An innovative method to obtain material J-R curve from test data using R6 failure assessment diagram

By

Mahesh Kumar

(ENGG01201004013)

Bhabha Atomic Research Centre, Mumbai

A thesis submitted to the

Board of Studies in Engineering Sciences

In partial fulfillment of requirements

for the Degree of

DOCTOR OF PHILOSOPHY

of

HOMI BHABHA NATIONAL INSTITUTE

January, 2019

Homi Bhabha National Institute

Recommendations of the Viva Voce Committee

As members of the Viva Voce Committee, we certify that we have read the dissertation prepared by **Mahesh Kumar** entitled "**An Innovative Method to Obtain Material J-R Curve from Test Data Using R6 Failure Assessment Diagram**" and recommend that it may be accepted as fulfilling the thesis requirement for the award of Degree of Doctor of Philosophy.

30/1/19

Chairman – Prof. T. A. Dwarkanath **Date:**

30/1/19

Guide / Convener – Prof. J. Chattopadhyay **Date:**

30.1.19

Co-guide - Prof. B. K. Dutta **Date:**

Examiner – Prof. Sanjib Kumar Acharyya **Date:** 30/01/19,

Member 1- Prof. R. Balasubramaniam **Date:** 30/1/19

Member 2- Prof. I. A. Khan **Date:** 30/1/19

Final approval and acceptance of this thesis is contingent upon the candidate's submission of the final copies of the thesis to HBNI.

We hereby certify that we have read this thesis prepared under our direction and recommend that it may be accepted as fulfilling the thesis requirement.

Date: 30/01/2019

Place: Mumbai

(Prof. B. K. Dutta) **(Prof. J. Chattopadhyay)**

Co-guide **Guide**

STATEMENT BY AUTHOR

This dissertation has been submitted in partial fulfillment of requirements for an advanced degree at Homi Bhabha National Institute (HBNI) and is deposited in the Library to be made available to borrowers under rules of the HBNI.

Brief quotations from this dissertation are allowable without special permission, provided that accurate acknowledgement of source is made. Requests for permission for extended quotation from or reproduction of this manuscript in whole or in part may be granted by the Competent Authority of HBNI when in his or her judgment the proposed use of the material is in the interests of scholarship. In all other instances, however, permission must be obtained from the author.

Mahesh Kumar

DECLARATION

I, hereby declare that the investigation presented in the thesis has been carried out by me. The work is original and has not been submitted earlier as a whole or in part for a degree / diploma at this or any other Institution / University.

Mahesh Kumar

List of Publications arising from the Thesis

International Journals

1. R. A. Ainsworth, M. Gintalas, **M. K. Sahu**, J. Chattopadhyay and B. K. Dutta (2016). "Application of failure assessment diagram methods to cracked straight pipes and elbows," *International Journal of Pressure Vessels and Piping,* 148, 26-35.
2. **M. K. Sahu**, J. Chattopadhyay, B.K. Dutta (2016). "Application of R6 failure assessment method to obtain fracture toughness. *Theoretical and Applied Fracture Mechanics*, 81, 67-75.
3. **M. K. Sahu**, J. Chattopadhyay, B.K. Dutta (2018). "Displacement based calculation of fracture toughness for cracked pipes using R6 method", *Theoretical and Applied Fracture Mechanics*, 93, 211-221.
4. **M. K. Sahu**, J. Chattopadhyay, B.K. Dutta. "Hybrid Approach for Calculation of J-R Curve Using R6", Theoretical and Applied Fracture Mechanics, status - (under review).

International Conferences

1. **M. K. Sahu**, J. Chattopadhyay, B.K. Dutta and K. K. Vaze (2012). "Implementation of FAD for Straight Pipes and Elbows with Circumferential Defects". ICCMS, IIT Hyderabad.
2. **M. K. Sahu**, J. Chattopadhyay, B.K. Dutta (2016), "Displacement Based Method for Calculation of Fracture Toughness using R6 Method for Cracked Pipes**".** 2nd International conference and exhibition on fatigue, durability and fracture mechanics. IISc, Bangalore.

Dedicated to

My beloved wife

ACKNOWLEDGEMENTS

I am deeply grateful to my beloved Deity Shiva for ushering me successfully in this journey of PhD investigation. His grace showered in the form of sincerity, dedication, patience, persistence, courage, etc. I genuinely feel that this work is expressed by him through me. May god fulfill me with more humility after completion of this work.

I am heartily thankful to my guide Dr. J. Chattopadhyay for his consistent motivation and critical technical assessment at appropriate stages of this investigation. His clarity of thought, decisiveness and promptness helped to complete this investigation.

I am also grateful to my co-guide Dr. B. K. Dutta for his motivation and essential 'push' at appropriate occasions. His attitude of curiosity and enthusiasm are naturally infectious.

I am also thankful to Doctoral committee members, Prof. T. A. Dwarkanath, Prof. R. Balasubramaniam, Prof. I. A. Khan and others for their important guidance in the course of the investigation.

I am grateful to my parent institute Bhabha Atomic Research Center for giving me opportunity for pursuance this work. The ample time and tips by knowledgeable colleagues helped to clear the doubts at times. I want to especially thank Dr. S. K. Gupta and Shri Punit Arora for their lucid explanation of complex technical issues.

I want to convey my special gratitude to Dr. Marius Gintalas for working with me. I learnt a lot from his very systematic approach, essential for the research work.

I also want to thank deeply the unsung heroes, the reviewers of my published journal papers. Without their critical assessment and suggestions, the work may have not reached to this final stage.

I am especially grateful to both the examiners for their critical assessment as well as kind appreciation of this work.

I am also deeply grateful to my parents and in-laws and, my children for their highly supportive attitude in the course of this investigation.

Finally, I am grateful to my beloved wife for her unconditional support during this long journey. I am sure that without her love, appreciation and motivation, this work could not have been completed.

Contents

List of Figures

List of Tables

Synopsis

Material fracture property J-R curve is an essential material parameter for assessing the integrity of any cracked component subjected to different loadings when the material is subjected to significant plastic deformation near crack tip. Obtained experimental results, load and load line displacement (LLD) from fracture test are conventionally post processed to material J-R curve using certain geometry parameters, η and γ. Thus, calculation of J-R curve is subjected to the availability of these parameters and the problem is that these parameters are available for very limited geometries. In this thesis, a simpler method is proposed to calculate J-R curve without using these η and γ parameters. For this purpose, R6 Failure Assessment Diagram (FAD) is employed. Conventionally, R6 FAD is widely used for failure assessment of cracked structures. However, in this work usage of R6 is extended for calculation of fracture property J-R curve from test data. In the steps of investigation, load approach, displacement approach and finally, hybrid (load and displacement) approach are proposed. The calculated J-R curves by hybrid R6 approach are in very good agreement for all investigated pipes and elbows. For this method, material tensile stress and strain properties, experimental load and displacement results with relevant crack growth data are required. The closed form expressions of stress intensity factor, K_I and limit load, P_L are also needed in the calculation procedure which are available for wider range of geometries unlike η and γ parameters . During this study, an innovative approach of calculation of reference stress and reference strain for R6 is proposed for deeply cracked pipes and elbows, using simple beam theory and curved bar theory respectively.

Nomenclature

a	Crack size
a_0	Initial crack size
Δa	Crack growth
B	Height between loading point and mid cross section of elbow in the test configuration
c	Half crack length
D_o	Outer diameter of pipe
E	Young's modulus
$E' = E/(1-\nu^2)$	Effective Young's modulus
F	Geometry factor for determination of crack driving force, K_I
F_b	F under bending moment
$H = \sqrt{B^2 + L^2}$	A length parameter of elbow test configuration
I	Moment of inertia of the cross section with respect to the neutral axis in beam theory
J	Total J-integral (summation of elastic and plastic)
$J_{0.2}$	Crack initiation toughness
J_{app}	Applied J −integral
J_e	Elastic J-integral
J_i^{TPB}	J-integral value corresponding to crack initiation of TPB fracture specimen
J_{ic}	Crack initiation material fracture toughness

J_{mat}	Material fracture toughness in plastically deformed regime
J_p	Plastic J-integral
K_I	Stress intensity factor
$K_{mat} = \sqrt{J_{mat}E'}$	Material fracture toughness
K_r=K_I/K_{mat}	Normalized crack driving force
L	Moment arm length in the test configuration of an elbow
$L_r = P/P_L$	Normalized remote loading
m_b	Geometry factor for including crack size effect on determination of M_L
M	Applied bending moment in pure beam
M_b	Bending moment
M_L	Limit bending moment
n	Ramberg-Osgood strain hardening exponent parameter
P	Applied load
$P_{0.2}$	Load corresponding to crack growth Δa =0.2mm
$P_{0.2}^{exp}$	Crack initiation load obtained by experiment
$P_{0.2}^{R6}$	Crack initiation load predicted by R6 method
P_L	Limit load
Q	Non dimensional stress triaxiality parameter
r	Radius of curvature of deformed beam
R_b	Bend radius of an elbow

R_m	Mean radius of cross section
t	Wall thickness
W	Width
X	Weakening factor due to crack on limit load of uncracked elbow
y	Distance from neutral axis
α	A coefficient in Ramberg – Osgood stress-strain equation
ε_e	Elastic strain
ε_{ref}	Reference strain
ε_y	Yield strain
θ	Half crack angle in circumferentially cracked pipes
ν	Poisson's ratio
$\xi = t/R_m$	Ratio of thickness to mean radius
σ_∞	Remote stress for uncracked cross section
σ_b	Bending stress for uncracked pipe cross section
σ_{ref}	Reference stress
σ_y	Yield strength of material
σ_u	Ultimate strength of material
$\phi = tan^{-1}\frac{\Delta}{C}$	Angular deformation of a pipe
$d\phi = tan^{-1}\frac{B}{L}$	Angular dimension of an elbow
$\Delta d\phi$	Angular deformation of a cracked elbow

Δ	Applied displacement
Δ_L	Applied displacement corresponding to limit load of load vs. load line displacement data
κ	A factor for getting reference strain by multiplication with normalized angular deformation $\Delta d\phi/d\phi$
η	A function used to multiply the area under load vs. load line deflection curve to get plastic J-integral
γ	A function used to get plastic J-integral under crack growth situation
$\lambda = \frac{tR_b}{R_m^2}$	Elbow factor

Chapter 1

Introduction

1.1 Motivation

Fracture mechanics was evolved to assess the structural integrity of the cracked structure under various loading conditions. On loading, the presence of crack intensifies the local stress level near crack tip which causes fracture of the structure. For a cracked structure, when the loading level is causing the global linear deformation, crack driving force is defined by single parameter K_I named as linear Stress Intensity Factor (SIF) by Irwin [1], Westergaard [2], etc. The material resistance to fracture is critical value of linear SIF K_I which is termed as K_{IC} and called material fracture toughness or fracture property of the material. The limitation of this parameter K_I is that allowed plastic zone size should be negligible compared to in-plane dimensions like thickness, remaining ligament, etc., of the cracked structure.

Engineering materials initially deform linearly, then after significant loading level it starts to deviate from linearity and undergo nonlinear deformation. For these cases, crack driving force K_I is not appropriate parameter and another parameter J-integral [3, 4] is proposed which is based on the assumption of nonlinear elastic deformation. The corresponding material fracture toughness is termed as J_{mat}. This parameter allows higher plastic deformation level near crack tip compared to SIF K_I. Fracture property of any ductile material is represented by J_{mat} vs. Δa curve, where Δa is the crack growth. This curve is called the J-R curve where 'R' stands for the fracture resistance of material. This curve is used to predict the unstable ductile tearing load of a cracked structure. The conditions for unstable ductile tearing are as follows:

$$J_{app} = J_{mat} \tag{1.1}$$

$$\left(\frac{\partial J}{\partial a}\right)_{app} \geq \left(\frac{dJ_{mat}}{da}\right) \tag{1. 2}$$

where, J_{app} is applied J-integral.

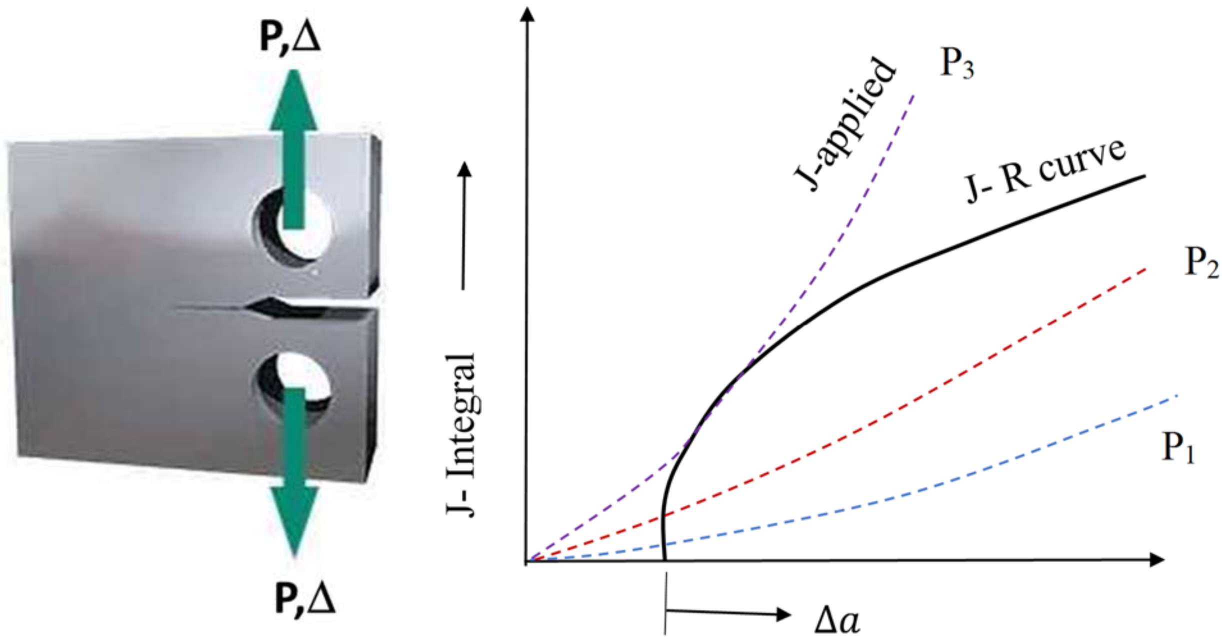

(a) (b)

Fig. 1.1. (a)Fracture specimen under loading for opening the crack. (b) Schematic representation of J-applied and J-R curve for determination of load level corresponding to unstable ductile tearing.

Fig. 1.1(a) shows the fracture specimen under loading and Fig. 1.1(b) shows the J-applied for different loading levels P_1, P_2 and P_3 with the fracture property J-R curve. The unstable ductile tearing point starts at load P_3, when Eqns. (1.1) and (1. 2) are satisfied. Thus, for predicting the load level corresponding to unstable ductile tearing, J-R curve is an essential material property. This concept is utilized in leak before break (LBB) concept which is used to design the primary heat transport (PHT) piping system of nuclear power plants [5] and other heat transporting pipes [6].

For an engineering material, fracture property J-R curve is found to be dependent on the geometry of cracked structure and loading configurations. The effect of geometries and loading configurations is quantified in terms of crack tip constraint parameter proposed by different researchers including O'Dowd and Shih [7]. Extensive research is still continuing for establishing this methodology for transferring the J-R curve from specimen to component using the crack tip constraint level [8]. Generally, the fracture property J-R curve is obtained from high constraint Compact Test (CT) fracture specimen irrespective of the constraint of the component geometry for which integrity is assessed. This method usually causes over conservatism in design and the higher fracture resistance property of the material remains unutilized. Hence, it is very important to predict the J-R curve from the fracture specimen that has identical stress triaxiality like the component for optimized design of the component for safety from unstable ductile tearing.

1.1.1 Conventional Methodology for J-R curve

The method of determination of J-R curve for fracture specimens have been discussed in detail in ASTM code E1820 [9] for Three Point Bend (TPB), CT and other standard fracture specimens. Experimental results like load, Load Line Displacement (LLD) and crack growth data are obtained by fracture tests conducted following the guidelines of the code. Load vs. LLD results are integrated numerically using certain geometry factors η and γ. This methodology is schematically shown in Fig. 1.2. Fig. 1.2 (a) shows schematically the typical test set up of TPB specimen which is loaded by applied load P or prescribed load line displacement(LLD) Δ. Fracture test results like load and LLD with relevant crack growth is obtained as shown schematically in Fig. 1.2(b). After deducting elastic displacement value from total LLD Δ, plastic displacement Δ_p is obtained. Now, load P vs. Δ_p curve is integrated using the geometry function η as shown in Fig. 1.2 (c) which is further corrected for crack

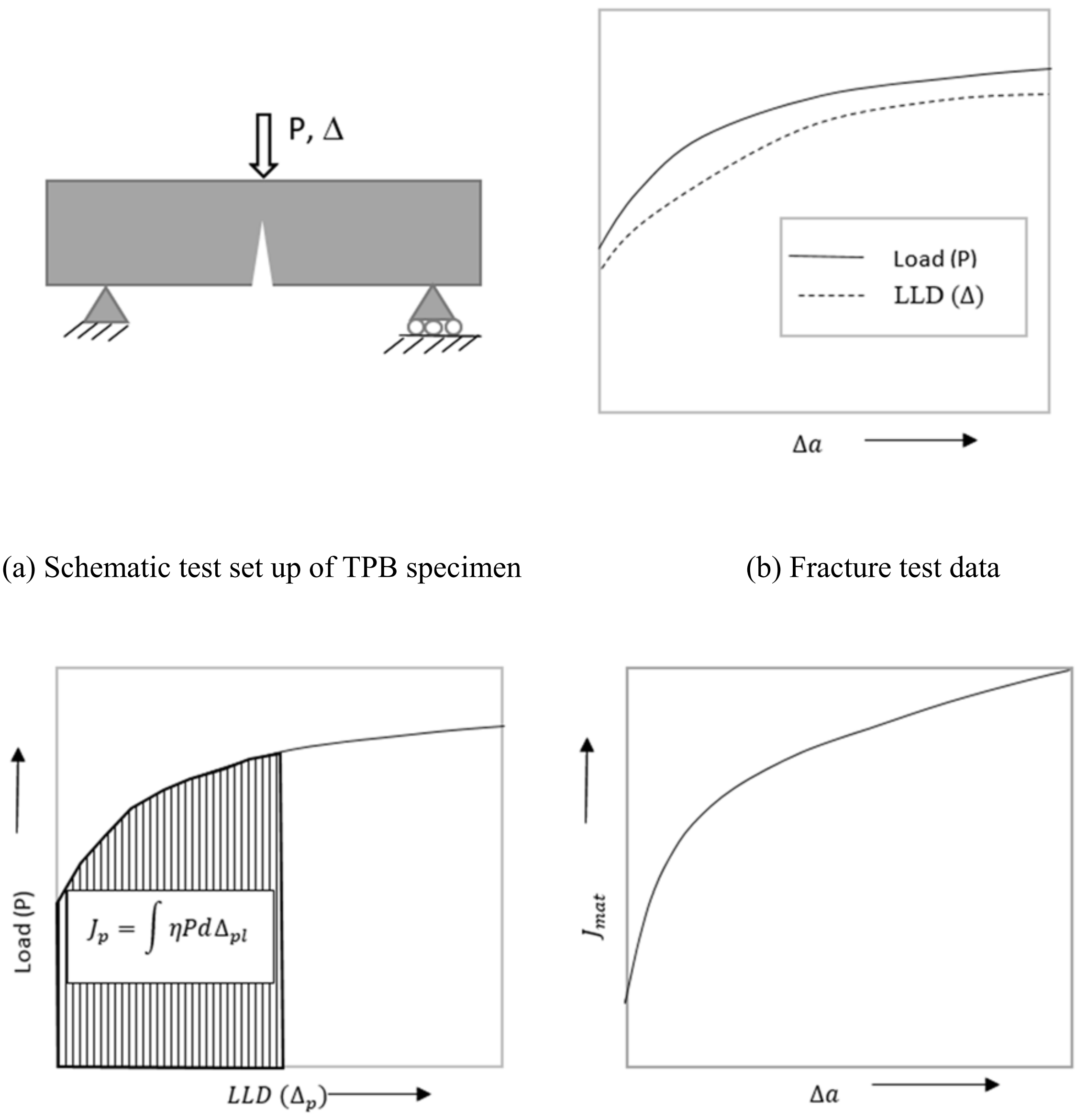

(a) Schematic test set up of TPB specimen

(b) Fracture test data

(c) Load vs. LLD integration

(d) J-R curve

Fig. 1.2. Schematic representation of methodology for fracture property J-R curve.

extension Δa using function γ for obtaining plastic part of J-integral, J_p. J-elastic (J_e) is obtained for this loading point using the closed form expressions of linear SIF, K_I. By combining elastic and plastic part, total value of J is obtained for this loading point which is material fracture toughness J_{mat} at this particular crack extension Δa . This method is applied for all values of crack extension Δa to obtain a complete J_{mat} vs. Δa curve i.e. J-R curve. This post processed typical J-R curve which is always a rising curve with crack extension Δa, is shown schematically in Fig. 1.2(d). The mathematical expression to evaluate J_p using experimental data is proposed by Ernts et.al. [10].

$$J_p = \int_0^{\Delta_{pl}} \eta_{pl}.P.d\,\Delta_{pl} + \int_{a_0}^{a} \gamma.J_p.da \tag{1. 3}$$

Where, P is applied load, Δ_{pl} is the plastic load line displacement due to crack only, a_0 and a are the initial and current length per crack tip and, η_{pl} and γ are two geometry and loading dependent functions. It should be noted that the η functions used here is associated with Δ_{pl}. Hence a subscript 'pl' is attached with η function in all the equations. However, for explanation purpose the term η is used for convenience instead of η_{pl}, further in this thesis.

This methodology is dependent on the availability of the functions η and γ. These functions depend on the geometry as well as loading configurations. Hence, these functions are available for limited geometries and standard loading configurations only. For post processing the fracture test data of any arbitrary geometry, these functions have to be obtained. While η function for an arbitrary crack geometry can be determined from extensive finite element analyses, γ function cannot be determined similarly. Chattopadhyay et. al. [11, 12] proposed limit load based general expressions of η and γ functions, however, they also need a limit load equation of the arbitrary crack geometry.

Hereafter, in this report this approach is referred as a conventional approach for determination of J-R curve.

1.1.2 Computational Approach for J-R curve

Using Gurson based continuum damage model GTN [13], fracture property J-R curve was estimated for some fracture specimens by Dutta et.al. [14] It should be noted that the identification of local damage parameters involves a lot of experimental works and numerical analyses and determination of these parameters with good repeatability is not very well established. This method is used to simulate the fracture test using large number of local material parameters. Additionally, computational time requirement is very high for this approach.

1.1.3 R6 Failure Assessment Diagram

R6 Failure Assessment Diagram (FAD) is a widely used simple method for failure assessment of any cracked component. In this methodology two failure modes, namely, brittle fracture and plastic collapse is included and in between ductile tearing is mapped [15] as

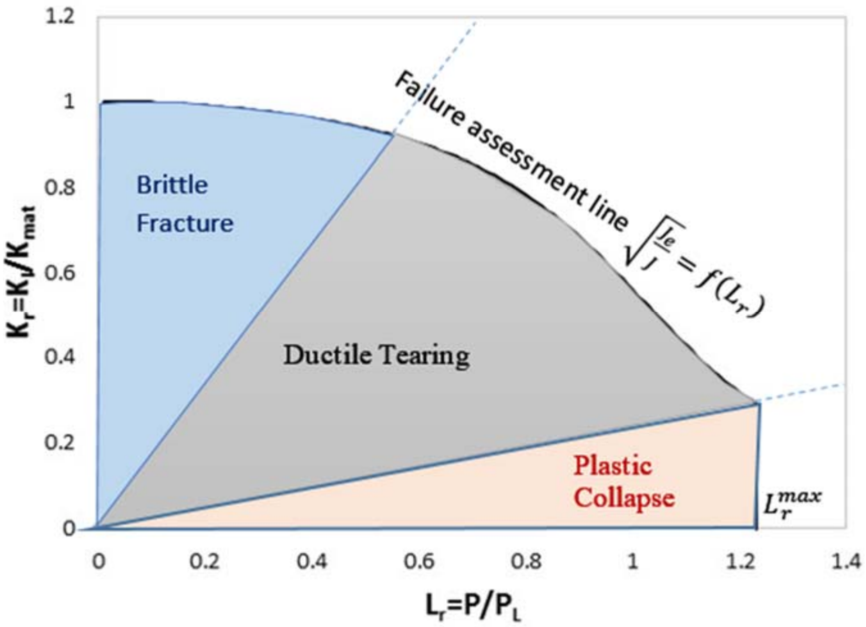

Fig. 1.3. Schematic representation of different modes of failure in R6

shown in Fig. 1.3.

British Energy researchers, Dowling and Townley [16] and Harrison [17] addressed the significant interaction of fracture and plastic collapse and proposed a two criterion failure assessment diagram (FAD), R6. A Failure Assessment Line (FAL) was proposed where normalized crack tip loading, $K_r = K_I/K_J$ was proposed as a function of normalized remote loading $L_r = P/P_L$. Here $K_J = \sqrt{JE'}$ where $E' = E$ for plane stress while $E/(1-\nu^2)$ for plane strain condition. P and P_L are applied load and limit load respectively for the assessed structure. With the evolution of finite element methodology the estimation of J became simpler and consequently values of J were reported extensively for different geometries with different material properties. Based of available J values, it was found that the earlier proposed R6 was non conservative for some cases.

The failure assessment line is simply variation of $\sqrt{J_e/J}$ with normalized loading L_r as shown in Fig. 1.3. Using finite element method, FAL can be estimated for the exact geometry and loading configurations with relevant material property. Hence, this estimated FAL is dependent on material and geometry and it is called option-3 curve. Using available J of different cracked geometries, Ainsworth [18] proposed reference stress based FAL which was almost independent of the cracked geometries. This FAL can be obtained using the material tensile stress strain data only. This is called option 2 curve and was more conservative than the option 3 curve. Further, considering that yield stress σ_y is corresponding to 0.2% yield for all the material, the failure point corresponding to $P_L(\sigma_y)$ is identical for all the materials. There was deviations in later part only i.e. beyond σ_y. This observation paved the way for proposal of a universal FAL. A lower bound curve was proposed and incorporated as option-1 in revision 4 of R6 [15] by British Energy. It is a universal curve because this curve is almost independent of material, geometry, type of loading and present flaw size.

In all the proposed methods in this thesis, option-1 failure assessment diagram is used for investigation which is a unique line and expressed by a simple exponential mathematical expression as shown in Eqn. (1.4).

$$K_r = f_1(L_r) = \left(1 + 0.5{L_r}^2\right)^{-1/2}\left[0.3 + 0.7exp\left(-0.6{L_r}^6\right)\right] \tag{1.4}$$

For assessment, mathematical solutions of elastic stress intensity factor, K_I and limit load P_L are required which are available for wider range of geometries than cases covered by η and γ functions.

R6 FAL is widely used for failure assessment of cracked structures under different loading configurations. However, in this thesis, the usage of R6 is extended for prediction of fracture property J-R curve. It should be noted that in this thesis, R6 failure assessment diagram is also quoted as simply 'R6' for convenience.

1.2 Objectives of the Thesis

Based on the extensive review of the literature, the following objectives are set for the present investigation:

1. To propose a simpler method to evaluate material J-R curve from test data using R6 failure assessment diagram without using geometry functions η and γ.
2. Application of the proposed methodologies for displacement controlled fracture tests.
3. To validate the proposed methodology for different geometries and loading configurations by comparing predicted J-R curves using R6 approach with already available conventionally calculated J-R curves using geometry functions η and γ.

For obtaining these objectives, based on the detail literature review, the following tasks have to be attempted.

1. R6 option 1 failure assessment line is made almost independent of material and geometries of the component and is a unique line. This efficacy of this failure

assessment line will be assessed for the piping material carbon steel SA333Gr6 for prediction of failure at ductile initiation.

2. Generally, R6 is utilized for determination of failure due to ductile initiation in terms of normalized remote loading L_r and crack tip loading K_r. Here, usage of this methodology will be extended to predict J_{mat} in ductile crack growth regime.
3. Reference stress σ_{ref} will be evaluated from experimental load value and consequent J-R curves will be compared with the conventional values.
4. For displacement controlled loading, displacement is established as a better parameter for quantification of fracture response especially for highly plastically deformed cases. Hence, applied displacement will be used for determination of J-R curves.
5. For task no. 4, displacement will be used for determination of reference stress σ_{ref} and reference strain ε_{ref} using tensile stress strain data of the material SA333Gr6. R6 failure assessment line is appropriate for smooth hardening material unlike the investigated material SA333Gr6, which has significant Luder band in tensile stress strain data at yield point. Hence, original tensile stress strain data will be converted to smooth hardening tensile stress strain data using appropriate exponential fitting.
6. For evaluating reference strain ε_{ref} using LLD, an innovative approach based on elastic beam theory and curved bar theory will be attempted.

1.3 Organization of the Thesis

The present research work proposes a new and simple method for calculation of J-R curve using R6 failure assessment diagram. This report comprises total seven chapters. The briefing of each chapter has been given as follows.

The second chapter includes exhaustive literature survey on different related areas like conventional approach of calculation of J-R curve using η and γ factors, referred experimental results like material tensile and fracture properties obtained from specimens, and fracture test data of pipes and elbows. Reference stress and reference strain R6 failure assessment methods have been also discussed in detail.

In the third chapter, utility of R6 FAD is assessed by predicting the crack initiation loads for pipes and elbows and comparison with experimental load values. This work ensures the efficacy of the R6 failure assessment diagram in predicting the ductile crack initiation for the investigated piping material carbon steel SA333Gr6.

The fourth chapter contains the proposal of load based approach for calculation of J-R curve using experimental load and relevant crack extension data. For total six pipes, the J-R curves are calculated and compared with already available results based on the conventional approach.

The fifth chapter explains the displacement as a better parameter than load for J_{mat} estimation. Thus, a displacement based approach is proposed for calculation of reference strain and reference stress and eventually, J-R curves for pipes.

In the sixth chapter, displacement based approach is extended to cracked elbows tested under bending moment. Based on the limitation of this approach for elbows, a hybrid approach is proposed where both parameters load and displacement are used for calculation of J-R curves. Thus, this approach is termed 'hybrid' approach. This approach is also validated for cracked pipes for calculation of J-R curves.

Finally, in the last chapter, important conclusions have been drawn for the present investigation.

Chapter 2

Literature Survey

2.1 Introduction

Large numbers of pipes and elbows of material SA333Gr6 with throughwall circumferential cracks were already tested by Chattopadhyay et.al. [19, 20] under monotonic bending moment. Consequent experimental results like load, Load Line Displacement (LLD), crack growth, etc., are available for further investigations. The relevant geometries and loading configurations of tested pipes and elbows are explained in this chapter. Conventional approach of calculation of J-R curve based on load vs. displacement data integration, is adopted for these test cases and calculated J-R curves are also reported. These J-R curves are used for validation of the proposed methods in later parts of the thesis.

Fracture mechanics-based approaches provide a means for constructing a correlation of crack size with applied loading as defined by the linear elastic stress intensity factor, K, or the elastic plastic parameter defined by J-integral [21]. Further developments in the engineering critical assessment methodology include the effect of plasticity on crack tip loading by adopting the concept of Failure Assessment Diagrams (FADs). A key feature of the FAD-based approach is the introduction of an user friendly frame work to explicitly address the potential interaction between stress-controlled cleavage fracture and plastic collapse to predict structural failure. The methodology thus provides an effective, although conservative, acceptance criterion for cracked structural components which relate the loading conditions with the critical applied load or critical crack size. Several flaw assessment procedures based upon the FAD concept, such as R6 approach [15] among others are now well established. These FAD approaches are widely adopted to analyse the significance of defects in terms of the assessment of structural integrity. For a highly plastically deformed cases under strain controlled loading, the limitation of load based approaches for defining the fracture response is discussed in detail. To address this issue, strain controlled R6 FAD has been proposed by Budden [22] and Budden and Ainsworth [23]. These approaches are available for very shallow cracked cases where uncracked strain can be assumed to be reference strain. Finally, the usage of R6 FAD for determination of crack driving force, J-integral is explained for very shallow cracked plate under axial loading. It should be noted that presently, there is no literature available to address failure of the deeply cracked cases using strain based R6 for significantly plastically deformed cases.

2.2 Experimental Results

2.2.1 Material Properties

Materials properties have been obtained from standard tensile tests and three-point bend (TPB) specimens for the SA333 Grade 6 carbon steel used in the pipe tests as discussed by Chattopadhyay et.al. [19] and Singh et.al. [24]. Pipes of two different diameters were tested. Although both the materials were SA333Gr6, however, material properties were slightly different due to heat to heat variation. Therefore, material properties were evaluated for both these two piping materials separately and expressed corresponding to pipe diameter. For getting material tensile properties and fracture properties, tests are performed according to ASTM standards E08 [25] and E1820 [9] respectively. Results are presented in Table 2.1; the yield stress, σ_y , ultimate stress, σ_u, and fracture toughness data for two different outer diameters of the pipe, D_o are tabulated. Ductile initiation fracture toughness values J_i^{TPB} were obtained using

Table 2.1: Properties of SA 333 Grade 6 steel for two different pipe diameters

D_0 [mm]	E [GPa]	ν	σ_y[MPa]	σ_u [MPa]	J_i^{TPB} [N/mm]
219	203	0.3	288	420	220
406	203	0.3	312	459	236

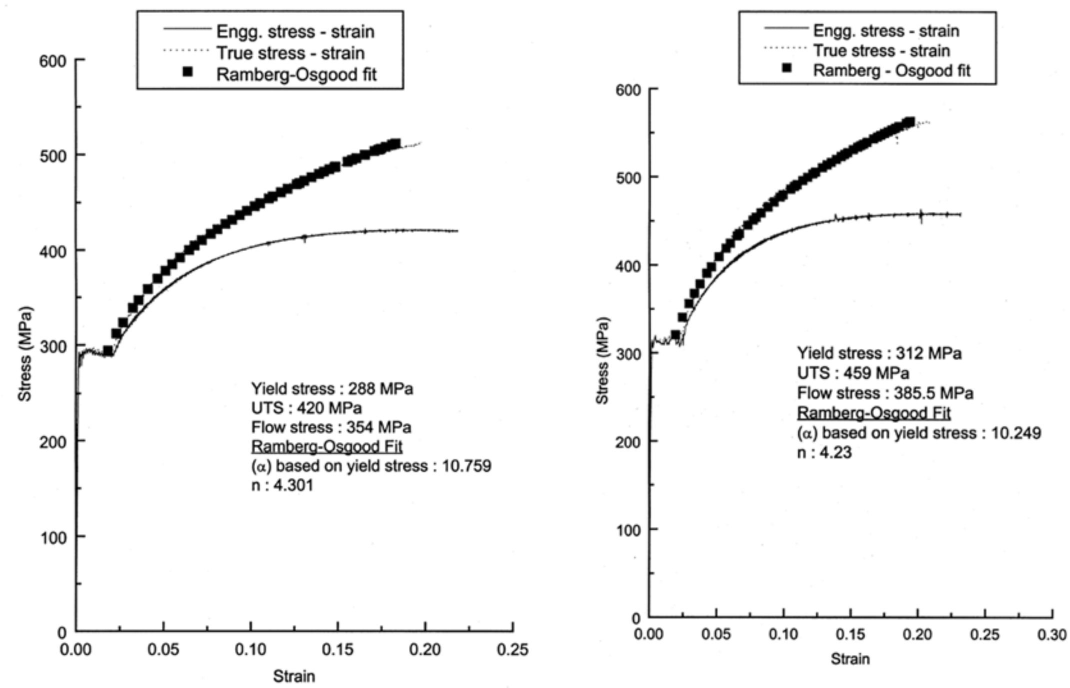

(a) (b)

Fig. 2.1. Tensile stress-strain properties used for further investigations for piping materials by Chattopadhyay et. al. [19]. (a) 8 inch piping material and (b) 16 inch piping material

stretch zone width (SZW) measurements at a crack growth of Δa =0.2mm. For the 219 mm (nominal 8 inch) pipe diameter, initiation toughness was determined from TPB8 specimens with a relative crack depth a/W=0.513 and for the 406mm (nominal 16 inch) pipe from TPB16 specimens with a/W=0.453 [26].

Tensile stress strain data obtained for the 8 inch and 16 inch piping materials by Chattopadhyay et.al. [19] are depicted in Fig. 2.1. These material properties are used for respective sizes of pipes and elbows chosen for the investigations in this research work.

2.2.2 Fracture Test Results: Pipes

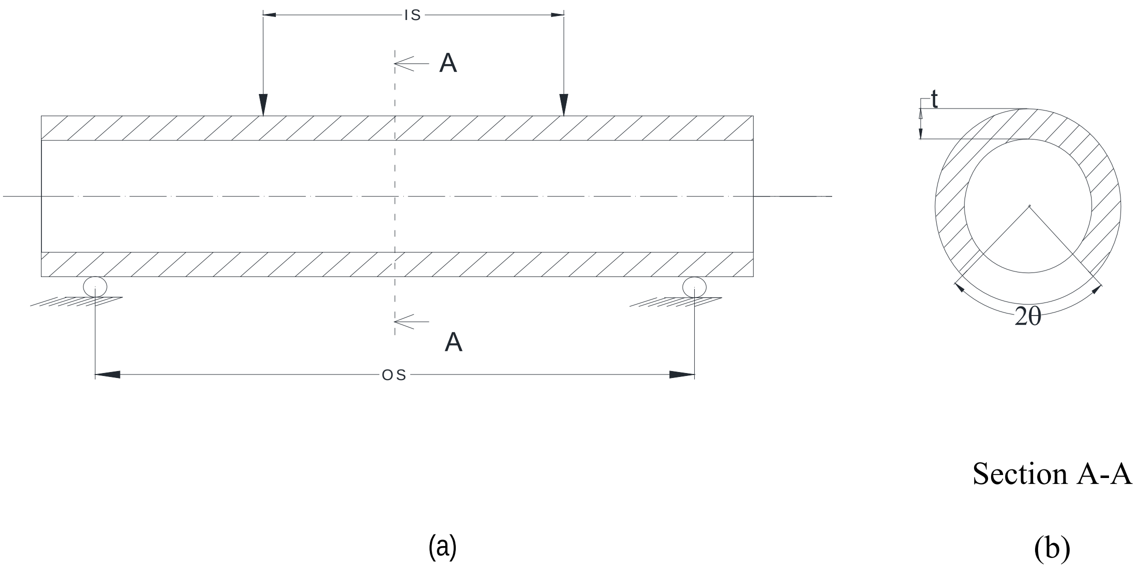

Fig. 2.2. (a) Loading configurations of pipes, where OS is outer span denoted by distance between supports and IS is inner span denoted by distance between loading points. (b) Cross sectional view of pipe with throughwall crack.

A comprehensive *Component Integrity Test Program* was initiated by Bhabha Atomic Research Centre (BARC), India in 1998. Under this program, large numbers of straight pipes and elbows with through wall cracks were tested at SERC (Structural Engineering Research Centre), Chennai, India by Chattopadhyay et.al. [19, 27]. Important aspects of those fracture tests on pipes are revisited here. In this program, four-point bending moment were applied quasi-statically during test. All straight pipes were fabricated with throughwall circumferential cracks of different sizes. The loading configuration is shown schematically in Fig. 2.2(a) and corresponding crack configuration in Fig. 2.2(b). Image processing system was employed to

Table 2. 2: Dimensions of pipes with circumferential cracks

Pipe Designation	Outer Diam-eter (D_0) (mm)	Thickne-ss (t)(mm)	R_m^*/t	Outer span (OS)(mm)	Inner span (IS) (mm)	crack angle (2θ) (degree)	θ/π	Crack initiation load ($P_{0.2}$) kN
SPBMTWC8-1	219	15.15	6.73	4000	1480	65.6	0.18	199.1
SPBMTWC8-2	219	15.1	6.75	4000	1480	93.9	0.26	155.9
SPBMTWC8-3	219	15.29	6.66	4000	1480	126.4	0.35	122.2
SPBMTW16-1	406	32.38	5.77	5820	1480	96.0	0.27	529.2
SPBMTW16-2	406	32.15	5.81	5820	1480	126.3	0.35	399.3
SPBMTW16-3	406	32.36	5.77	5820	1480	157.8	0.44	288.4

* mean radius, $R_m = (D_0 - t)/2$

measure crack growth during pipe fracture experiments. Therefore, picking exact crack initiation point in load vs. crack growth curve was not possible. Hence, crack initiation load was determined at crack growth $\Delta a = 0.2$mm for more repeatability in choosing the initiation point. This load corresponding to this crack extension of 0.2mm is named as $P_{0.2}$. In this study we have chosen total 6 straight pipes; 3 numbers each of both 8 inch and 16 inch nominal diameter sizes. Relevant dimensions of pipes are shown in Table 2. 2. All pipes were fatigue pre-cracked to produce very sharp crack tip from machined crack. A static and monotonic load was applied on the pipe specimens under displacement control. Different instrumentations were mounted on test configurations for monitoring and recording different experimental results like total applied load, crack growth, LLD, etc.

2.2.3 Fracture Test Results: Elbows

The testing of these elbows has been performed under the component integrity test program by

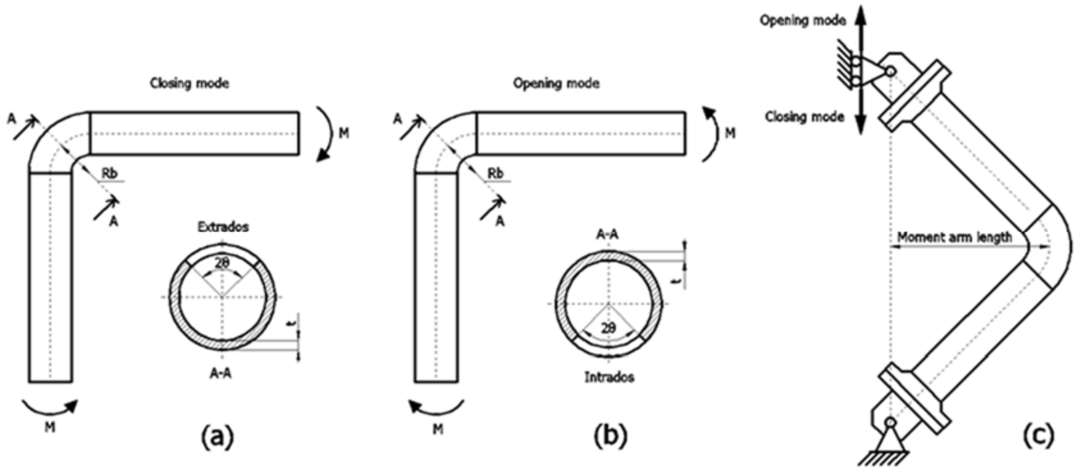

Fig. 2.3. Loading configuration of an elbow, under in plane bending moment: a) crack at extrados – closing mode, b) crack at intrados – opening mode; c) test set up

Chattopadhyay et al. [20]. The test specimens selected for the investigation consist of 90 degree elbows with circumferential throughwall crack, either at intrados or extrados having two sizes; nominal bore 200 mm (8 inch) and 400 mm (16 inch). Cracks have been machined on the elbow by milling process. Before carrying out the fracture tests, each elbow was fatigue pre-cracked through remote loading by around 3-10 mm on each side of the crack to have sharp crack tips. These tests have been carried out by applying in-plane bending moment.

The elbows which were cracked at the extrados were tested under closing mode and those cracked at the intrados were tested under opening mode. Straight pipes were welded to each side of an elbow and to flanges, bolted to circular plates, for connection to the loading. Fig. 2.3 is a schematic representation of an elbow test set up.

Table 2.3. Elbows having extrados throughwall crack: tested under closing mode of moment

Designation	R_b (Bend radius)	D_o (Outer Diamet-er.)	t (thick ness)	R_m/t	2θ (crack angle)	$P_{0.2}$ (Crack initiate-on load)	L (moment arm length)
	(mm)	(mm)	(mm)		(degree)	kN	(mm)
ELTWEX16-4	609	406	35.7	5.19	94.11	1004.2	840
ELTWEX16-5	609	406	37.6	4.90	124	748.4	840

Table 2.4. Elbows having intrados throughwall crack: tested under opening mode of moment.

Designation	R_b (Bend radius)	D_o (Outer Diameter)	t (thickness)	R_m/t	2θ (crack angle)	$P_{0.2}$ ((crack initiation load)	L (moment arm length)
	(mm)	(mm)	(mm)		(degree)	kN	(mm)
ELTWIN8-2	207	219	18.8	5.32	125.16	89.7	826
ELTWIN16-1	609	406	36.43	5.07	95.89	647.6	840
ELTWIN16-2	609	406	36.85	5.01	122.79	594.3	840

Total 5 nos. of elbows with circumferential through-wall cracks, either at the intrados or extrados have been picked up for the present study. They were tested by applying monotonic and quasi-static in-plane bending moment. Relevant data for FAD analyses for the elbows tested under closing mode of bending moment with extrados throughwall cracks has been given in Table 2.3.

Similar information is given in Table 2.4 for elbows tested under opening mode of bending moment. Crack initiation loads for all the elbows have been also interpolated from the load vs. crack growth data, corresponding to the crack growth of 0.2mm, termed as $P_{0.2}$.These experimental data of cracked pipes and elbows have been used for further investigation by Chattopadhyay group using FE analyses and available closed form expressions of limit load. The predicted crack initiation loads [28-31] and limit loads [32] are in good agreement with experimental values. Using Gurson based continuum damage model, GTN model [13, 33], one pipe and one elbow have been simulated using micromechanical properties of the material by Dutta et.al. [14]. The computed results of load vs. crack growth curve and load vs. LLD curve are found to be in very good agreement with corresponding fracture test results. These earlier investigations validate the experimental results obtained from the fracture tests.

2.3 Fracture Parameters

For a cracked body loaded globally up to linear elastic deformation, the crack driving force is defined by linear Stress Intensity Factor (SIF), K_I. This parameter fully characterizes the stress and strain field near crack tip. The corresponding material fracture toughness is critical value of SIF which is named as K_{IC}. The limitation for this parameter is that the plastic zone size near the crack tip should be contained and very small compared to other dimensions of the cracked body. The mathematical expressions of stresses and strains near crack tip were simultaneously derived by Irwin [1], Westergaard [2], Sneddon [34] and Williams [35]. These expressions showed that the stresses vary with the amplitude of SIF and SIF can be written in the following form

$$K_I = F\sigma_\infty\sqrt{\pi a} \qquad (2.\ 1)$$

Where σ_∞ is the remote stress acting for opening the crack, a is the crack size per crack tip and

F is a factor based on the geometry and loading configurations which is available in open literature for wide range of geometries.

One increasing the load, the plastic zone size near the crack tip increases and after some point the plastic zone size is no longer negligible compared to the plane dimensions of cracked geometry. This is reflected as nonlinear deformation globally and SIF K_I is no longer a valid parameter. With assumption of nonlinear elastic deformation, a fracture parameter J-integral was proposed which was valid for larger level of plastic deformation. Rice [3] showed that this parameter was equivalent to energy release rate for stationary crack under monotonic loading. Hutchinson [4] and, Rice and Rosengren [36] had shown that crack tip stresses and strains can be uniquely characterized by this parameter. Hence it can be viewed as stress intensity parameter as well as an energy release rate parameter for nonlinear elastic material. The corresponding material fracture toughness is denoted as J_{mat} for nonlinear material. This parameter is valid upto limited plastic deformation level only. However, J-integral allows significantly larger plastic deformation near crack tip compared to K_I.

2.4 Crack Tip Constraint Parameter

The concept of "similitude" in fracture mechanics is inherent. In this approach, it is assumed that the near tip stress and strain fields that govern the micro-structural fracture processes are similar in any two cracked bodies (e.g., specimen and component). Traditionally, these fields were uniquely characterized by a single parameter (i.e. the crack driving force), which, depending on the level of loading could be either of K or J . Later it was observed that such a single parameter description is only valid for certain configurations those exhibit high level of crack tip stress triaxialities [37]. Therefore, two parameter approaches evolved, which

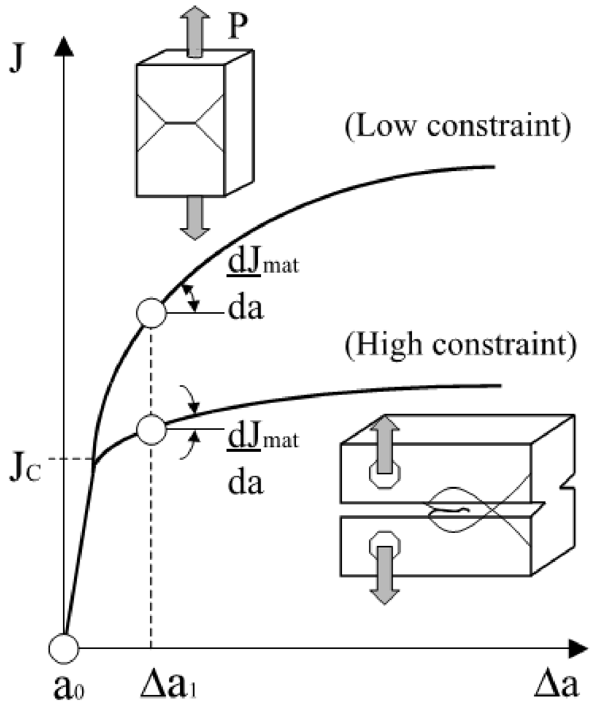

Fig. 2.4. Variation of J-R curves with the level of crack tip constraints [38]

introduced additional "crack tip constraint/ stress triaxiality" parameter, in addition to the crack driving force to characterize the near tip fields.

It is now well known that transferability of J-R curve from specimen to component is mainly governed by constraint ahead of crack tip which is depicted by Zhu and Jang [38] as shown in Fig. 2.4. There are several parameters to quantify the crack tip constraint, such as T-stress [39], Q parameter [7, 40], multi-axiality quotient (q) [41], stress triaxiality factor (h) [42], A_2 parameter [43], etc. In this thesis, stress triaxiality parameter, Q is used as a measure of triaxiality.

O'Dowd and Shih [7] introduced the non-dimensional parameter, 'Q', to quantify the crack tip constraint. By this theory, the laboratory specimen must match the constraint of the component for transferability of fracture toughness property. Q is defined as,

$$Q = \frac{[\sigma_{\theta\theta} - (\sigma_{\theta\theta})_{ref}]}{\sigma_y} \qquad at\ \theta = 0, \qquad r = \frac{2J}{\sigma_y} \tag{2.2}$$

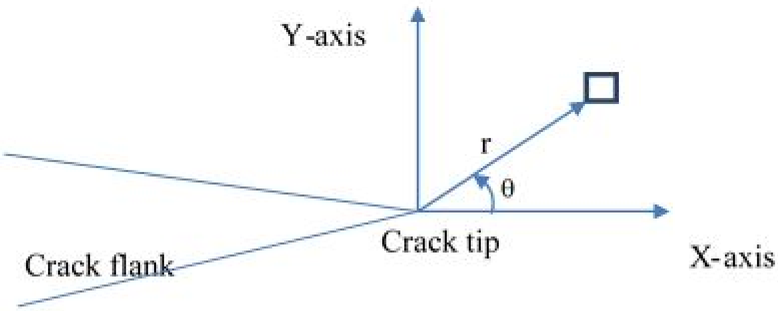

Fig. 2.5. Definition of co-ordinate axis ahead of crack tip

Where, r and θ are polar co-ordinates of the point of interest with origin situated at the crack tip (as shown in Fig. 2.5). $\sigma_{\theta\theta}$ is the existing stress field ahead of the crack tip of the actual specimen or component, $(\sigma_{\theta\theta})_{ref}$ is reference solution obtained from standard plain strain small scale yielding solution $(\sigma_{\theta\theta})_{SSY,\ T=0}$ or HRR field. It is found that the SSY (Small Scale Yielding) solution gives better reproducibility for reference stress solution. Therefore, it is widely used for determination of Q. Recently in 2017, Larrosa and Ainsworth [44] have utilized the stress triaxiality parameter Q for quantifying the crack tip constraints of different standard and non-standard fracture specimens, and surface cracked pipes. Based on this investigation, the use of nonstandard specimen with lower crack tip constraint instead of standard fracture specimen CT, has been recommended for avoiding excessive conservatism in the fracture assessment of a surface cracked pipe. For another set of standard and nonstandard fracture specimens, Yang [45] has also reported the crack tip constraint levels and validated by corresponding material J-R curves, obtained experimentally for those fracture specimens.

2.5 Conventional Approach for Calculation of J-R Curve

The method of determination of J-R curve for fracture specimens have been discussed in details in ASTM code E1820 [9] for standard fracture specimens, Three Point Bend (TPB), Compact Tension (CT) and Disc Shaped Compact (DSC) specimens. Experimental results like load, LLD and crack growth data are obtained by fracture tests conducted following the guidelines of the code. Load vs. LLD results are integrated numerically using geometry factors η and γ. Conventional approach of evaluation of J-integral requires certain geometry parameters (η and γ functions) proposed by Rice et.al. [46] and Ernst et.al. [47]. For simpler geometries and loading configurations, these parameters are available in open literature [10, 47-49]. For complex geometries, these parameters are not easily available; thus calculation of J-R curve from fracture test results is difficult using conventional approach. Chattopadhyay et. al. [11, 12, 50] proposed limit load based general expressions of 'η' and 'γ' and utilized them to derive these functions for cracked pipe and elbow geometries. These geometric functions were utilized for calculation of J-R curves. These curves are reported by Chattopadhyay et. al. [11, 19, 20, 51] for all the investigated pipes and elbows, in this thesis.

J-integral at any loading point can be divided as following:

$$J = J_e + J_p \tag{2.3}$$

where J_e and J_p are the elastic and plastic part of J-integral respectively.

where, J_e is evaluated as $J_e = K_I^2/E'$, where $E' = E$ for plane stress while $E/(1-\nu^2)$ for plane strain case, E is the Young's modulus and ν is the Poisson's ratio. J_p is obtained by numerical integration of load and LLD.

$$J_{p(i)} = \left[J_{p(i-1)} + \eta_{p(i-1)}\left[U_{p(i)} - U_{p(i-1)}\right]\right]\left[1 + \gamma_{(i-1)}\left(a_{(i)} - a_{(i-1)}\right)\right] \tag{2.4}$$

with

$$\left[U_{p(i)} - U_{p(i-1)}\right] = \frac{\left(P_{(i-1)} + P_{(i)}\right)}{2}\left(\Delta_{p(i)} - \Delta_{p(i-1)}\right) \tag{2.5}$$

where P, Δ_p are total applied load and plastic load line displacement respectively. U_p is the area under P vs. Δ_p curve. Geometry functions, η_p and γ are factors depending on the instantaneous geometries and loading configurations. The subscripts '(i)' and '$(i-1)$' indicate values corresponding to current and previous load steps respectively.

2.6 R6 Failure Assessment Diagram

It should be recognized that for failure assessment or structural integrity assessment different codes/procedures are used. SINTAP (Structural Integrity Assessment Procedures) [52] is developed by cooperative European project for European industry. British Standards document BS7910 [53] and Swedish safety assessment procedure by Anderson et. al. [54] are also popular procedure for flaw assessment of any cracked structure. A handbook in Japan is produced namely Japan Society of Mechanical Engineers fitness-for-purpose code by Kobayashi group [55, 56]. Lei et.al. [57] proposed Chinese national standard containing procedure for flaw assessment. A comprehensive guide for fitness-for-purpose is API 579 published by the American Petroleum Institute by Anderson and Osage [58]. RSE-M code [59] is also a widely used procedure for flaw assessment of nuclear components. R6 [15] proposed a simplified failure assessment technique where failure and involved margin can be predicted and visualized graphically.

2.6.1 Earlier Developments of R6 Method

Interaction diagrams have been already used in engineering. It is widely recognized that the brittle fracture and plastic collapse caused by overloading are competing failure modes in cracked structural components made of sufficient toughness material. Using strip-yield model of Bilby et.al. [60] and Heald et.al. [61], a simplified mathematical relation was developed to combine elastic fracture with plastic collapse. Further, Dowling and Townley [16] addressed the potential interaction between fracture and plastic collapse which introduced the concept of a two-criterion failure assessment diagram (most often referred as FAD) to describe the mechanical integrity of flawed structures. Harrison et al. [62] modified the earlier expression and proposed a more useful relationship.

$$K_r = S_r[(8/\pi^2) ln \sec(\pi S_r/2)]^{-1/2} \tag{2.6}$$

Where,

$$K_r = \frac{K_I(P,a)}{K_{mat}} \tag{2.7}$$

$$S_r = \frac{P}{P_L(a,\sigma_f)} \tag{2.8}$$

The first parameter, K_r is governing the elastic fracture which is defined in terms of elastic stress intensity factor K_I in terms of applied load P and present crack size a, and material fracture toughness K_{mat}. Second term S_r is the normalized loading which is normalized by plastic collapse load P_L defined for flow stress σ_f, where σ_f is taken average of yield stress σ_y and ultimate stress σ_u.This failure assessment diagram is depicted in Fig. 2.6, from where it is clear that LEFM and plastic collapse, are corresponding to $K_r = 1$ and $S_r = 1$ respectively. In between region is corresponding to elastic-plastic fracture where both mechanisms are interacting and adding to total failure inflicted on the loaded cracked structure.

The R6 procedures underwent further improvement by Harrison et.al. [17, 63]. The underlying

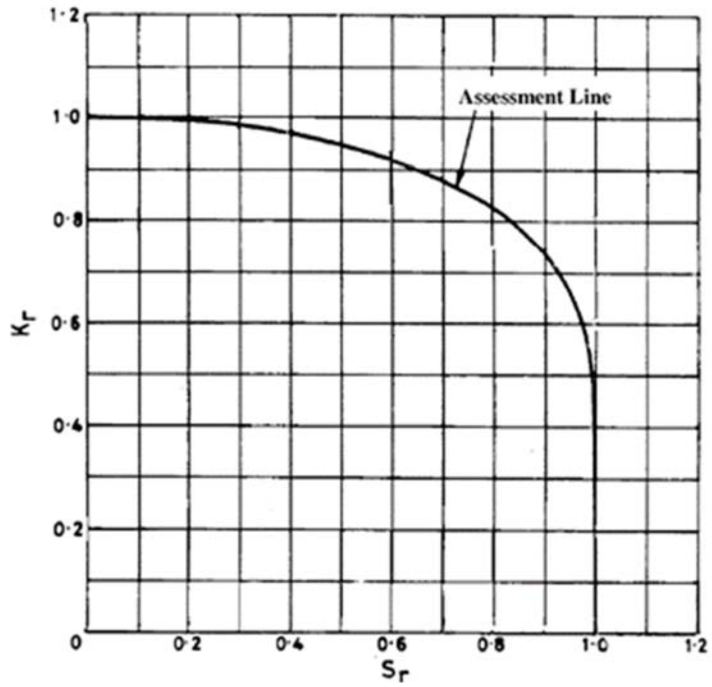

Fig. 2.6. FAD in the first version of R6 by Harrison et.al. [62]

principles of R6 were used in other codes and standards and were found to be consistent with emerging elastic-plastic fracture parameters COD and J-integral. This basic principle of interaction of LEFM and plastic collapse remain unchanged till today with so much extensive development in this field. This proves the power of the work carried out by the earlier researchers.

2.6.2 Reference Stress Based R6

In post yield fracture mechanics (PYFM), it is established that the onset of crack growth and small amount of crack extension can be estimated by a better fracture parameter, J instead of K_I. Finite element method has been widely used for determination of J but it is relatively difficult because it involves significant computational effort and expertise. To counter this, many simplified PYFM methods such as CEGB failure assessment route as shown in Eqn. (2.6) [64] , the $J-$design curve [65] and $J-$ estimation schemes [66] had evolved. These schemes are mainly based on materials such as A533B and some metals for which the ratio of ultimate stress to yield stress is low i.e. the strain hardening is low. In these materials, the strain hardening property can be satisfactorily fitted by pure power hardening (as in the $J-$estimation schemes) for plastic strain. Stress vs. strain property of many materials, does not fit properly to simple power hardening so the use of $J-$ estimation schemes based on pure hardening rule is not justified for those materials. Milne [67] showed that neither of these approaches is satisfactorily for significant strain hardening response of materials where yield and ultimate strengths are significantly different. Shih [68] had derived estimations of J-integral for strain hardening materials in the small scale yielding to large scale yielding range in antiplane shear using available elastic solutions and fully plastic solutions [69, 70].

Shih and Hutchinson [71] extended that J-estimation to elastic plastic case for plane stress crack problems. Earlier $J-$ estimation scheme was dependent on the power law fit of the material. For many materials, material stress strain curve shows very poor fitting in power law equation used and the strain hardening parameter n of Ramberg Osgood equation is very sensitive to the range of stress strain curve chosen for fitting. These reasons may result in to significant erroneous estimate of J.

2.6.2.1 Option-2 Failure Assessment Line

Because of development of elastic-plastic fracture mechanics and evaluation of numerical values of J by Bloom and Malik [72] and Bloom [73, 74], it was found that these proposed FADs are non-conservative in same cases.

Ainsworth [18] used the extensive J solutions proposed by Kumar et.al. [75] and proposed a simple approach for elastic–plastic J-estimation using the actual material stress strain curve of the material. Milne [76] performed extensive work for treatment of ductile tearing using FAD approach.

This $J-$ estimation is proposed which is based on reference stress, σ_{ref}, which is defined based on earlier developed creep analysis methodology [77]. Reference stress based methods proposed by Ainsworth [18] to calculate Failure Assessment Line (FAL) provided convenient approach to calculate FAL for different materials using material stress – strain data. With the development of finite element method and introduction of reference stress method, detailed comparison of the FAD method with FE results for range of elastic-plastic material behaviour were performed by Miller and Ainsworth [78]. Finally, a modified reference stress based FAD to include the more accurate small scale yielding effect was proposed in revision 3 of R6 by Milne et.al. [79, 80].

$$K_r^{-2} = \frac{E\varepsilon_{ref}}{\sigma_{ref}} + \frac{1}{2}\left(\frac{L_r^2}{E\varepsilon_{ref}/\sigma_{ref}}\right) \tag{2.9}$$

Which can be further rearranged as Eqn.(2.10) for better explanation of fracture response.

$$J \approx J_e\left[1 + \frac{1}{2}\left(\frac{L_r^2}{E\varepsilon_{ref}/\sigma_{ref}}\right)\right] + J_e\left[\frac{E\varepsilon_{ref}}{\sigma_{ref}} - 1\right] \tag{2.10}$$

$$L_r = \frac{P}{P_L(a, \sigma_y)} = \frac{\sigma_{ref}}{\sigma_y} \tag{2.11}$$

Where ε_{ref} is total (elastic plus plastic) strain at the reference stress, σ_{ref} and J_e is elastic part of total J. The first term of the right hand side of Eqn.(2.10) is the elastic contribution multiplied by a small scale yielding correction and the second term is the fully plastic contribution. Introduction of reference strain and reference stress takes into account the material hardening in calculation of J. Furthermore, the geometric features of the cracked body are also included implicitly via elastic stress intensity factor, K which is in the form of J_e. Thus, the final expression of failure assessment curve in terms of reference stress, is written as,

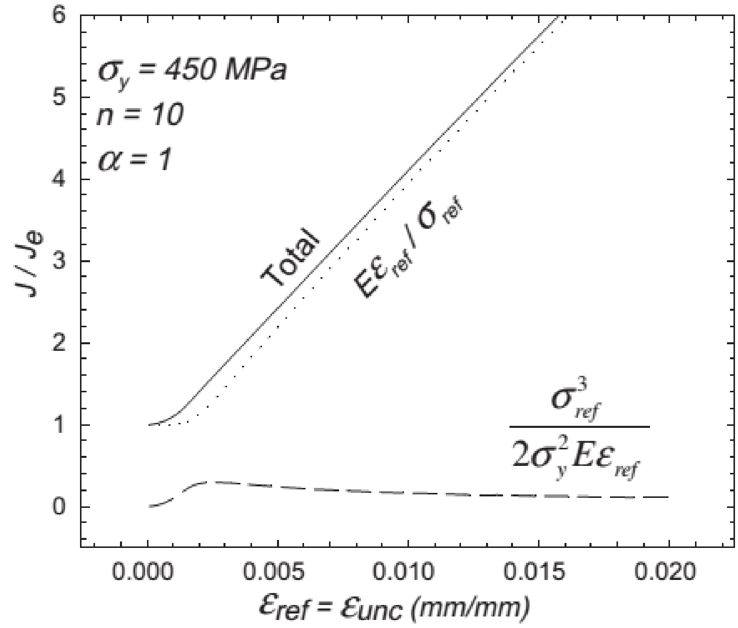

Fig. 2.7. Influence of plasticity correction term in small scale yielding on the fracture response of surface cracked pipe under bending moment. [82]

$$K_r^{-2} = f_2(L_r) = \frac{E\varepsilon_{ref}}{\sigma_{ref}} + \frac{\sigma_{ref}^3}{2\sigma_y^2 E\varepsilon_{ref}} \tag{2.12}$$

The first term in Eqn. (2.12), $E\varepsilon_{ref}/\sigma_{ref}$ gives value of elastic value of J_e without considering the plastic zone formed when the specimen is globally elastic, $\sigma_{ref} \leq \sigma_y$. In case of larger plastic loading, $\sigma_{ref} \gg \sigma_y$, $E\varepsilon_{ref}/\sigma_{ref}$ defines a factor, which gives total J, when it is multiplied with J_e. The second term, $\sigma_{ref}^3/2\sigma_0^2 E\varepsilon_{ref}$, represents the factor for modification of J_e for plastic zone correction in SSY region and becomes significant in the loading region, $\sigma_{ref} \approx \sigma_y$. This factor has negligible effect in the elastic domain, $\sigma_{ref} \ll \sigma_y$ and fully plastic domain, $E\varepsilon_{ref}/\sigma_{ref} \gg 1$ [81]. Fig. 2.7 (by assuming equality of reference strain and applied strain) shows that minor plasticity correction term, $\sigma_{ref}^3/2\sigma_0^2 E\varepsilon_{ref}$ becomes significant when the loading is in regime of SSY, $\sigma_{ref} \approx \sigma_y$ while it is negligible when the loading is purely elastic or purely plastic. It can be observed that this factor has negligible effect on fracture response for strains larger than 1% [82].

2.6.2.2 Option-1 Failure Assessment Line

Using the material tensile stress-strain data, FADs are developed for a range of austenitic and ferritic steels by Milne et.al. [80]. The curves were found to be almost insensitive to the material chosen because the yield stress is defined at 0.2% proof stress for all cases. Thus, there were almost negligible differences in failure quantity up to $L_r \approx 1$. This observation led the way for proposal of a universal curve for failure assessment. An empirical curve was proposed by Milne et.al. [79] in R6 revision 3 which is further modified by Ainsworth et.al. [83, 84] and incorporated as option-1 in revision 4 of R6 [85] by British Energy in 2001.

Eqn. (1.4) for failure line is called option1 curve which gives most conservative assessment. $f_1(L_r)$ is plotted up to maximum , L_r called $L_{r_{max}}$, which is defined as,

$$L_{r_{max}} = \frac{\left(\sigma_y + \sigma_u\right)}{2\sigma_y} \tag{2.13}$$

It was a universal curve in the same sense as original FAD curve presented as Eqn.(2.6) because this curve is also independent of material, geometry, type of loading and present flaw size. In the present study, option 1 failure assessment curve is adopted for all the investigations carried out.

Thus R6 contained a hierarchy of failure assessment lines: the universal curve of option 1 $f_1(L_r)$, the material dependent curve option 2 $f_2(L_r)$ which required a completer stress-strain data in terms of true stress strain data and option 3 curve

$$f_3(L_r) = (J_e/J)^{-1/2} \tag{2.14}$$

Which require a specific evaluation of J for the considered geometry with relevant loading configurations.

It should be noted that in this thesis, for all R6 related calculation, option-1 failure assessment line is used. Hence, for convenience purpose, employed option-1 FAL is termed as simply '$f(L_r)$' instead of $f_1(L_r)$ in many places in the thesis.

2.6.3 Closed Form Solutions of K_I and P_L

For failure assessment of any arbitrary loading point, stress intensity factor K_I and limit load solutions P_L are essential. These expressions are easily available in the literature for cracked pipes under bending moment because of simpler geometry and loading configuration. However, the development of these functions for elbows is more challenging compared to pipes. Hence, availability of these functions has been limited and continuous improvement is still going on. For example, for elbows the elastic stress distribution is still not available in defect free elbow under in-plane bending moment and research is being continued in this area [86]. Generally, elbow section is assumed to be of constant thickness with perfect circular shape. However, during fabrication process thickness varies across the circumference and cross section undergoes ovalization during deformation process.. The effect of these shape imperfections have been studied in detail by Micheal et.al. [87] and Buckshumian et.al. [88] for closing and bending moment respectively. Some attempts have been done to include material strain hardening property also in the limit load expression by Zhang et.al. [89]. However, now it is well established that the limit load is dependent on the material yield stress σ_y and elbow and existing crack geometries only [90]. Recently there have been many proposals of limit load solutions [32, 91-93] and stress intensity factors [94-96] for cracked pipes and elbows.

2.6.4 Reference Strain Based R6

Current procedures for engineering critical assessment (ECA) for structural integrity and fitness-for-service codes and standards (for example BS 7910 [97] and API [98]) are based on the assumptions that the component is subjected to load-controlled loading and failure can be predicted by the amount of the load subjected. Initially, Bratfos [99], Schwalbe [100] , Wang et.al. [101] and Linkens et.al. [102] had attempted the problems in the light of strain based

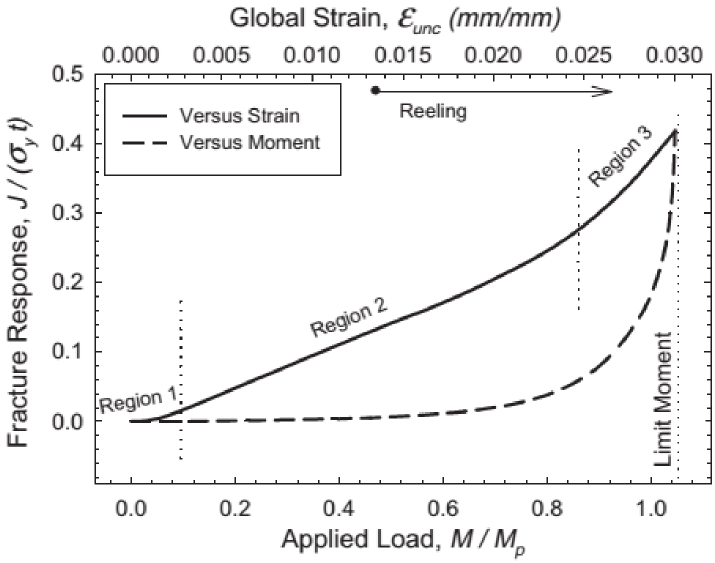

Fig. 2.8. Fracture response of a circumferentially cracked pipeline as a function of the global strain (solid line) and load (dashed line) by Nourpanah et. al. [82].

fracture when the component was subjected to displacement controlled loading and material had undergone significant plastic deformation.

Jayadevan et al. [103] and Otsby et al. [104] investigated the fracture response of pipelines subjected to large plastic deformation under, tension and bending respectively. Otsby [105] have also reported the large scale experimental investigation which incorporates significant plastic deformation under displacement controlled loading. Their results clearly indicated the benefit of using the total strain in formulating the fracture response under large plastic strains over the traditional stress based approaches. The fracture response of a pipe with circumferential surface crack under bending, characterized by ($J/\sigma_y t$), is shown in Fig. 2.8, which shows that fracture response is increasing gradually with applied strain (solid line) while it increases rapidly with applied moment (dotted line) near plastic collapse. Hence, strain is better parameter to quantify the fracture response instead of applied moment in highly plastically deformed cases [82]. Parise at.al. [106] have proposed mathematical expressions of

J in terms of remotely applied strain for circumferential surface cracked pipe subjected to reeling.

Limited articles are available in open literature where strain based R6 has been investigated and usage of R6 for estimation of J-integral is again very rare. Linkens et.al. [102] proposed a method to convert reference stress to reference strain in R6. Tkaczyk et.al. [107] have utilized the modified reference stress approach proposed by Kim and Budden [108] to optimize the limit load solutions of Kastner et.al. [109] to account for additional failure in displacement controlled loading. In parallel, the strain based failure assessment diagram is proposed and validated for creep induced crack growth in creep-brittle steels [110, 111].

No literature is available for deeply cracked pipes to adopt directly for calculation of J-R curves using R6. Budden [23] have also studied the limitations of load based R6 failure assessment and proposed a displacement/strain based approach for calculation of J-integral using R6. It is well known that, for displacement-controlled loads, the basic R6 approach calculations becomes over-conservative particularly beyond limit load point in the component. Section III.14 of R6 [15] proposes an alternative approach that takes into account the post-yield effect in the failure by Ainsworth [112]. In this investigation, Budden has used the finite element calculations of Lei [113-116] for surface semi elliptical defects in plates under mechanical and thermal loads to validate the proposed reference strain based approximations. Displacement based estimation of J has been re-cast into reference strain based failure assessment diagram.

Budden [22, 117] has observed that the proposed strain-based FAD becomes non-conservative in some cases, especially for deeply cracked cases and/or for the material with high value of strain hardening coefficient, 'n'. Budden and Ainsworth [118] further improved the strain-based failure assessment methodology for integrity assessment of highly strained component under plastic deformation. Proposed strain based failure assessment method is validated by finite element results [113, 119]. Further, Ainsworth et.al. [120] have advanced the method for including the secondary strains in the calculations in strain based failure assessment diagram.

2.7 Closure

For calculating the J-R curve from experimental fracture data load, LLD (load line displacement) with related crack growth data are essential. For post processing these fracture test data using conventional load vs. LLD integration technique certain, geometry functions η and γ are essential. These functions are available in open literature for limited geometries and loading configurations only. Thus, post processing the fracture test data of the cracked component without availability of these geometry functions is not possible. The fracture test data like load, LLD with relevant crack extension data are available for cracked pipes and elbows tested under bending moment. For these test cases, geometry functions η and γ have been developed by using a limit load based general expressions and reported already. Using these functions, all these fracture test data have been post processed to obtain the J-R curve using load and displacement integration technique. These conventionally calculated J-R curves are already reported, which are used in this thesis for validation of the proposed methodologies. An attempt is made in the present work to propose a simpler and alternative methodology for calculating J-R curve, using R6 failure assessment diagram (FAD). R6 represents a failure line which maps brittle fracture, plastic collapse and in between elastic-plastic ductile tearing. In the elastic plastic ductile tearing regime, the failure line corresponds to ductile initiation. With more and more development in R6, a unique failure line is proposed which is almost independent of material and geometry, which is called Option 1 failure line. In this work for all the investigations, option-1 failure line of R6 is employed.

For R6 failure analysis, linear stress intensity factor K_I and limit load P_L are required. These functions are available for wider range of geometries in open literature than geometry functions η and γ. Geometric details and loading configurations are available for these pipes and elbows to evaluate corresponding stress intensity factor K_I and limit load P_L values. Material properties tensile stress strain data and crack initiation toughness J_{ic} is also available for the piping material SA333Gr6. Crack initiation toughness J_{ic} is termed as J_i^{TPB} because it is corresponding to crack initiation of TPB specimens fabricated using the same piping/elbow material carbon steel SA333Gr6.

For displacement controlled loading cases, the present load based R6 have been found to be over conservative and for these cases strain based R6 failure assessment diagram have been proposed. However, the proposed strain based R6 is appropriate for a very shallow cracked component. For deeply cracked cases, available strain based R6 becomes again highly non-conservative.

In this work, R6 failure assessment diagram will be utilized for calculation of fracture property J-R curve. The already available experimental results like load, LLD with related crack growth of pipes and elbows will be used for predictions. Already available conventionally obtained J-R curves will be used to validate the predicted J-R curves using R6 failure assessment diagram in the following chapters. Before using R6 failure assessment line option-1 curve for calculation of J-R curve, first, this $f(L_r)$ will be validated at crack initiation point for the investigated pipes and elbows in next chapter.

Chapter 3

Prediction of Crack Initiation Loads using R6 and Validation

3.1 Introduction

In a wide range of industries, the structural integrity assessment of piping components containing defects is required to demonstrate safe and reliable operation. For example, Leak-Before-Break (LBB) assessments of primary piping systems of some nuclear power plant postulate the presence of cracks and demonstrate that such cracks lead to detectable leakage before pipe burst. There have been many studies addressing the defect tolerance of piping components, some addressing the influence of defects on the collapse load, others addressing fracture using linear and non-linear fracture mechanics. This has led to the inclusion of procedures for assessment of piping components within more general fracture assessment approaches such as R6 [15] and RSE-M code [59] and others. Recently there have been developments in both stress intensity factor and limit load solutions for defective straight pipes and elbows [32, 91-94, 121]. Using these expressions and experimental test data, applicability of fracture assessment method R6 for predicting the crack initiation loads and its comparison with experimental data is performed. This work is important because in next chapters the utility of R6 is extended beyond crack initiation point to crack growth regime for calculation of J-R curve. Hence, the efficacy of R6 in prediction of crack initiation loads for the chosen cases are very important.

3.2 Analytical Solutions for Input to the Fracture Assessments

3.2.1 Stress Intensity Factor for Pipes

In order to apply FAD methods, it is necessary to evaluate the stress intensity factor, K_I. The following solution for circumferentially through-wall cracked pipes under in-plane bending moment proposed in R6 [15, 95], was used:

$$K_I = F_b \sigma_b \sqrt{\pi a} \tag{3.1}$$

where, the bending stress, σ_b, is defined in terms of the bending moment M_b as

$$\sigma_b = M_b / (\pi R_m^2 t) \tag{3.2}$$

The correction function, F_b, in Eqn. (3.1) is

$$F_b = 1 + A[4.5967(\theta/\pi)^{1.5} + 2.6422(\theta/\pi)^{4.24}] \text{ for } 0 < \theta/\pi \leq 0.55 \tag{3.3}$$

where

$$A = [0.125(R_m/t) - 0.25]^{0.25} \text{ for } 5 \leq R_m/t \leq 10 \tag{3.4}$$

Here 2θ is the total circumferential throughwall crack for the pipe to be investigated. For all the pipes studied, θ/π and R_m/t are within the validity limits, in Eqns.(3.3) and (3.4) respectively.

3.2.2 Limit Moment for Pipes

For failure assessment using R6 failure methodology, limit load, P_L, is also essential to calculate $L_r = P/P_L$. Closed form expression of limit moment, M_L, is available in R6 [15, 122] for straight pipes under bending moment as,

$$M_L = 4{R_m}^2 t m_b \sigma_y \tag{3.5}$$

where, weakening factor m_b due to crack is,

$$m_b = f_b(\xi)\sin\beta - 0.5 f_c(\xi)\sin\theta \quad (3.6)$$

and σ_y is the yield strength of the piping materials as shown in Table 2.1

where,

$$f_b(\xi) = 1 + \xi^2/12,\ \ f_c(\xi) = 1 + \xi^2/6,\ \ \beta = (\pi - \theta)/2 \text{ and } \xi = t/R_m \quad (3.7)$$

3.2.3 Stress Intensity Factor for Elbows

Table 3.1. Values of the function F_b for a crack at the centre of the elbow extrados – under closing moment

R_m/t	R_b/R_m	θ/π			
		0.1	0.2	0.3	0.5
3	2	0.609	0.856	1.189	2.176
	3	0.751	0.978	1.280	2.219
	4	0.846	1.057	1.336	2.239
5	2	0.374	0.722	1.231	2.601
	3	0.570	0.901	1.347	2.541
	4	0.727	1.036	1.429	2.512
10	2	-	-	1.119	3.509
	3	-	0.505	1.322	3.287
	4	0.273	0.749	1.481	3.131

In order to calculate the stress intensity factor for elbows, the solution recently developed in [94] has been used using Eqns. (3.1) and (3.2). However, F_b is given in tabular form as a functions of R_b/R_m, R_m/t and θ/π. These parameters can be calculated from geometrical details given for elbows in Table 2.3 and Table 2.4. Values of F_b are only given for solutions where the crack fully opens (see [94]). The relevant part of the tabulated values of F_b from literature, are shown in Table 3.1 and Table 3.2, which cover all the elbows investigated. For some parametric values in the tables, the values of F_b are not given which is related to crack closure cases. However, for all investigated cases here, the crack opens due to loading configurations. It should be noted that the different parameters R_b/R_m, R_m/t and θ/π shown Table 3.1 and Table 3.2 cover all the elbows investigated.

Table 3.2. Values of the function F_b for a crack at the centre of the elbow intrados – under opening moment

R_m/t	R_b/R_m	θ/π			
		0.1	0.2	0.3	0.5
3	2	1.037	1.335	1.706	2.726
	3	1.072	1.305	1.616	2.593
	4	1.076	1.275	1.558	2.517
5	2	0.765	1.257	1.884	3.313
	3	0.892	1.288	1.783	3.068
	4	0.964	1.281	1.703	2.918
10	2	-	0.792	2.02	4.625
	3	0.359	0.993	1.996	4.193
	4	0.510	1.099	1.930	3.896

3.2.4 Limit Load Solutions for Elbows

3.2.4.1 Closing Mode

The limit moment for a defective elbow is taken as the product of the limit moment for an defect-free elbow M_0 and a weakening factor X:

$$M_L = M_0 X \tag{3.8}$$

The solution for a defect free elbow under closing moment was recently developed in [93]:

$$\frac{M_0}{M_L^P} = \begin{cases} \left(1 + \frac{0.22}{\lambda^{1.028+0.12(R_b/R_m)}}\right)^{-1} & for\ \lambda \leq 1 \\ \left(1 + \frac{0.22}{\lambda^{1.313}}\right)^{-1} & for\ \lambda > 1 \end{cases} \tag{3.9}$$

where M_L^P is the limit moment for the uncracked straight pipe:

$$M_L^P = 4R_m^2 t\sigma_y \tag{3.10}$$

and λ is the elbow factor defined as,

$$\lambda = \frac{tR_b}{R_m^2} \tag{3.11}$$

The weakening factor due to the presence of the crack is [91]:

$$X = \begin{cases} 0 & \text{for} \quad 0 \leq \theta/\pi < 0.21 \\ 1.44 - 2.1(\theta/\pi) & \text{for} \quad 0.21 \leq \theta/\pi \leq< 0.5 \\ 3.12(1-\theta/\pi)^3 & \text{for} \quad 0.5 \leq \theta/\pi \leq 1 \end{cases} \tag{3.12}$$

3.2.4.2 Opening Mode

The limit moment solution for a defective pipe bend is again taken as the product of the solution for an un-cracked elbow M_0 and a weakening factor X as in Eqn. (3.8). The solution for a defect free elbow under opening moment was again recently developed in [93] as:

$$\frac{M_0}{M_L^P} = 0.8908 + 0.2502\ln(\lambda) \quad \text{for} \quad 0.1 \leq \lambda \leq 1.0 \tag{3.13}$$

where the uncracked straight pipe limit moment is again given by Eqn. (3.10). After a lot of comparative study of different expressions of weakening factor X in these cases, the expressions of Chattopadhyay et.al. [27] as given in Eqn. (3.14) was found to be the most accurate and is used for these investigations:

$$X = 0.127 - 1.8108(\theta/\pi) \quad \text{for} \quad 0.125 \leq \theta/\pi \leq 0.41 \tag{3.14}$$

3.3 Defect Assessment Results

Using Eqns. (2.7) and (2.11) the assessment point (L_r,K_r) corresponding to experimental crack initiation load, $P_{0.2}^{exp}$ is calculated. Material fracture toughness K_{mat} corresponding to crack initiation is obtained from $J_{mat} = J_i^{TPB}$ which is given for piping material in Table 2.1. The required solutions of K_I and P_L are already discussed for relevant cracked pipes and elbows.

For prediction of crack initiation loads corresponding to failure assessment line following

Table 3.3. Comparison of experimental and predicted initiation loads for pipes.

<table>
<tr><th rowspan="2">Test Number</th><th colspan="2">Experimental Initiation Load $P_{0.2}^{exp}$, kN</th><th colspan="2">Predicted Initiation Load using R6 $P_{0.2}^{R6}$, kN</th><th rowspan="2">Difference, % $\frac{\left(P_{0.2}^{R6} - P_{0.2}^{exp}\right)}{P_{0.2}^{exp}} 100$</th></tr>
<tr><th>L_r</th><th>K_r</th><th>L_r</th><th>K_r</th></tr>
<tr><td rowspan="2">SPBMTWC8-1</td><td colspan="2">199.1</td><td colspan="2">186.6</td><td rowspan="2">-6.3</td></tr>
<tr><td>1.0027</td><td>0.6779</td><td>0.9399</td><td>0.6353</td></tr>
<tr><td rowspan="2">SPBMTWC8-2</td><td colspan="2">155.9</td><td colspan="2">142.6</td><td rowspan="2">-8.6</td></tr>
<tr><td>0.9830</td><td>0.7483</td><td>0.8986</td><td>0.6840</td></tr>
<tr><td rowspan="2">SPBMTWC8-3</td><td colspan="2">122.2</td><td colspan="2">104.7</td><td rowspan="2">-14.3</td></tr>
<tr><td>1.0374</td><td>0.8106</td><td>0.8891</td><td>0.6946</td></tr>
<tr><td rowspan="2">SPBMTWC16-1</td><td colspan="2">529.2</td><td colspan="2">539.9</td><td rowspan="2">2.0</td></tr>
<tr><td>0.7483</td><td>0.7951</td><td>0.7634</td><td>0.8110</td></tr>
<tr><td rowspan="2">SPBMTWC16-2</td><td colspan="2">399.3</td><td colspan="2">397.2</td><td rowspan="2">-0.5</td></tr>
<tr><td>0.7586</td><td>0.8220</td><td>0.7546</td><td>0.8175</td></tr>
<tr><td rowspan="2">SPBMTWC16-3</td><td colspan="2">288.4</td><td colspan="2">289.6</td><td rowspan="2">0.4</td></tr>
<tr><td>0.7857</td><td>0.7874</td><td>0.7892</td><td>0.7907</td></tr>
</table>

relation is used:

$$J_{ic} = J_i^{tpb} = J_e[f(L_r)]^{-2} \tag{3.15}$$

where, J_e is evaluated as $J_e = {K_I}^2/E'$, where $E' = E$ for plane stress while $E/(1-\nu^2)$ for plane strain case. Where E is Young's modulus and ν is the Poisson's ratio. Crack initiation

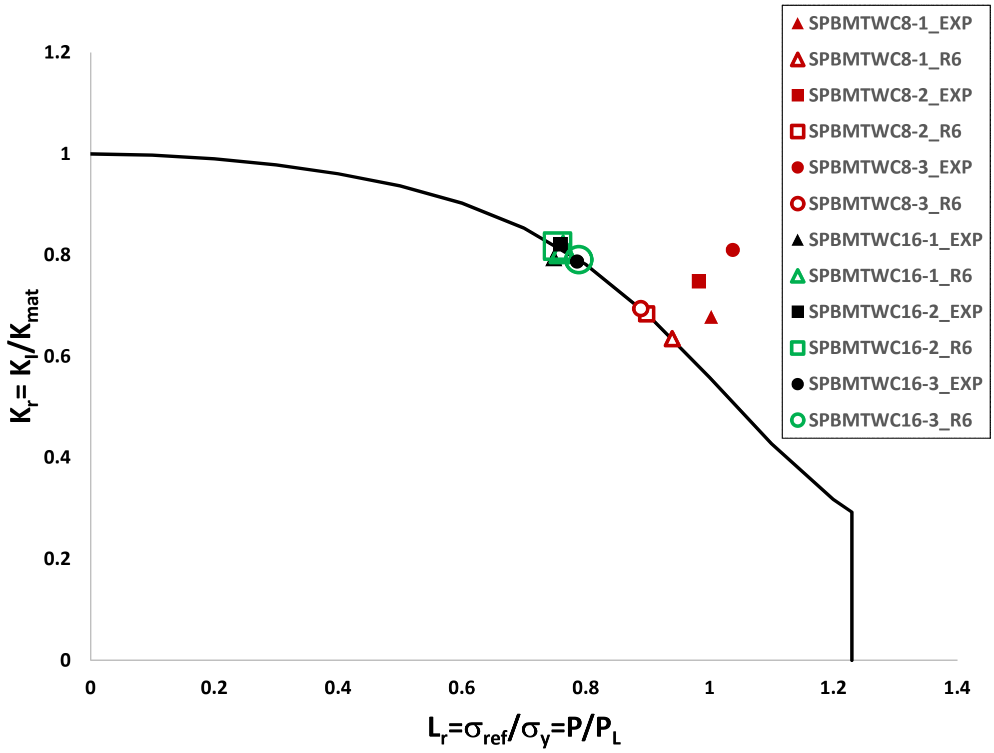

Fig. 3.1. Circumferentially through-wall cracked pipes. Predicted and experimental initiation load points on FAD.

toughness, J_i^{TPB} is already available from TPB specimen test. J_e and L_r are linear functions of applied load P. The instantaneous crack size a for calculation of K_I and P_L is obtained by adding the crack extension $\Delta a = 0.2mm$ to initial crack size because predicted crack initiation load will be compared with experimental crack initiation load P corresponding to $\Delta a = 0.2mm$, which is termed as $P_{0.2}^{exp}$. It should be noted that $f(L_r)$ is option 1 failure assessment line as shown in Eqn. (1.4), which is a unique exponential function. Thus, by iterative way value of P is determined corresponding to J_i^{tpb}, which will be predicted crack initiation load $P_{0.2}^{R6}$ based on R6.

3.3.1 Pipes

For total 6 straight pipes under pure bending, the predicted crack initiation loads are compared with the experimental initiation loads in Table 3.3. Also included in the table are the values of L_r and K_r at the predicted crack initiation loads. Fig. 3.1 shows pictorially the assessment points (L_r,K_r) evaluated at the experimental crack initiation loads and the predicted initiation loads, and plotted on the FAD. Of course, the assessment points for the predicted loads lie on the failure assessment curve because the prediction is based on the failure assessment line only. It can be observed that the predicted initiation loads are close to the experimental loads and ductile initiation occurs before plastic collapse. These results are tabulated with the percentage differences in Table 3.3.

3.3.2 Elbows

Using Eqns. (2.7) and (2.11) the assessment point (L_r,K_r) corresponding to experimental crack initiation load, $P_{0.2}^{exp}$ is calculated. Material fracture toughness K_{mat}, corresponding to crack initiation is obtained from initiation fracture toughness J_i^{tpb} for piping material given in Table 2.1.

For the all five elbows under opening or closing bending, the predicted ductile initiation loads are compared with the experimental initiation loads in Table 3.4. Also included in the table are the values of L_r and K_r at the predicted initiation loads. Fig. 3.2 shows the assessment points (L_r,K_r) evaluated at the experimental and predicted initiation loads, and plotted on the FAD. It can be seen that the predicted initiation loads generally exceed the experimental loads, with the percentage differences given in Table 3.4, and that ductile initiation occurs before plastic collapse, although often close to $L_r = 1$.

Table 3.4. Comparison of experimental and predicted initiation loads for elbows.

Test Number	Experimental Initiation Load $P_{0.2}^{exp}$, kN		Predicted Initiation Load using R6 $P_{0.2}^{R6}$, kN		Difference, % $\frac{\left(P_{0.2}^{R6} - P_{0.2}^{exp}\right)}{P_{0.2}^{exp}} 100$
	L_r	K_r	L_r	K_r	
ELTWIN8-2	89.7		80.4		-10.4
	0.9872	0.7808	0.8846	0.6995	
ELTWIN16-1	647.6		734.6		13.4
	0.6783	0.7110	0.7694	0.8065	
ELTWIN16-2	594.3		544.8		-8.3
	0.7781	0.9223	0.7133	0.8454	
ELTWEX16-4	1004.2		927.8		-7.6
	0.8814	0.8326	0.8144	0.7692	
ELTWEX16-5	748.4		690.1		-7.8
	0.7642	0.9225	0.7047	0.8506	

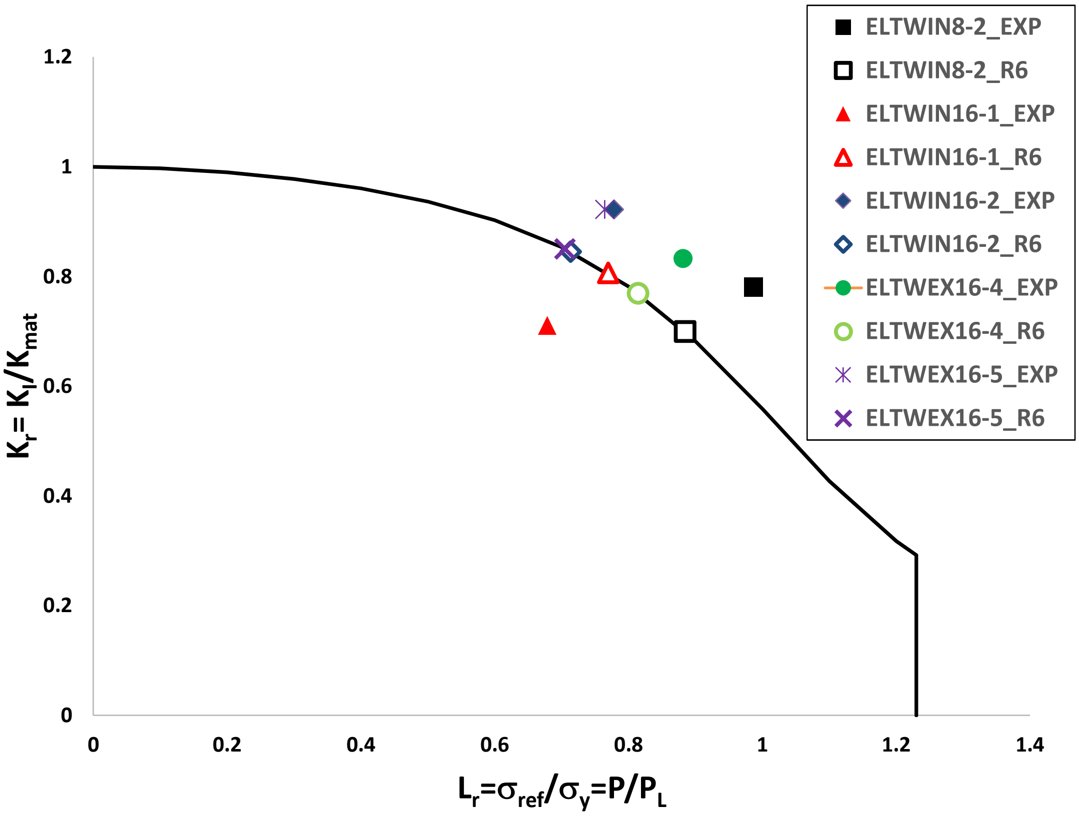

Fig. 3.2. Circumferentially through-wall cracked elbows. Predicted and experimental initiation load points on FAD.

3.4 Relative Variability of R6 Predictions

The predicted crack initiation loads are showing deviations from experimental values upto approximately ±14%. For comparing the different predictions of crack initiation loads $P_{0.2}^{R6}$, it is normalized with respect to corresponding experimental valueP_{exp}^{R6} , because the load is highly dependent on the pipe size. Hence, the deviation from experimental value is quantified in terms of normalized crack initiation load values $p = P_{0.2}^{R6}/P_{0.2}^{exp}$. These values of p are calculated using tabulated values of $P_{0.2}^{R6}$ and $P_{0.2}^{exp}$for pipes and elbows from Table 3.3 and Table 3.4

respectively. For both the sizes of the pipes/the elbows, these normalized crack initiation loads p are comparable statistically, instead of load values $P_{0.2}^{R6}$.

For assessment of the overall variability of the predictions p_i, relative variability or Coefficient of Variation (CV) parameter corresponding to normal distribution, are predicted for both the pipes and the elbows. In the steps of this calculation, different parameters, namely mean value $\bar{p}$, standard deviation, s, and coefficient of variation (CV) are calculated separately for the pipes and the elbows. The lower/higher value of CV represents the more repeatability/variability in the sample data set. The mathematical formula for calculation of these parameters are shown below:

mean value of data points p_i,

$$\bar{p} = \sum_{i=1}^{N} p_i \tag{3.16}$$

standard deviation,

$$s = \sqrt{\frac{\sum_{i=1}^{N}(p_i - \bar{p})^2}{N-1}} \tag{3.17}$$

relative variability or coefficient of variation,

$$CV = \frac{s}{\bar{p}} \times 100 \tag{3.18}$$

where N is the total number of data points. For the present calculation, values of N for the pipes and the elbows are 6 and 5 respectively.

The mean value $\bar{p}$, standard deviation s and coefficient of variation (CV) are calculated using the Eqns. (3.16), (3.17) and (3.18) respectively, for the normalized load values p. These calculated values are shown in Table 3.5 for the pipes and the elbows, separately. Relative variability parameter CVs are 6.3% and 10.3% for the pipes and elbows respectively. Thus, predictability of crack initiation loads by R6 is reasonably acceptable for these pipes and elbows because of these lower values of CVs which represents the good repeatability in predictions of crack initiation loads for all the pipes. It can also be observed that the R6 predictions are better for pipes than the elbows because of lower relative variability 6.3%.

Table 3.5. Relative variability of the R6 predictions

Normal distribution parameters	Pipes						Elbows				
	SPBMTWC8-1	SPBMTWC8-2	SPBMTWC8-3	SPBMTWC16-1	SPBMTWC16-2	SPBMTWC16-3	ELTWIN8-2	ELTWIN16-1	ELTWIN16-2	ELTWEX16-4	ELTWEX16-5
Normalized loads, $p = P_{0.2}^{R6}/P_{0.2}^{exp}$	0.93	0.91	0.85	1.02	0.99	1.00	0.89	1.13	0.92	0.92	0.92
Mean value $\bar{p}$	0.95						0.96				
Standard deviation s	0.06						0.10				
Coefficient of variation (%) (CV)	6.3%						10.3%				

3.5 Closure

Assessments of the loads for ductile crack initiation in 11 large-scale piping tests, consisting of 6 straight pipes and 5 elbows has been calculated using R6. It has been shown that the use of modern solutions for stress intensity factor and limit load, recently presented in the literature, in conjunction with standard failure assessment diagram R6, leads to generally accurate assessments of the loads for ductile crack initiation, with a tendency for some small conservatism i.e. predicted initiation loads are lower than the experimental values. The predicted values are showing greater variations from experimental values in case of elbows than straight pipes. Considering the reasonably good efficacy of R6 at crack initiation points, in next chapter this methodology will be extended beyond crack initiation point to crack growth regime for calculation of fracture toughness J_{mat}.

Chapter 4

Load Based Approach for Calculation of J-R Curve Using R6

4.1 Introduction

Fracture experimental results have to be post processed to determine J-R curve i.e. J-Resistance vs. crack extension data. Conventional approach of evaluation of J-integral requires certain geometry parameters (η and γ functions) proposed by Rice et.al. [46] and Ernst et.al. [47]. For simpler geometry and loading configurations, these parameters are widely available in open literature. However, for complex geometries and/or with complex loading configurations, these parameters are not available; thus calculation of J-R curve from fracture test results is difficult using conventional approach. In this study, one simpler approach is proposed for calculation of J-R curve using R6 failure assessment diagram. R6 failure assessment method is based on two criterion approaches where brittle fracture and plastic collapse are combined and a failure assessment line is proposed which also covers in between, ductile initiation in elastic plastic deformation regime [15]. Here utility of the R6 method is extended beyond crack initiation point to consider crack growth for determination of J-R curve. This approach is used for determination of J-R curve for total six pipes of 8 inch and 16 inch nominal diameters. These curves are compared with the conventionally calculated J-R curves. Further, it can be observed that the slope of J-R curves for 8 inch pipes are higher than 16 inch pipes. This difference is investigated in the light of prevalent crack tip constraints which are computed in terms of stress triaxiality parameters, Q.

4.2 R6 Methodology for Determination of J-R curve

Eqn. (3.15) is relation between crack initiation toughness and applied loading using failure assessment line. That equation is used for determination of crack initiation load $P_{0.2}^{R6}$ using initiation fracture toughness, J_i^{TPB} which was estimated using TPB specimens for both piping materials as shown in Table 2.1 by Tarafder et.al. [26]. It is already discussed in previous chapter that the predicted crack initiation loads $P_{0.2}^{R6}$ are in reasonably good agreement with experimental value $P_{0.2}^{exp}$. This observation ensures that the failure assessment diagram is efficient in predicting the crack initiation load using R6 method. It can be also said that the applied crack driving force J-integral is also almost equal to material crack initiation toughness J_i^{TPB} at crack initiation point. Further, this approach is used in reverse way using experimental load P vs. crack extension data Δa for getting J-R curve. This approach is extended beyond crack initiation point to further crack growth points of experimental fracture results. In this approach, using experimental load value corresponding to any arbitrary crack extension $P(\Delta a)$, crack driving force J-integral is calculated. It should be noted that these are corresponding to the actual experimental data. Hence, the calculated crack driving force J −integral is basically value of material fracture toughness J_{mat} for that crack growth value Δa.

$$J_{mat}(\Delta a) = J_e(a_0 + \Delta a)[f(L_r)]^{-2} \tag{4.1}$$

Using Eqn. (4.1) fracture toughness, J_{mat} can be calculated for applied normalised loading L_r using FAD assessment line. This methodology is explained graphically in Fig. 4.1. A typical experimentally obtained load vs. crack extension curve is shown in Fig. 4.1(a).At loading point 1, the total crack size a_1, used for calculation will be $a_1 = a_0 + \Delta a_1$, where $a_0$is initial crack size and Δa_1 is the instantaneous crack extension. For this loading point, values of $K_I(P_1, a_1)$

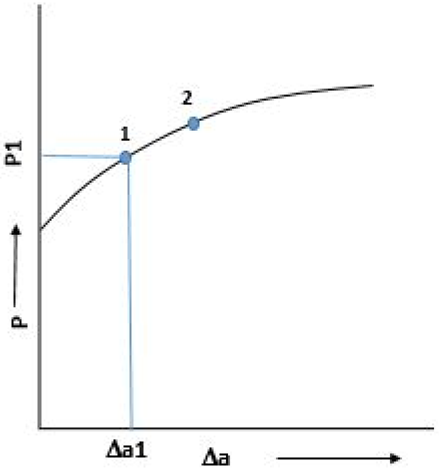

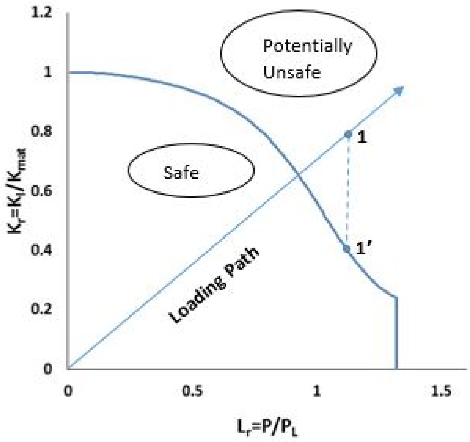

(a) (b)

Fig. 4.1. (a) Typical load vs. crack extension curve. (b) Schematic Illustration of the FAD methodology for J-R curve for experimental load point 1.

and $P_L(a_1, \sigma_{ys})$ are calculated using closed form expressions available in the literature. Suppose we choose that assessment point corresponding to load point,1 beyond failure line (ductile crack initiation). Now, for getting J_{mat}, for loading 1, the assessment point is moved vertically on FAD assessment line, $f(L_r)$which is shown as point 1' as shown in Fig. 4.1(b). Finally value of J_{mat} is obtained using Eqn. (4.1) for crack extension of Δa_1. For further points (for example point 2 in Fig. 4.1 (a)) same calculation is repeated for getting J_{mat} corresponding to load P_2 and crack extension Δa_2. These calculations for all data points of load vs. crack extension curve will give the entire fracture toughness property, J-R curve.

4.3 Relevant Experimental Results and Closed Form Expressions

Tensile and fracture material properties obtained for the piping material carbon steel SA333Gr6 is already reported in Table 2.1 (Section 2.2.1). Relevant geometry and loading configurations are also discussed in Section 2.2.2 for cracked pipes tested under four point bending moment and tabulated in Table 2. 2.

Closed form expression of stress intensity factor, K_I and limit load P_L, is as discussed in previous Sections 3.2.1 and 3.2.2 respectively for the pipes, are used here for calculation of material fracture parameters, J-R curves.

4.4 Steps for Determination of J-R Curve Using R6

a) Updating the crack size, a: Corresponding to first value of crack extension Δa, load $= P$ is obtained from the experimental P-Δa curve. For this point, the crack size a is updated using the present crack extension Δa and adding with initial crack size a_0 i.e. $a = a_0 + \Delta a$.

b) Calculation of 'L_r': Using the Eqns. (3.5), (3.6) and (3.7) limit load P_L corresponding to the material yield stress σ_y is calculated. Now using Eqn.(2.11) reference stress σ_{ref} or nominal loading L_r is calculated using the applied load P. Thus the second term $f(L_r)$ of the Eqn. (4.1) is obtained by evaluating the normalized reference stress $L_r = \sigma_{ref}/\sigma_y$.

c) Calculation of 'J_e': Bending stress, σ_b is calculated by using Eqn. (3.2) corresponding to the experimentally applied load P. First applied moment M is evaluated using the loading configurations as $M = P(OS - IS)/4$ as shown in Fig. 2.2(a) and corresponding to this moment, bending stress σ_b is obtained. Corresponding to the instantaneous crack size a, the geometry factor F_b is calculated using Eqn.(3.3). Using these parameters, stress intensity factor K_I is obtained which is converted to $\mathrm{J_e}$ as $\mathrm{J_e} = \mathrm{K_I^2}/E'$. This is the first term of the Eqn.(2.11).

Using these J_e and L_r values, J_{mat} is calculated using the relation $J_{mat} = J_e[f(L_r)]^{-2}$. Steps (a), (b) and (c) are repeated for further Load vs. crack extension data points to obtain whole J-

R curve for a pipe.

This calculation procedure is shown as a flowchart as shown in Fig. 4. 2. This procedure is

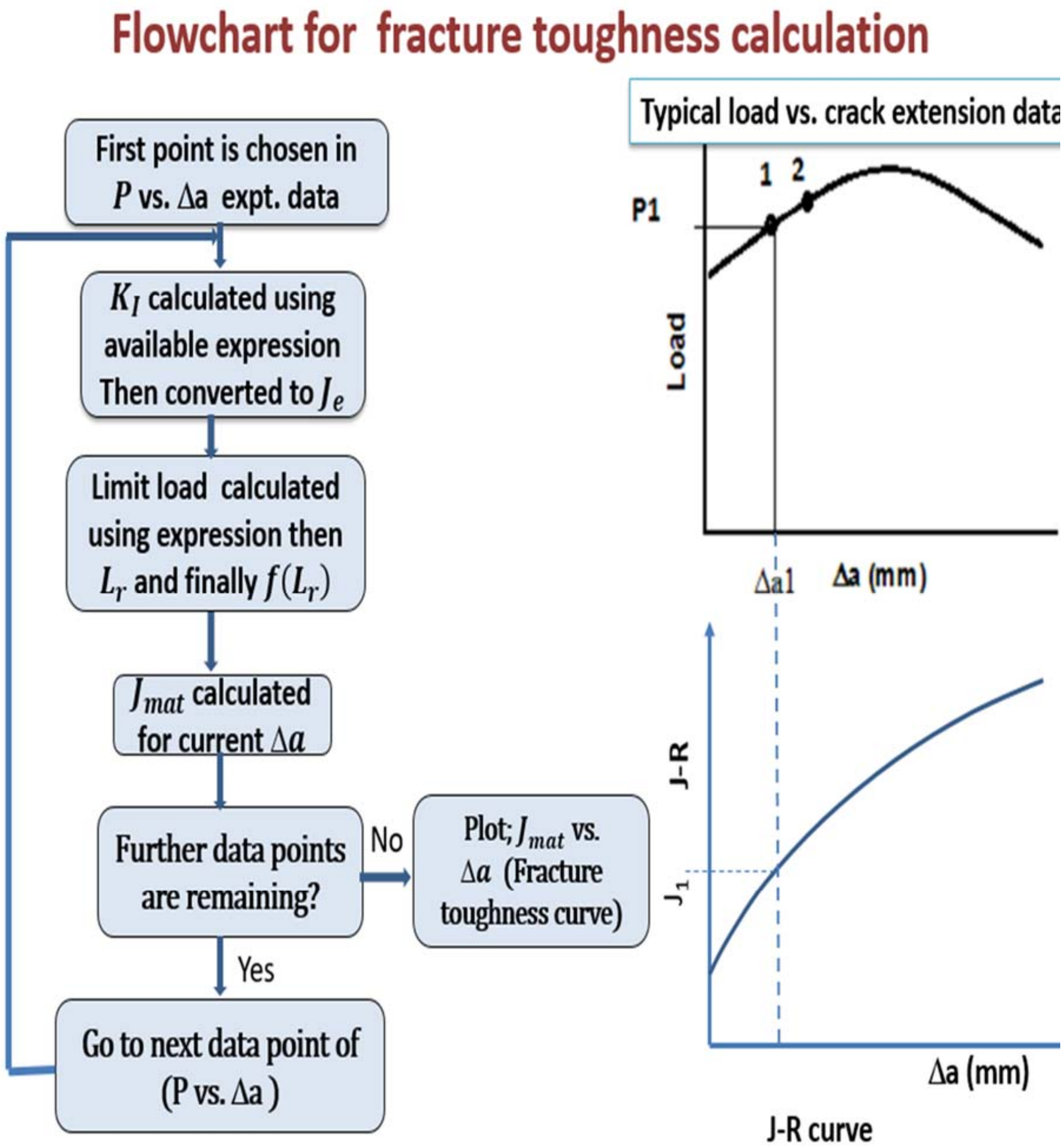

Fig. 4. 2 Flowchart showing the load based R6 approach for prediction of J-R curve by using experimental load vs. crack extension data

used to convert load vs. crack extension data to J_{mat} vs. crack extension data i.e. material fracture property J-R curve.

4.5 J-R Curve Results

Using experimental load vs. crack extension data, J-R curves for all pipes are calculated using R6 method and shown for all pipes from Fig. 4.3 to Fig. 4.8. It should be noted that these plots also depict conventional J-R curves calculated using relevant η and γ parameters and reported by Chattopadhyay et.al. [19]. It can be observed that for SPBMTWC8-1, R6 J-R curve is showing good agreement with conventionally computed that one as shown in Fig. 4.3. However, For SPBMTWC8-2 and SPBMTWC8-3 pipes, R6 methodology are over predicting the J-R curves than conventional approach especially for higher loadings as depicted in Fig. 4.4 and Fig. 4.5. For 16 inch pipe SPBMTWC16-1, the R-6 estimated J-R curve is significantly lower than that one calculated using conventional approach as shown in Fig. Fig. 4.6. For remaining two 16 inch pipes SPBMTWC16-2 and SPBMTWC16-3, the J-R curves calculated by both approaches are reasonably in good agreements as shown in Fig. 4.7 and Fig. 4.8. However, more extensive investigations are needed in future to establish this methodology for calculation of $J-R$ curve.

All the J-R curves are shown simultaneously in Fig. 4.9 and can be observed that J-R curves are segregated based on the sizes of the pipes. In other words, for all 8 inch pipes J-R curves are higher than all 16 inch pipes. This variation may be due to the higher thickness at crack front for 16 inch pipes than 8 inch pipes. Higher thickness may be causing more crack tip constraint and it may be causing lower fracture toughness for 16 inch pipes. To investigate this issue the crack tip constraint is computed further, in terms of stress triaxiality parameter, Q.

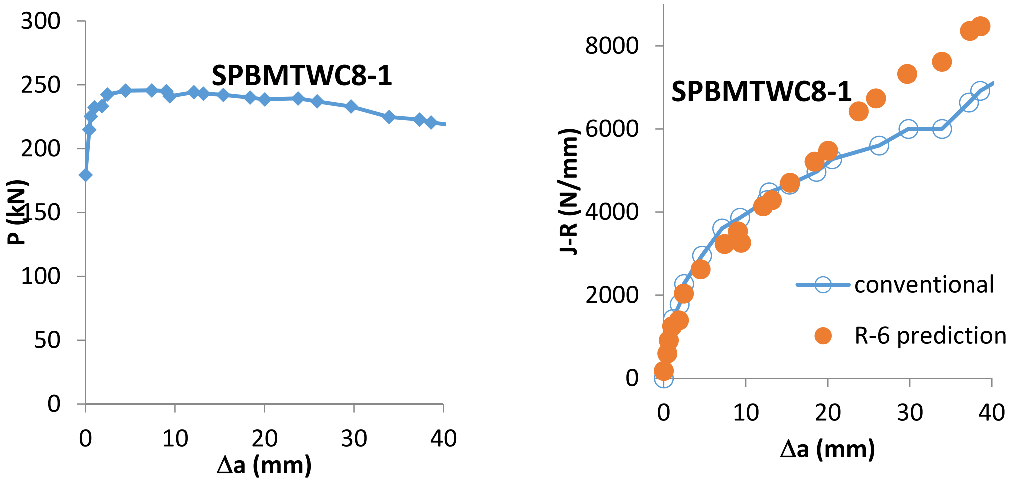

(a)Experimental load vs. crack extension plot

(b)R6 prediction is compared with conventional

Fig. 4.3. Results of pipe SPBMTWC8-1

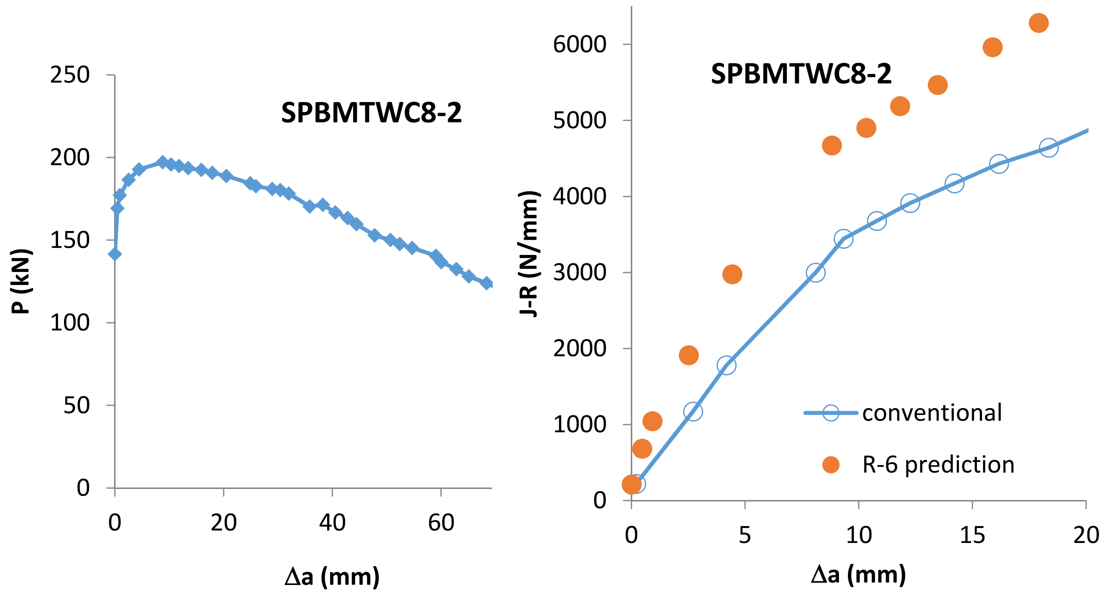

(a) Experimental load vs. crack extension plot

(b) R6 prediction is compared with conventional

Fig. 4.4. Results of pipe SPBMTWC8-2

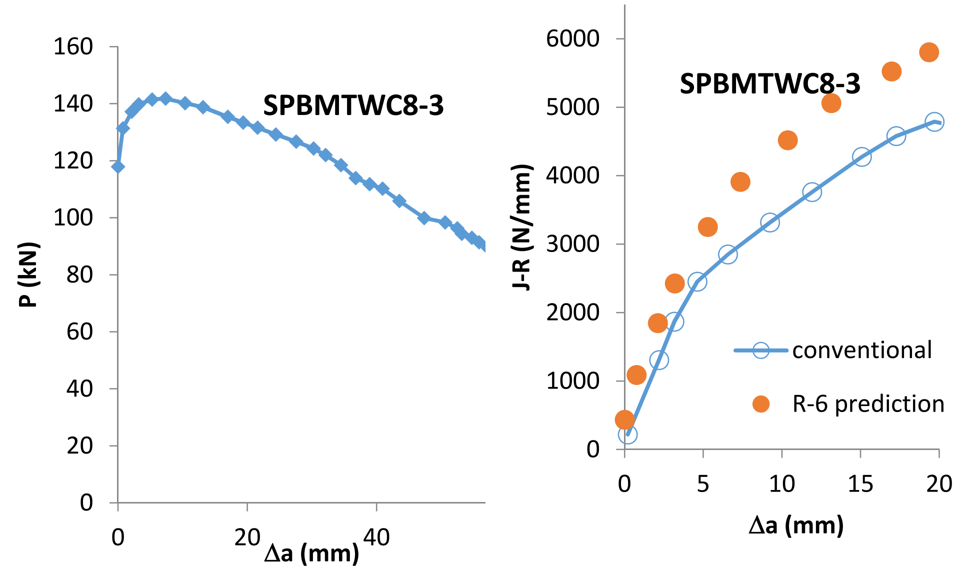

(a) Experimental load vs. crack extension plot

(b) R6 prediction is compared with conventional

Fig. 4.5. Results of pipe SPBMTWC8-3

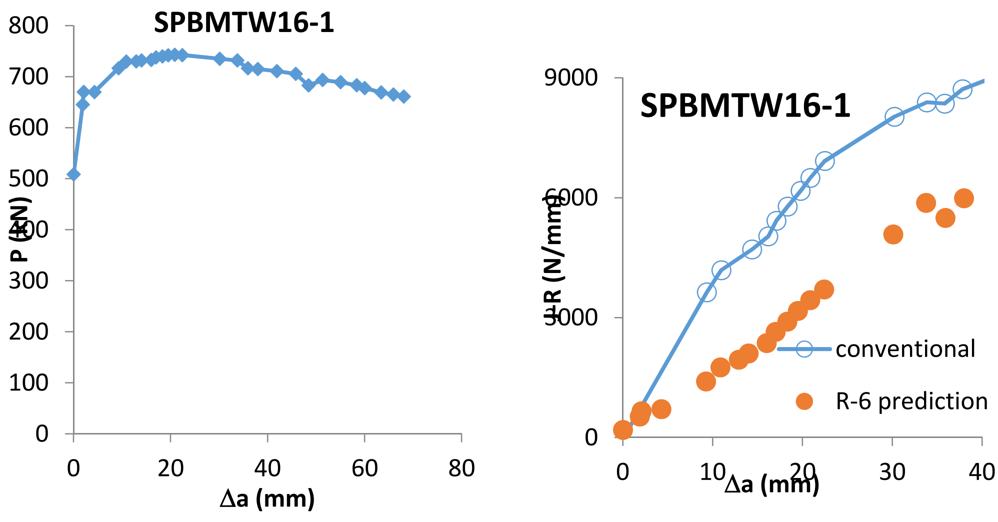

(a)Experimental load vs. crack extension plot

(b) R6 prediction is compared with conventional

Fig. 4.6. Results of pipe SPBMTWC16-1

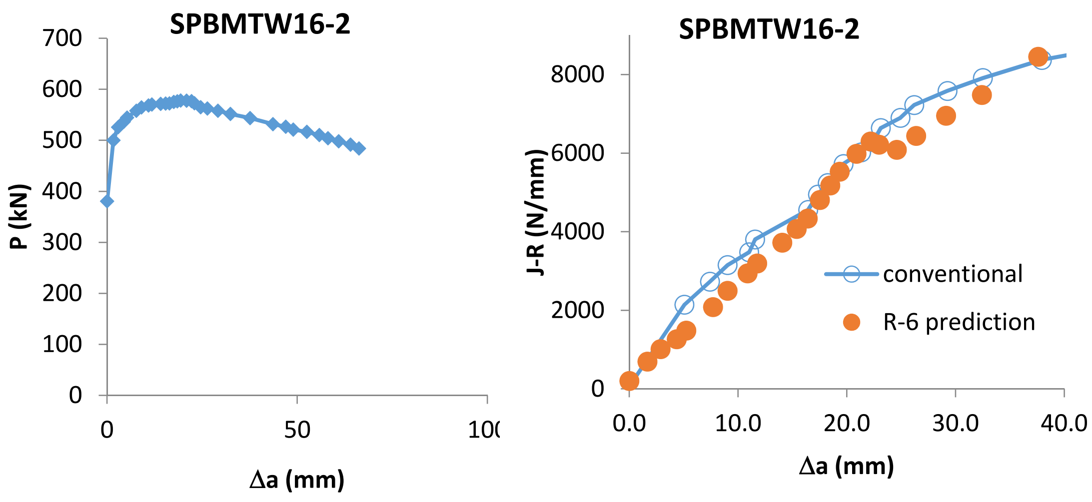

(a) Experimental load vs. crack extension plot

(b) R6 prediction is compared with conventional

Fig. 4.7. Results of pipe SPBMTWC16-2

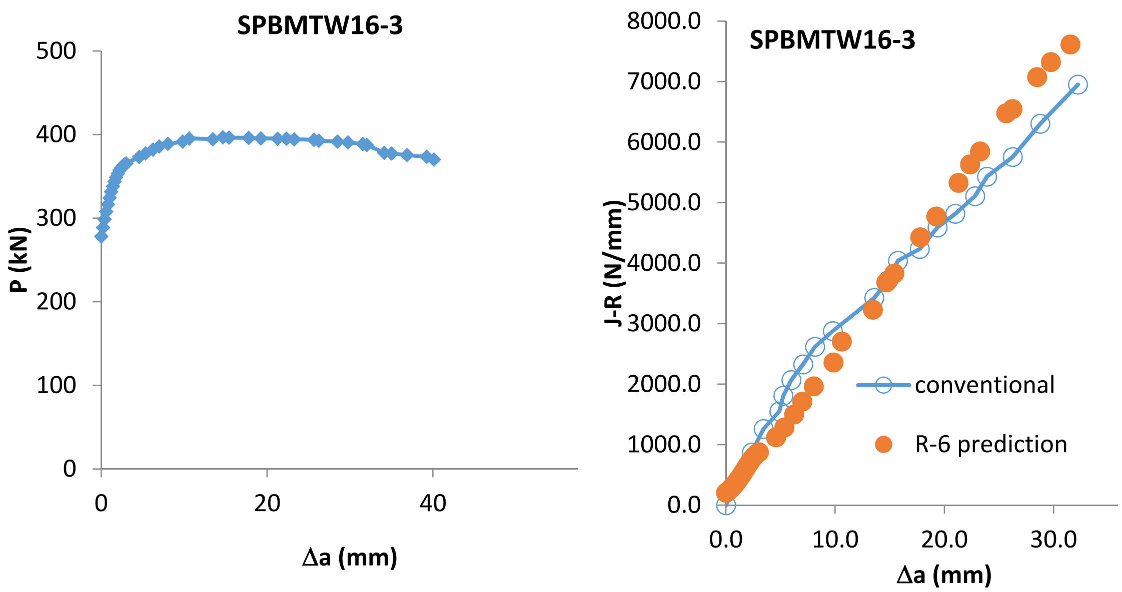

(a)Experimental load vs. crack extension plot

(b) R6 prediction is compared with conventional

Fig. 4.8. Results of pipe SPBMTWC16-3

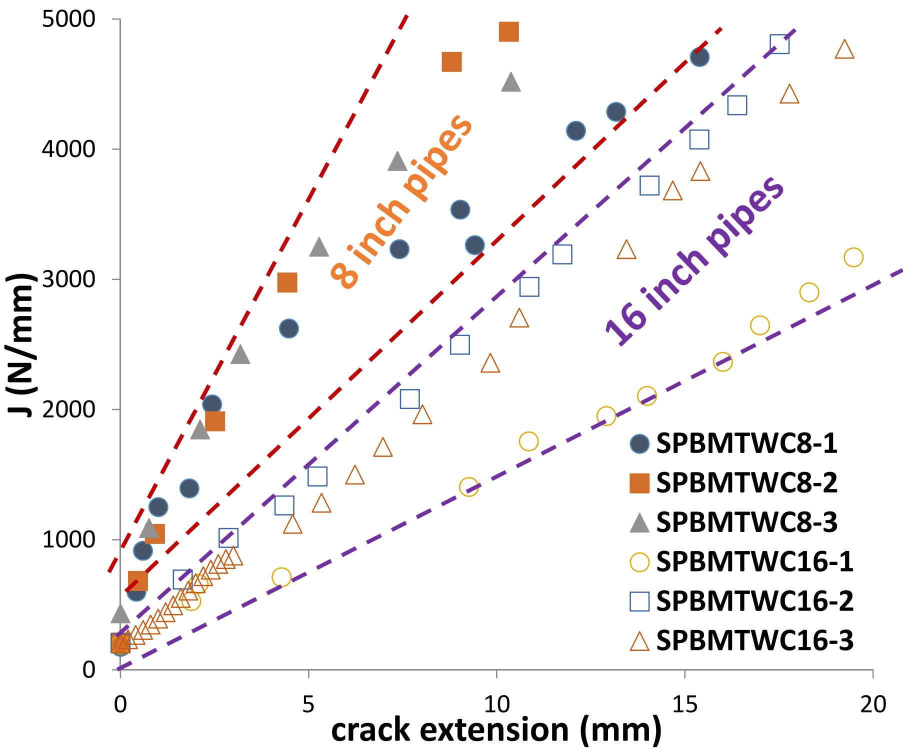

Fig. 4.9 J-R curves are segregated based on the size of the pipes

4.6 Stress Triaxiality Results

O'Dowd and Shih [7] introduced the non-dimensional parameter, 'Q', to quantify the crack tip constraint. By this theory, the laboratory specimen must match the constraint of the component for transferability of fracture toughness property. Stress triaxiality parameter Q is defined as,

$$Q = \frac{\left[\sigma_{\theta\theta} - (\sigma_{\theta\theta})_{ref}\right]}{\sigma_{ys}} \qquad at\ \theta = 0 - 90^{o}, \qquad r = \frac{2J}{\sigma_y} \tag{4.2}$$

where, r and θ are polar co-ordinates with origin situated at the crack tip. $\sigma_{\theta\theta}$ is existing stress field ahead of the crack tip of the actual specimen or component as shown in Fig. 2.5, $(\sigma_{\theta\theta})_{ref}$ is reference solution obtained from standard plane strain small scale yielding (SSY) solution $(\sigma_{\theta\theta})_{SSY}$ as explained by O'Dowd and Shih [40]. In this work, all the calculations about Q, are performed at remaining ligament i.e. $\theta = 0$.

4.6.1 Three Dimensional Finite Element Analysis of pipes

Three dimensional finite element analyses (FEA) are carried out for all six pipes. The details of used piping material properties true stress vs. true strain are already explained by Chattopadhyay et.al [19] and reproduced here as Fig. 2.1 have been used here in FEA of pipes. Other relevant material properties like modulus of elasticity, E, and Poisson's ratio, ν are provided in Table 2.1.The detailed methodology of meshing crack tip using spider web mesh technique is shown in Fig. 4.10.

4.6.2 Variations of Stress Triaxiality Parameters

The stress triaxiality parameter, Q, is dependent on applied loading and consequent crack driving force, J. Hence one specific loading point has to be chosen for comparing crack tip constraint. It is established that at crack initiation point the applied crack driving force J-integral $= J_i^{TPB}$, where J_i^{TPB} is crack initiation toughness obtained here by fracture testing of TPB specimen for respective pipes, which is established as a material property.

4.6.2.1 8 inch and 16 inch Pipes

For these piping materials, the reported value of J_i^{TPB} are 220N/mm and 236N/mm for 8 inch and 16 inch piping material as shown in Table 2.1. Hence for all cases, the loading point chosen for computation of Q is corresponding to J-integral $=J_i^{TPB}$ of related piping material. Crack opening stress and thus, stress triaxiality is the highest at the centre of the crack front for all pipes Hence, for getting conservative estimate, the stress triaxiality has been computed at the centre of crack front. The crack opening stress is obtained at distance of cJ/σ_y (where c = 1, 2, 3, 4, 5) ahead of crack tip at $\theta = 0$. The variations of stress triaxialities in the remaining ligament are depicted in Fig. 4.11 for all six pipes. Based on these findings it can be stated that the crack tip constraints are higher for 16 inch pipes than 8 inch pipes, which explains the lower

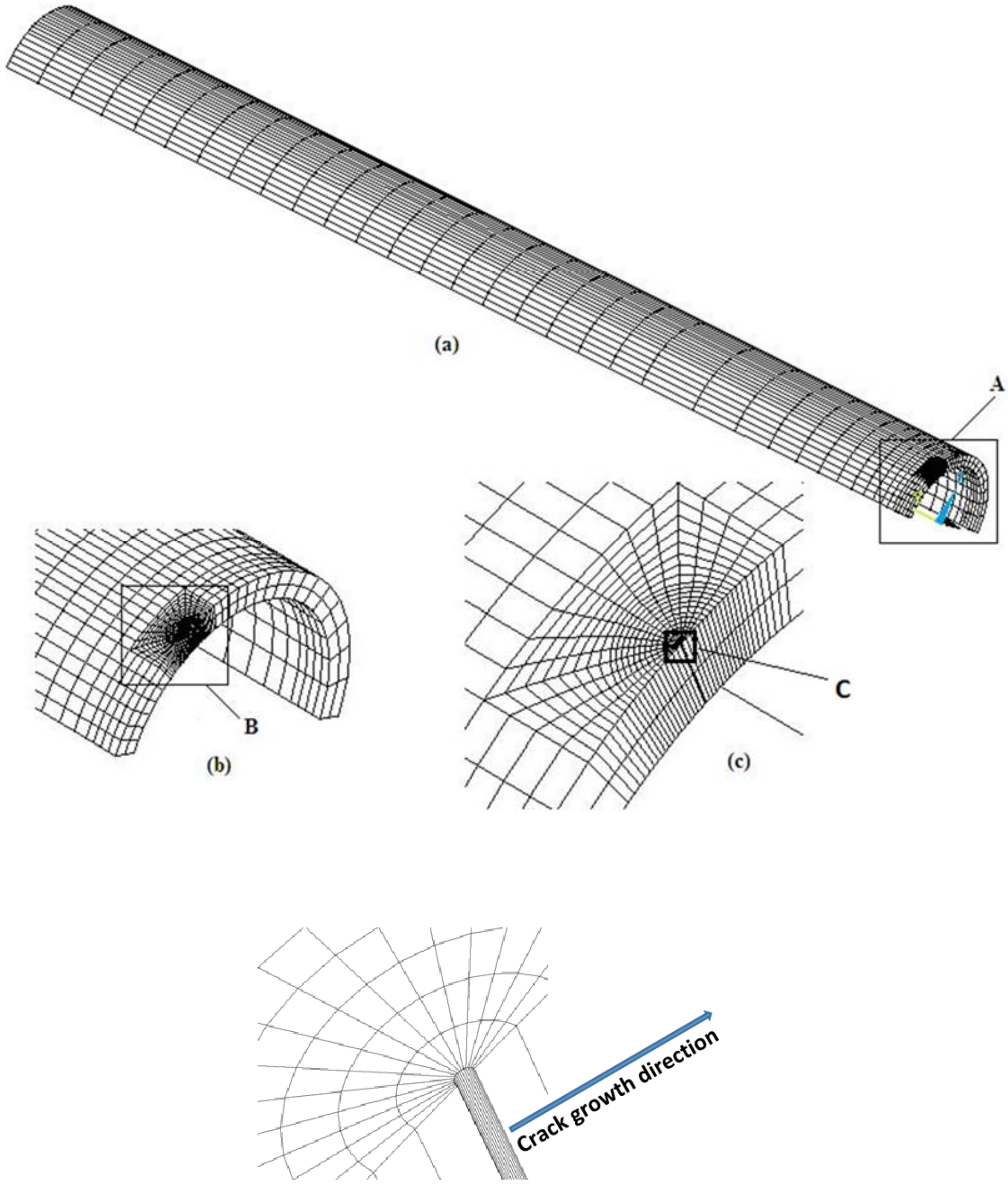

(d)

Fig. 4.10: (a) Typical finite element mesh used for straight pipes having throughwall crack, (b) Detailed mesh in region A, (c) Detailed mesh in region B, (d) detailed mesh in region C with a notch having notch tip radius of 0.1mm.

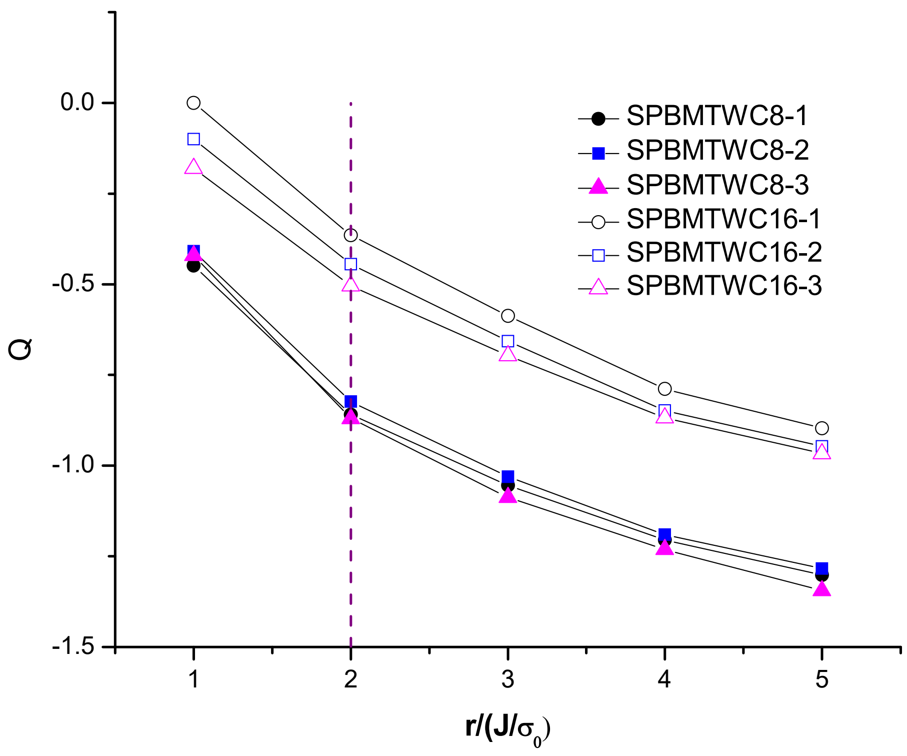

Fig. 4.11 Variations of stress triaxiality parameters, Q, on remaining ligament

J-R curve for 16 inch pipes in comparison to 8 inch pipes (Fig. 4.9). It is also observed that crack tip constraints are significantly dependent on the size of pipes instead the crack sizes.

4.6.2.2 8 inch Pipes and TPB specimen

Larrosa and Ainsworth [44] have calculated the stress triaxiality parameters Q using FEA for standard fracture specimen CT, and non-standard fracture specimens, SENT and notched CTs. These parameters are also calculated for surface cracked pipes under two separate loadings, global bending and internal pressure. It was found the crack tip constraint level is similar for surface cracked pipe and non-standard fracture specimen SENT. Hence, usage of SENT specimen instead of standard CT specimen is recommended for fracture assessment of surface cracked pipe to avoid excessive conservatism in fracture assessment. Sahu et.al. [123] had already reported for variation of Q in remaining ligament for the fracture specimen TPB8

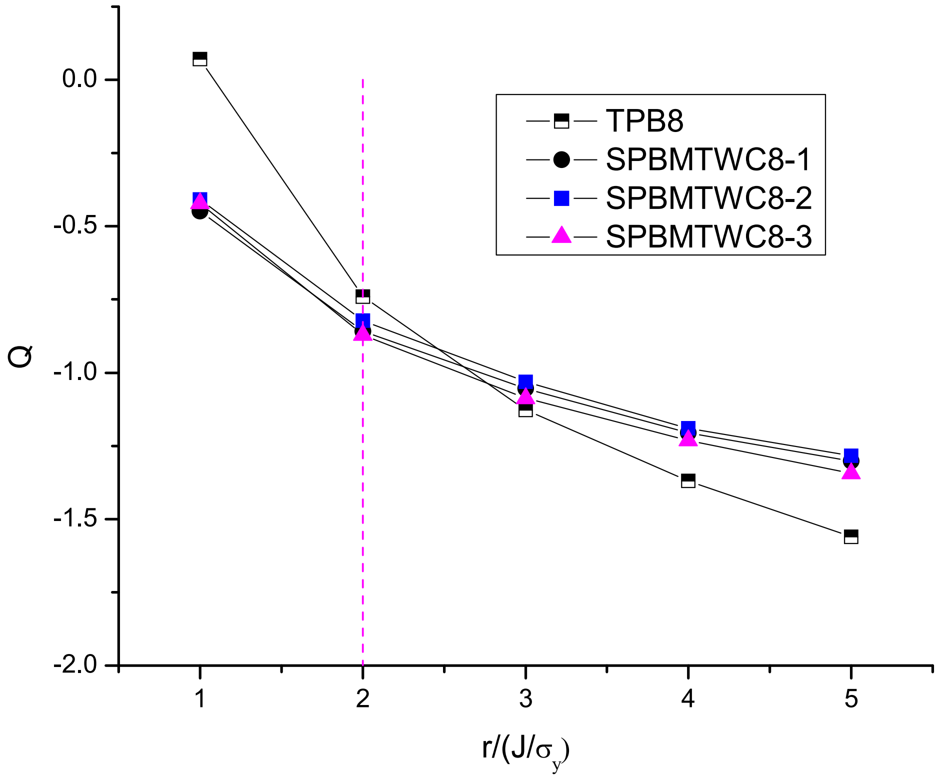

Fig. 4.12 Variations of Qs for the 8 inch pipes and TPB8 specimen

corresponding to crack driving force $J \approx J_i^{TPB} = 220$N/mm. Here, that result is comparatively plotted with the 'Q's of the 8 inch pipes in Fig. 4.12. It can be observed that the crack tip constraint level is almost same at characteristic distance $r = 2\frac{J}{\sigma_0}$ from crack tip for the TPB8 specimen as well for all the 8 inch pipes. Hence, usage of J_i^{TPB} as crack initiation material fracture toughness J_{ic} is justified, and will not cause any over conservatism in fracture assessment.

4.7 Closure

A simpler R6 based approach is proposed for evaluation of J-R curve from experimental load vs. crack growth data. It is utilized to calculate J-R curves of total six pipes of 8 inch and 16 inch diameter pipes with throughwall circumferential cracks under four point bending load. The J-R curves thus calculated are showing good agreement for three out of total six cases. Thus, further extensive study is essential to get confidence in this methodology. It is also found that J-R curves for 16 inch pipes are lower than those of 8 inch pipes. This difference has been attributed to prevalent higher crack tip constraints for 16 inch pipes than 8 inch pipes. It is expected that the methodology suggested in this work will greatly simplify the calculation of constraint dependent J-R curve from experimental data. The limitation of this methodology is that it is based on single point experimental data unlike conventional approach, where entire history of load vs. displacement results is integrated. Thus, in the presently proposed method, error at arbitrary experimental data point will lead to significantly erroneous fracture toughness data at that particular point. Based on extensive literature survey, it is already established that for quantifying the fracture response, applied displacement instead of applied load is a better parameter for highly plastically deformed cases. In the investigated pipes, the loading level is significantly going beyond limit load and undergoing significant plastic deformation. Hence, the adopted load based approach may be responsible for the deviations between conventional and predicted J-R curves. In the next chapter, displacement based approach will be attempted for calculation of J-R curves.

Chapter 5

Displacement Based Approach for Calculation of J-R Curve Using R6

5.1 Introduction

Load based R6 approach was used for calculations of J-R curves for pipes in previous chapter. The calculated results were showing good agreement for some cases while for few cases there were significant deviations suggesting scope for further improvement. Jaydevan et. al. [103] and Otsby et. al. [104] had shown that applied strain is a better parameter than applied load/stress for defining the fracture response, J-integral in plastically deformed pipes. Budden [23] have also studied the limitations of load based R6 failure assessment and proposed a displacement/strain based approach for calculation of J-integral using R6. The studied pipes in this work are loaded significantly higher than the limit load and subjected to considerable plastic deformation near crack tip. Considering the limitations of application of stress based R6 method, a better approach is proposed in this chapter where applied displacement is used for calculating reference strain and stress, which are eventually used for calculation of fracture property. In this procedure mathematical expressions of stress intensity factor, K_I and limit load, P_L are required which are available in literature for wider range of geometries. Material stress-strain data is an additional input in this procedure for calculation of reference stress from evaluated reference strain. J-R curves calculated by the displacement based R6 approach are compared with the results already obtained by conventional and load based R6 approaches.

5.2 Limitation of Load Based Failure Assessment

Jayadevan et al. [103] and Otsby et al. [104] showed the benefit of using the total strain in formulating the fracture response under large plastic strains over the traditional stress based approaches.

It should be noted that the failure assessment point, (L_r, K_r), in R6 FAD is a linear function of applied load/moment as per Eqns. (2.7) and (2.11). Thus, in the R6 load based approach, no additional crack driving force or energy will be estimated for increased strain if the applied load is almost asymptotic for an arbitrary cracked component. However, it is evident that the component is absorbing energy because applied strain is continuously increasing, which should be reflected in terms of higher crack driving force, $J -$ integral. This higher J, should reflect in terms of higher failure amount in the assessment of the component. Hence, the greater applied strain should reflect in terms of higher failure amount which is not possible in the load based R6 approach. It is evident that present approach of calculation of reference stress from applied load is no longer applicable when the structure is subjected to large plastic deformation under displacement controlled loading. Hence, for strain controlled failure cases, a strain based method is proposed to calculate fracture property using R6 FAD.

5.3 Displacement Based R6 Approach

For pipes, $J - R$ curves using load–based R6 methodology and conventional approach have been already compared by Sahu et.al [124] where it is observed that the load based R6, $J - R$ curves, are showing good agreement with conventional values for some cases, while for few cases the predicted values are significantly higher/ non-conservative with respect to conventional $J - R$ values. Here, that load-based R6 approach is modified for better prediction of $J - R$ curve.

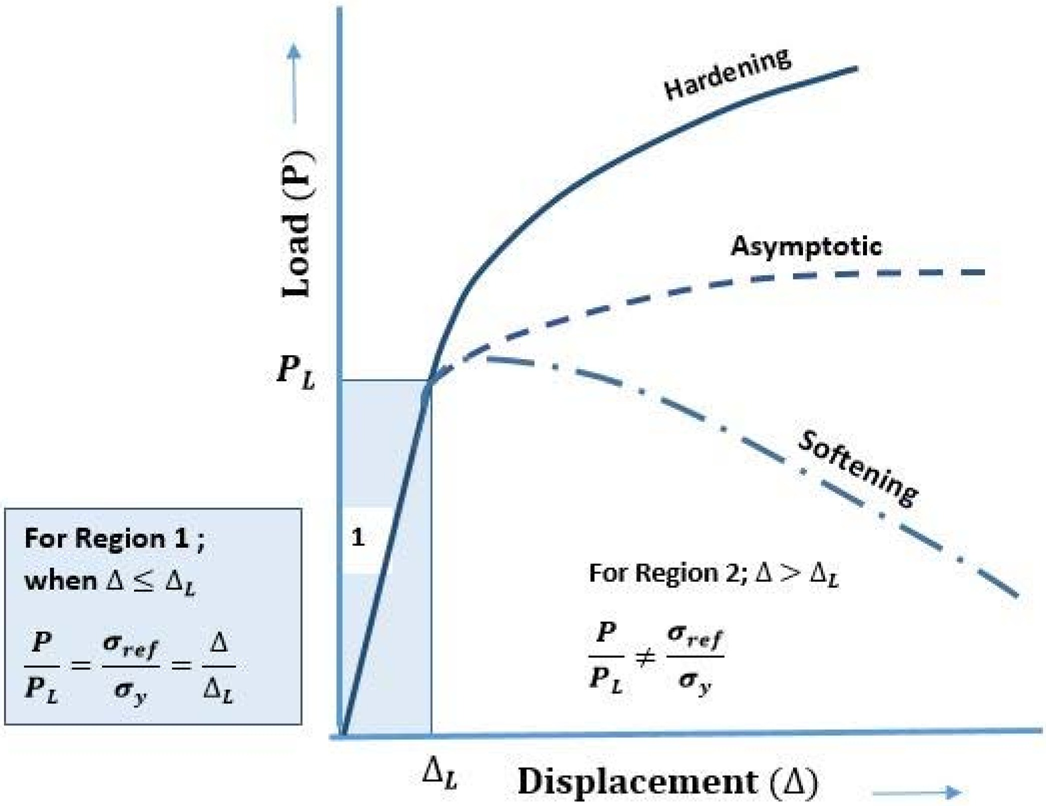

Fig. 5.1. Schematic diagram of typical behaviour of load vs. applied displacement curves under displacement controlled loadings.

It should be noted that reference stress based R6 methodology is used for calculation of fracture toughness where reference stress, σ_{ref} is directly calculated using the applied load, P using Eqn. (2.11). This approach will work with reasonable accuracy when applied displacement, Δ is lower or equal to limit displacement (displacement corresponding to limit load), $\Delta_L(P_L)$ i.e. $\Delta \leq \Delta_L$. Basically in this region when $P \leq P_L$, deformation is linear; so the relation $L_r = P/P_L = \Delta/\Delta_L$ will be valid. But it may not necessarily work beyond limit point because the load vs. displacement curve may show hardening, asymptotic or softening behaviour based on the loaded geometry, loading configurations and strain hardening property of the material as shown in Fig. 5.1. The pipes under investigation are tested by displacement controlled loading and applied displacement is going significantly higher than limit displacement, D_L. To address such issue, Budden and Ainsworth [118, 23] proposed the strain-based failure assessment methodology to investigate the component under large plastic deformation. The difference in load and displacement based approaches for failure assessment, becomes more and more significant when the loading goes beyond limit displacement i.e. enters Large Scale Yielding (LSY) regime, $\Delta \gg \Delta_L$. It should be noted that all the chosen pipes are loaded significantly beyond the limit point resulting in to large scale nonlinear deformation near crack tip. Hence, the displacement based approach is more appropriate for calculation of failure/fracture property instead of conventional load based approach.

5.3.1 Simplification of Cracked Pipes for Beam Theory

Limited articles are available in open literature where strain based R6 has been investigated and usage of R6 for estimation of J-integral is again very rare. No literature is available for deeply cracked pipes to adopt directly for calculation of J-R curves using R6. Budden [118] proposed the strain-based J estimation scheme using R6 for very shallow cracked plate under uniaxial applied displacement. In the proposed approach, the reference stress is calculated using the applied strain instead of applied load. This method is used for calculating the applied crack driving force, J, by Budden while in this work that method is applied for calculating the material $J-$ Resistance , J_{mat}.

Here, that approach is extended for deeply cracked pipes tested under displacement controlled four point bending. The chosen case is different from the case of shallow cracked plate investigated by Budden [118] because of the two facts; one is that the chosen geometry is deeply cracked pipe unlike very shallow cracked case and second is that the present loading is four point bending instead of uniaxial tension. The reference strain is calculated after simplification of cracked pipe to a beam using simple beam theory. Simplification of pipe is explained in detail as following:

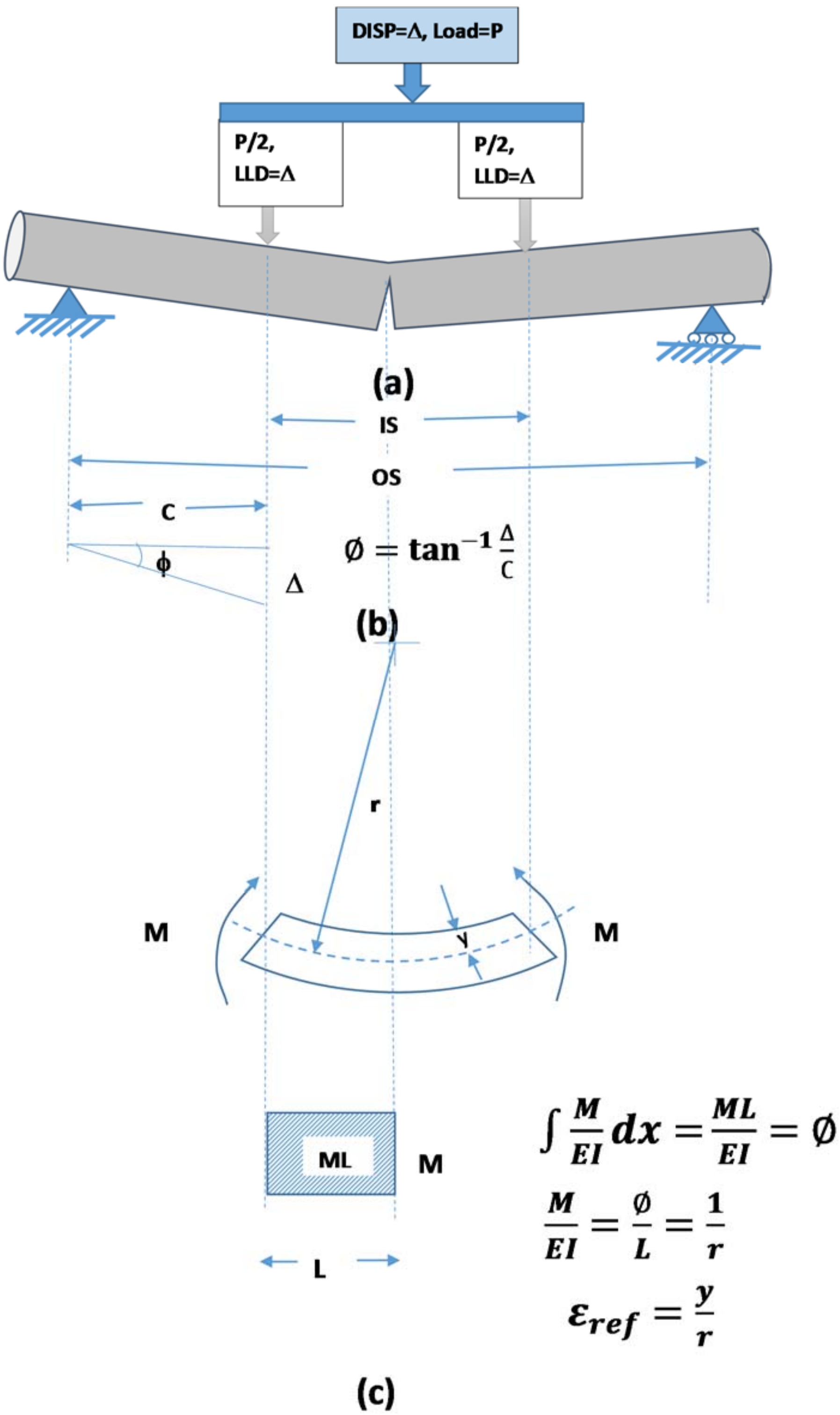

Fig. 5.2. (a) Typically deformed pipe with throughwall cracks under four point bend load (b) determination of slope using LLD, (c) determination of reference strain based on virtual beam using experimental slope ϕ obtained from cracked pipe.

The schematic diagram of pipe after deformation is shown schematically in Fig. 5.2(a), which shows that the deformation is essentially localized at the cracked section because of the deep crack in pipe. In this condition, it can be assumed that the other part of pipe is acting just as a load transferring stiff arm. With this assumption, the slope of pipe, ϕ, at loading point can be calculated (Fig. 5.2(b)) as,

$$\emptyset = \tan^{-1}\frac{\Delta}{C} \tag{5.1}$$

where Δ is the Load Line Displacement (LLD) and $C = (OS - IS)/2$.

First, slope $\emptyset$ of deformation of pipe is calculated by the assumption explained by Fig. 4(a) using applied LLD (load line displacement). Now, for using this $\emptyset$ for calculation of reference strain ε_{ref}, a virtual beam is assumed with length IS and height of $2y$ as shown in Fig. 4(c).With this assumption, the pipe block within IS is virtualized as a beam under constant bending moment, M, whose slope is changing from ϕ at loading point to zero at center as shown in Fig. 5.2 (c). Based on this condition,

$$\int \frac{M}{EI}dx = \frac{ML}{EI} = \emptyset \tag{5.2}$$

where $L = IS/2$.

Further, radius of curvature, r, can be determined using following relation,

$$\frac{M}{EI} = \frac{\emptyset}{L} = \frac{1}{r} \tag{5.3}$$

It should be noted that the radius of curvature, r, is calculated in terms of applied LLD, Δ, instead of applied load, P. Subsequently, reference strain, ε_{ref}, is calculated using following relation,

$$\varepsilon_{ref} = \frac{y}{r} = \frac{\tan^{-1}(\Delta/C)}{L}y \tag{5.4}$$

where , y, is the effective distance from the neutral axis as shown in Fig. 5.2(c), which is an unknown value for the virtualized beam till now. This y will be calculated within elastic loading regime and will be used as a constant in further plastic loading range for calculation of reference strain.

5.3.2 Determination of Fracture Property J-R Curve

Tensile stress-strain properties of 8 inch piping material shows typical Luder band just after yield point as shown in Fig. 5.3, where stress remains almost constant with increase in strain for some strain range. After Luder band stress starts increasing again with strain which represents prevalent strain hardening. For uniaxial tensile properties, the Ramberg – Osgood (RO) parameters, α and n are calculated for this strain hardening region of stress and strain [19]. However, in the R6 methodology the reference stress and strain is tensile property of the material which should also represent the crack driving force, J of the cracked component under loading. Consequently, reference stress and reference strain should strain harden smoothly in the whole range including Luder region of stress-strain property so that increase in strain should reflect in terms of smooth increase in crack driving force. Thus, the curve fitting is done from yield point (including luder region) to ultimate stress point with continuous hardening. Nourpanah and Taheri [82] have already studied three curve fitting schemes, elastic, average and post yield for material stress strain data as shown in Fig. 5.3, in the light of fracture response, J-integral for a surface cracked pipe under bending moment.

It has been observed that most accurate prediction of fracture response is predicted by the average fitting of material stress strain data in terms of reference stress and strain. The average curve fitting using RO equation as shown in Eqn.(5.5) is done from yield stress (point A) to ultimate stress point (point B) of material true stress strain data as shown in Fig. 5.3.

$$\frac{\varepsilon_{ref}}{\varepsilon_y} = \frac{\sigma_{ref}}{\sigma_y} + \alpha\left(\frac{\sigma_{ref}}{\sigma_y}\right)^n \tag{5.5}$$

This RO constants, α and n of average fitting are already reported by Chattopadhyay [28] for material of 8 inch pipes which is used in this work for further calculations. However, these constants have not been reported for 16 inch piping material. 16 inch piping

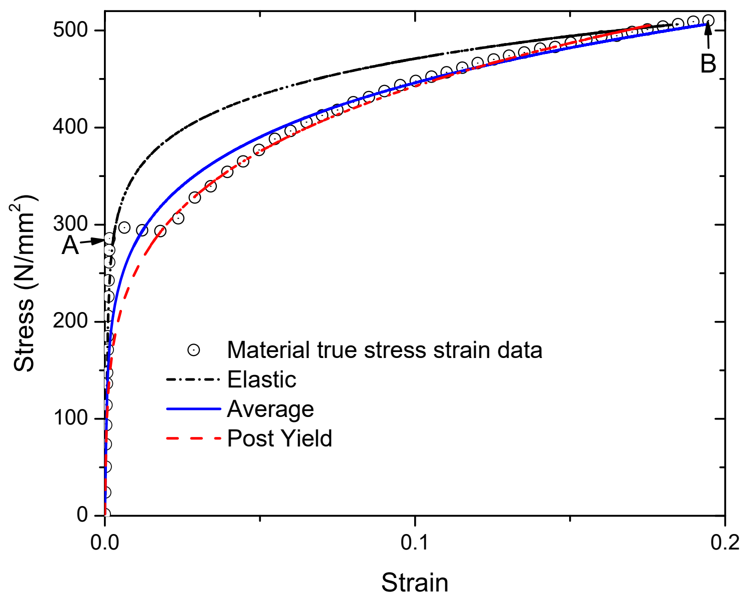

Fig. 5.3. Ramberg – Osgood fitting of 8 inch piping material stress strain data

material tensile stress–strain property is similar to 8 inch piping material with slight variations in yield and ultimate stress [19]. Ramberg-Osgood constants, α and n are calculated for 16 inch piping material and shown with 8 inch piping material in Table 5.1.

Table 5.1. Ramberg – Osgood constants

Pipe nominal diameter	α	n
8 inch	6.71	5.30
16 inch	6.27	5.27

Reference stress and strain should be linear in the elastic deformation regime as shown in Fig. 5.4 as shaded region 1. Consequently, strain hardening exponent is taken as $n = 1$ to ensure linear variation of reference stress. Putting $n = 1$ in Eqn.(5.6), reference stress can be calculated using applied load, P corresponding to crack initiation load, P_i, using Eqn. (2.11).

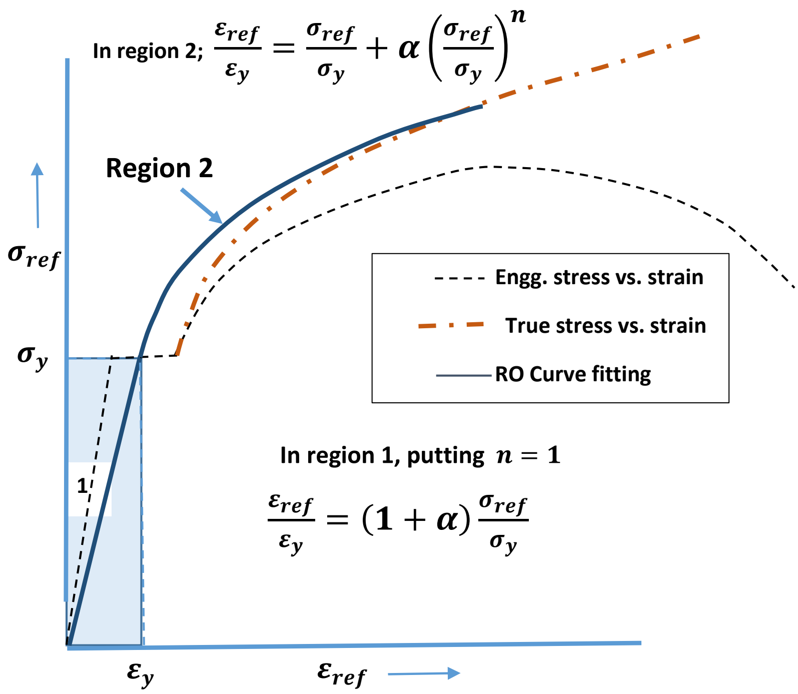

Fig. 5.4. Schematic R-O equation fitting of the material stress strain data beyond yield point

$$\frac{\varepsilon_{ref}}{\varepsilon_y} = (1+\alpha)\frac{\sigma_{ref}}{\sigma_y} = (1+\alpha)\frac{P_i}{P_L(\sigma_y)} \tag{5.6}$$

It should be noted that for all studied pipes the crack initiation loads are within the limit loads. Hence, the variation of load and reference stress in this region can be assumed linearly proportional and so use of Eqn. (2.11). Using above equation (5.6), ε_{ref} is calculated in the linear region of Fig. 5.4. This value is used in Eqn. (5.4) with LLD= Δ_i where 'i' stands for crack initiation point for calculation of 'y', of virtual beam, which is assumed constant for all further calculations for a pipe chosen.

$$\mathrm{y} = \varepsilon_y(1+\alpha)\frac{P_i}{P_L(\sigma_y)}\cdot\frac{L}{\tan^{-1}(\Delta_i/C)} \tag{5.7}$$

For a pipe, in light of known 'y', reference strain, ε_{ref}, is calculated using Eqn. (5.4) for any arbitrary applied LLD = Δ. Subsequently, reference stress, σ_{ref} corresponding to ε_{ref} is calculated using the Ramberg - Osgood relation as shown in the Fig. 5.4 in region 2 which is beyond yield point. If the applied displacement is lower than limit load point displacement of load vs. LLD data then usual relation of Eqn. (2.11) is used for calculation of reference stress, σ_{ref} using applied load, P.

Applied moment for cracked pipe in terms of σ_{ref} is used for the calculation of the stress equivalent to bending stress for uncracked section, σ_b, using the following relation,

$$4R_m^2 t m_b \sigma_{ref} = \pi R_m^2 t \sigma_b \tag{5.8}$$

where the bending moment is equalized for cracked and uncracked section of pipes in terms of reference stress, σ_{ref}, and bending stress, σ_b, respectively. Left hand side of the Eqn.(5.8) represent the limit moment of the cracked pipe which contains the geometry factor m_b, which is a function of dimensions of the pipe R_m and t, and prevalent crack size θ.

$$\sigma_b = 4m_b \sigma_{ref}/\pi \tag{5.9}$$

Finally SIF, K_I, is calculated for this σ_b.Normalized loading, L_r, is also calculated using the reference stress, σ_{ref} i.e. $L_r = \sigma_{ref}/\sigma_y$.

It should be noted that L_r is calculated using applied displacement, Δ, in this proposed methodology instead of conventional way of applied load, P. Using these parameters, K_I and L_r, and finally material fracture toughness, J_{mat} is calculated using Eqn. (4.1). This calculation is repeated for all displacement data points corresponding to further crack extension values, which provides the variation of J_{mat} vs. Δa i.e. whole material fracture toughness curve.

5.3.3 Steps for Determination of J-R curve

Experimental results of applied load P, LLD Δ and crack extension Δa are post processed to material J-R curve using this approach. Assuming elastic beam theory, 'y' is calculated for load and LLD value corresponding to crack initiation point for a pipe.

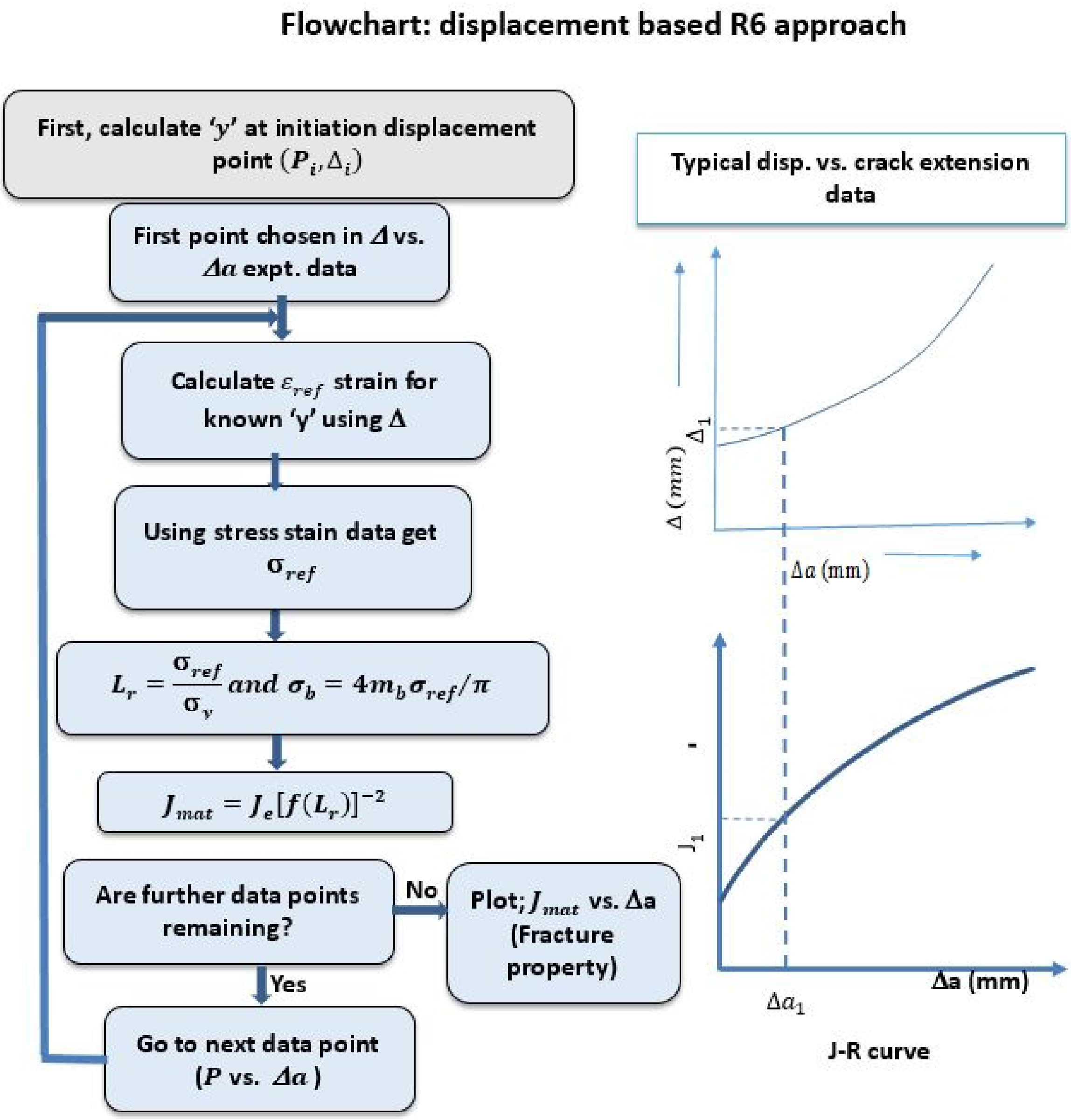

Fig. 5.5. Flowchart diagram depicting the steps of displacement based R6 approach for calculation of J-R curve using experimental displacement vs. crack extension data.

a) Calculation of 'y': First data point is chosen corresponding to LLD vs. crack extension experimental results, which is corresponding to $\Delta a = 0$. The load and LLD value corresponding to this crack initiation point are denoted as P_i and Δ_i respectively. For initial crack size a, limit load P_L is calculated corresponding to material yield stress, σ_y using the available mathematical expression [15]. Now using Eqn. (5.7) 'y' is calculated. This 'y' is assumed constant for the whole calculation of J-R curve for the pipe.

b) Calculation of 'L_r': Corresponding to next value of crack extension Δa, LLD $= \Delta$ is chosen for calculation. Now using Eqn.(5.4) reference strain ε_{ref} is calculated with already available 'y'. If the reference strain is below yield point; $\varepsilon_{ref} \leq (1+\alpha)\varepsilon_y$, then reference stress σ_{ref} is calculated by using the linear relationship as shown as region 1 in Fig. 5.4. However, if the reference strain is beyond yield point. Then reference stress, σ_{ref} is estimated using Ramberg –Osgood Eqn. (5.5) as shown in Fig. 5.4 as region 2. Further, normalized loading, L_r is calculated as $L_r = \sigma_{ref}/\sigma_y$.

c) Calculation of 'J_e': Crack size a is increased by Δa for calculation of stress intensity factor, K_I. Bending stress, σ_b is calculated by using Eqn. (5.9) from reference stress, σ_{ref}. Using this σ_b, stress intensity factor is calculated using the closed form equation available in R6 [15], which is converted to $\mathrm{J_e}$ as $\mathrm{J_e} = \mathrm{K_I^2}/E'$.

Using these J_e and L_r values, J_{mat} is calculated using the relation $J_{mat} = J_e[f(L_r)]^{-2}$. Steps (b) and (c) are repeated for further LLD vs. crack extension data points to obtain whole J-R curve for a pipe. This methodology is shown in Fig. 5.5 showing different steps in form of flow chart to convert displacement vs. crack extension data to material J-R curve. It should be noted that in this approach only displacement vs. crack extension data is required and experimental load data is not needed.

5.4 Results

Fracture properties calculated using conventional approach of load vs. LLD integration is reported by Chattopadhyay et. al. [19] using corresponding geometry parameters η and γ as already discussed. Similarly, same set of fracture properties are also estimated by applying load based approach using R6 FAD by Sahu et.al. [124]. Fracture properties, thus calculated are reproduced here to compare with present calculations, which are carried out by using proposed displacement based approach. The load and displacement values at crack initiation point (P_i and Δ_i) are given in Table 5.2. The effective distance, y, from neutral axis of virtual beam also calculated and given in the table.

Table 5.2. Different parameters at crack initiation point during J-R curve calculation.

Pipe Designation	P_i (KN)	Δ_i (mm)	'y' (mm)	$\varepsilon_{ref(i)}/\varepsilon_y$	$L_{r(i)} = \sigma_{ref(i)}/\sigma_y$	$J_{e(i)}$ (N/mm)
SPBMTWC8-1	179.5	20.87	449.2	7.09	0.92	84.3
SPBMTWC8-2	141.6	18.39	498.6	6.93	0.9	102.3
SPBMTWC8-3	117.9	19.99	515.5	7.79	1.01	136.1
SPBMTW16-1	508.6	29.87	373.7	4.52	0.62	102.2
SPBMTW16-2	380.6	25.67	437.6	4.55	0.62	107.5
SPBMTW16-3	278.2	24.51	479.2	4.75	0.65	100.3

Different important parameters corresponding to crack initiation point, which are calculated in the steps of final calculation of J_{mat} are reference strain $\varepsilon_{ref(i)}$, reference stress $\sigma_{ref(i)}$ and J –elastic $J_{e(i)}$. These parameters are also reported in Table 5.2 for all pipes.

5.4.1 Detailed Results of Pipe SPBMTWC8-1

Using the proposed approach, experimental LLD vs. crack extension results is converted to J-R curve. Experimental LLD vs. crack extension data is shown in Fig. 5.6 (a) for pipe SPBMTWC8-1. From Fig. 5.6(b) to (e), variations of different parameters with crack extension Δa are plotted. Finally comparative plot of J-R curves calculated by different methods are shown in Fig. 5.6(f).

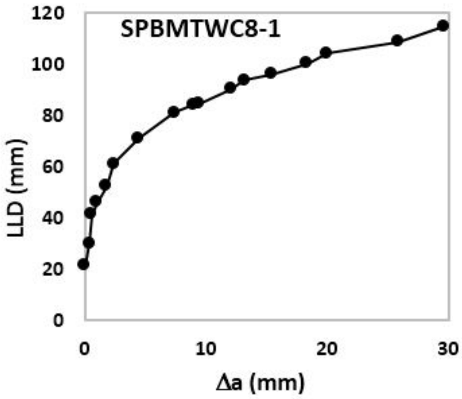

(a)

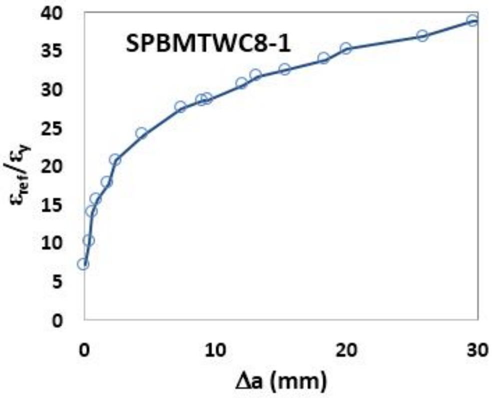

(b)

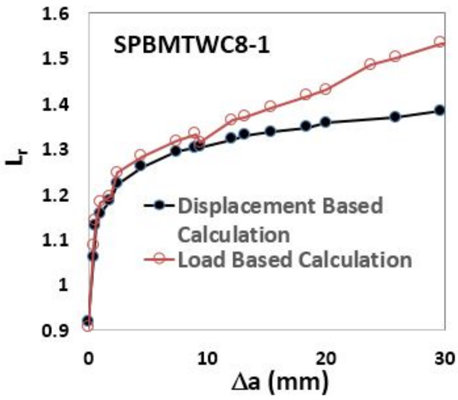

(c)

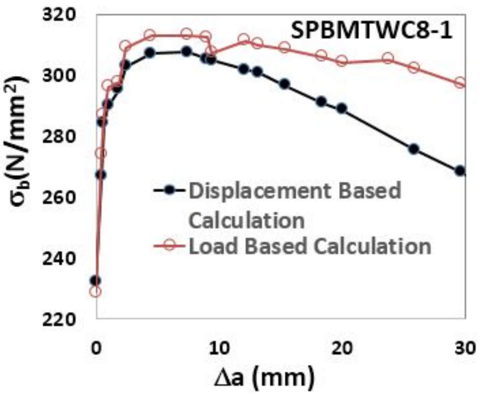

(d)

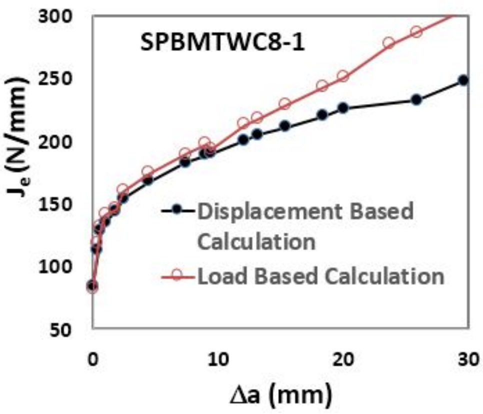

(e)

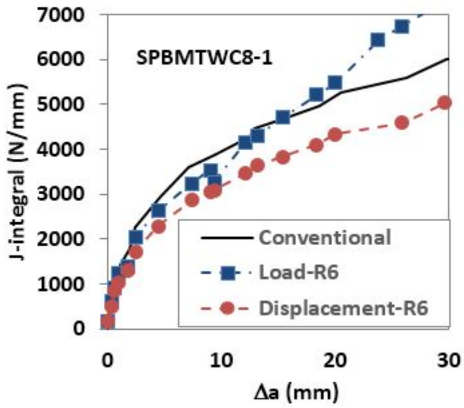

(f)

Fig. 5.6. Variation of different parameters with crack extension Δa for pipe PRSPTWC8-1. (a) Experimental LLD (b) Normalized reference strain, $\varepsilon_{ref}/\varepsilon_y$. (c) Normalized reference stress, $L_r = \sigma_{ref}/\sigma_y$. (d) Bending stress, σ_b for uncracked section. (e) J-elastic, J_e and (f) Comparison of J-R curves calculated by different methods.

5.4.2 Displacement Based J-R Curves for Remaining Pipes

For remaining pipes, only the plot of experimental LLD vs. crack extension and finally calculated J-R curves are shown. For the pipe SPBMTWC8-2, experimental LLD vs. crack extension data and finally calculated J-R curves are depicted in Fig. 5.7 (a) and (b) respectively. Similar results are shown for remaining pipes SPBMTWC8-3, SPBMTWC16-1, SPBMTWC16-2 and SPBMTWC16-3 in Fig. 5.8, Fig. 5.9, Fig. 5.10 and Fig. 5.11 respectively. It can be observed that the proposed displacement based approach is able to predict the fracture properties which are in better agreement with the conventional J-R curves for all the pipes compare to the earlier approach of load based calculation.

5.5 Further Improvement in Displacement Based R6 Approach

It should be noted that the present approach is based on the assumption that the whole deformation is concentrated only on the cracked section of the pipe. This assumption is used for calculation of effective distance, y, from neutral axis of the virtual beam. This assumption is more applicable for the pipes with large crack sizes. If we move towards smaller crack size cases, we are deviating from the assumption that the deformation is concentrated on the crack section only. It should be observed that the calculated results are showing better agreement for the pipes with larger crack sizes compared to small crack sizes. Comparing all 8 inch pipes, it is observed that all geometric parameters are identical except the prevalent crack sizes as shown in Table 2. 2. This observation is also true for the 16 inch pipes. Accordingly, it can be assumed that the variation in y is due to initial crack sizes for the same size pipes having identical diameters. Hence, calculation of y is more valid for the pipe with the deepest crack size.

To observe the effect of crack size on calculated y, variation of y is shown with respect to

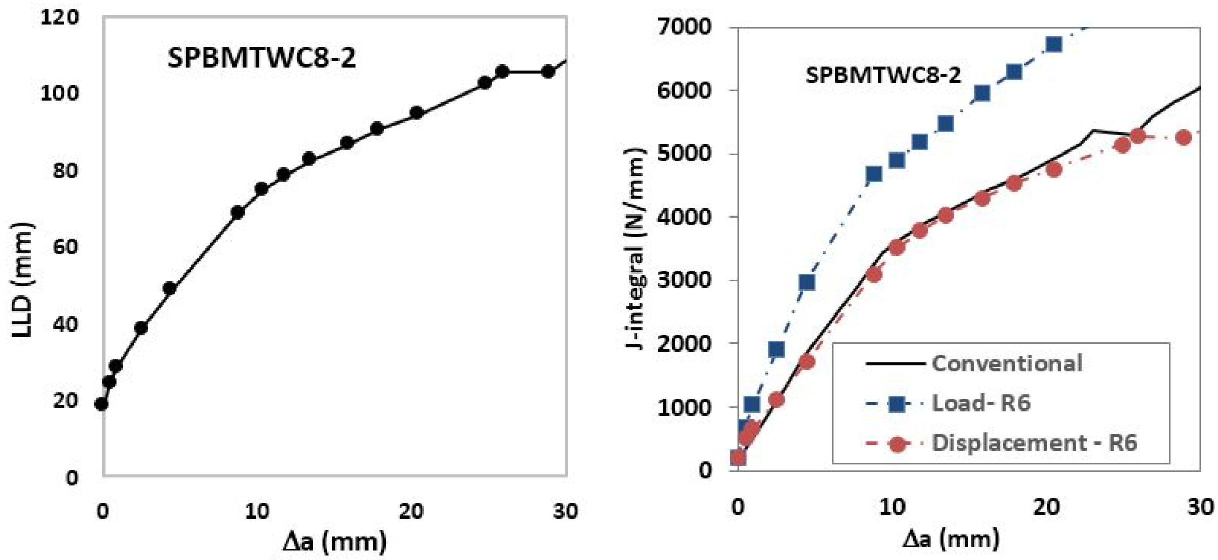

(a) (b)

Fig. 5.7. Different plots for pipe SPBMTWC8-2. (a) Experimental LLD vs. crack extension data. (b)J-R curve calculated using displacement based approach and comparison with already available results.

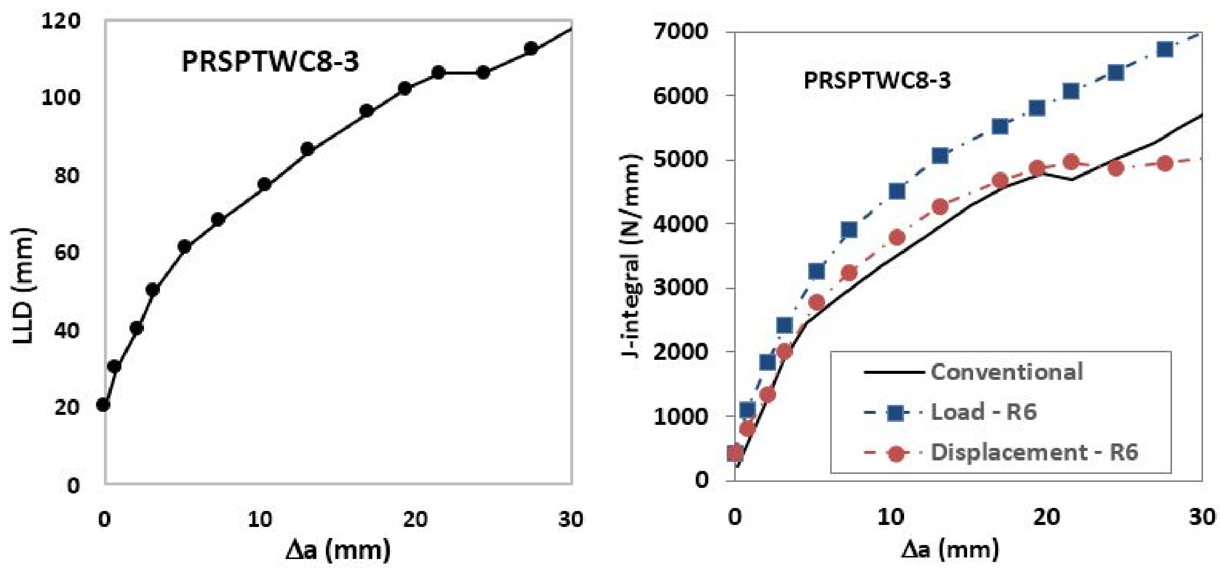

(a) (b)

Fig. 5.8. Different plots for pipe SPBMTWC8-3. (a) Experimental LLD vs. crack extension data. (b)J-R curve calculated using displacement based approach and comparison with already available results.

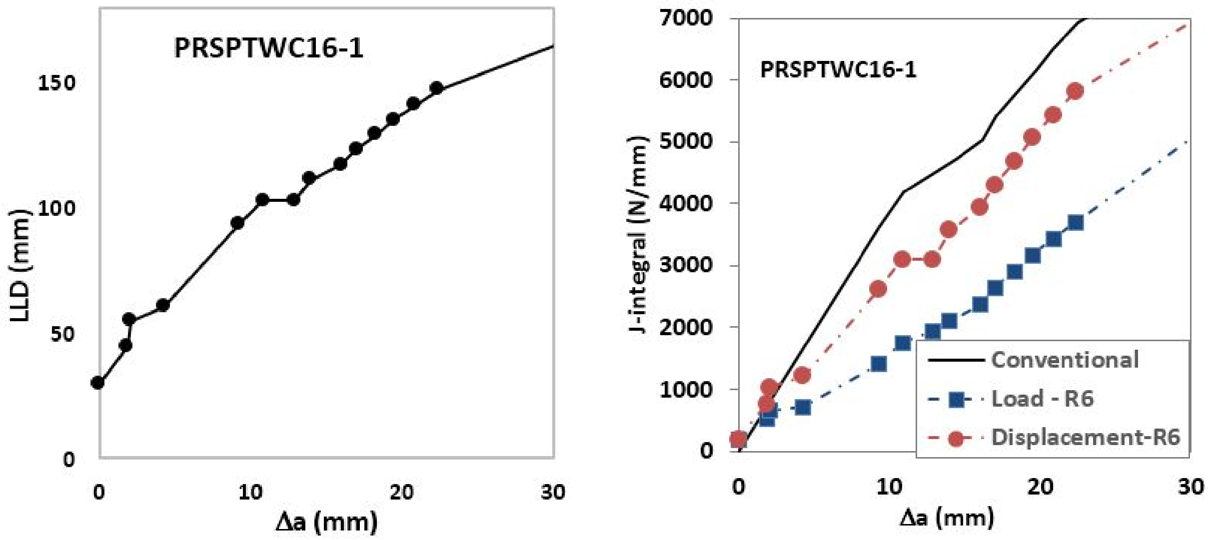

(a) (b)

Fig. 5.9. Different plots for pipe SPBMTWC16-1. (a) Experimental LLD vs. crack extension data. (b)J-R curve calculated using displacement based approach and comparison with already available results.

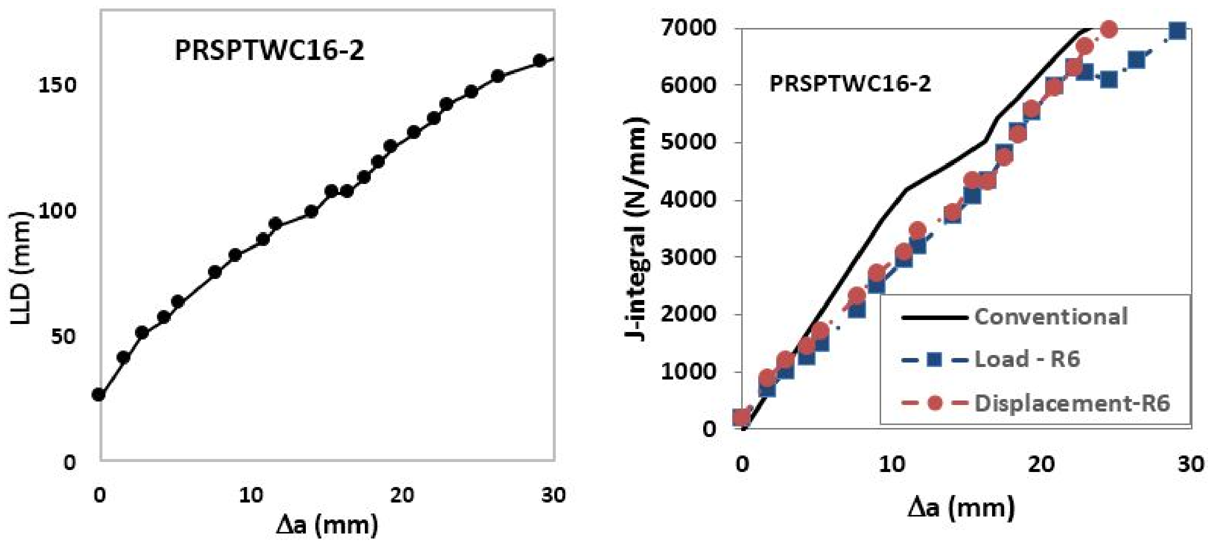

(a) (b)

Fig. 5.10. Different plots for pipe SPBMTWC16-2. (a) Experimental LLD vs. crack extension data. (b)J-R curve calculated using displacement based approach and comparison with already available results.

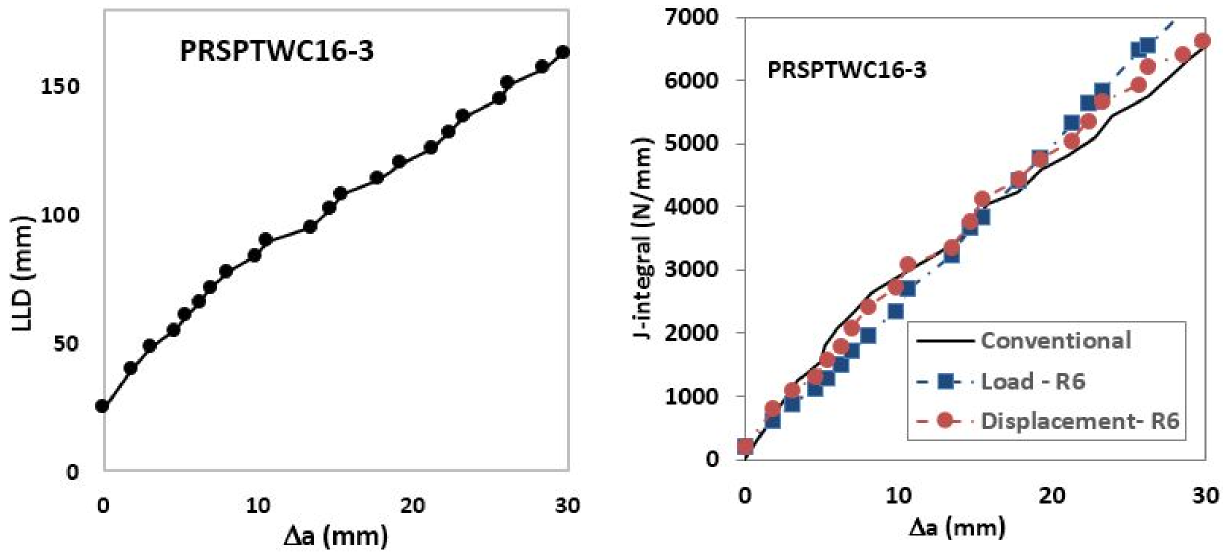

(a) (b)

Fig. 5.11. Different plots for pipe SPBMTWC16-3. (a) Experimental LLD vs. crack extension data. (b)J-R curve calculated using displacement based approach and comparison with already available results.

normalized crack size, θ/π in Fig. 5.12. It can be observed that y tends to asymptote with higher crack size for both 8 inch and 16 inch pipes.

Considering these facts, the calculated, y, corresponding to the deepest crack sized pipe is used for recalculation of fracture properties for all remaining pipes. In case of 8 inch pipes, value of y of deepest cracked pipe, SPBMTWC8-3 is 515.5mm as shown in Table 5.2. This value is used for recalculation of reference strain, ε_{ref} for other two pipes SPBMTWC8-1 and SPBMTWC8-2 using improved approach. Eventually, fracture toughness curves for pipes SPBMTWC8-1 and SPBMTWC8-2 are recalculated and depicted in Fig. 5.13 and Fig. 5.14 respectively. For 16 inch pipes also fracture properties are recalculated using this improved approach for relatively small size cracked pipes, SPBMTWC16-1 and SPBMTWC16-2. The already calculated value of y for 16 inch pipe with deepest crack size, SPBMTWC16-3 is 479.2mm as shown in Table 5.2, which is used for recalculation of fracture properties for remaining two 16 inch pipes. The recalculated fracture properties are shown in Fig. 5.15 and

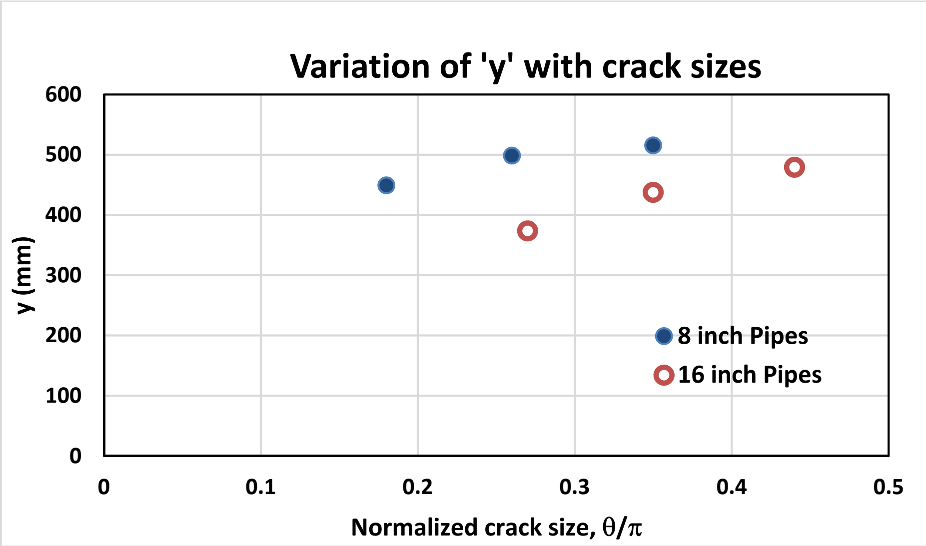

Fig. 5.12. Variation of y with crack size for pipes shows the convergence tendency of y for higher crack sizes for both 8 and 16 inch pipes.

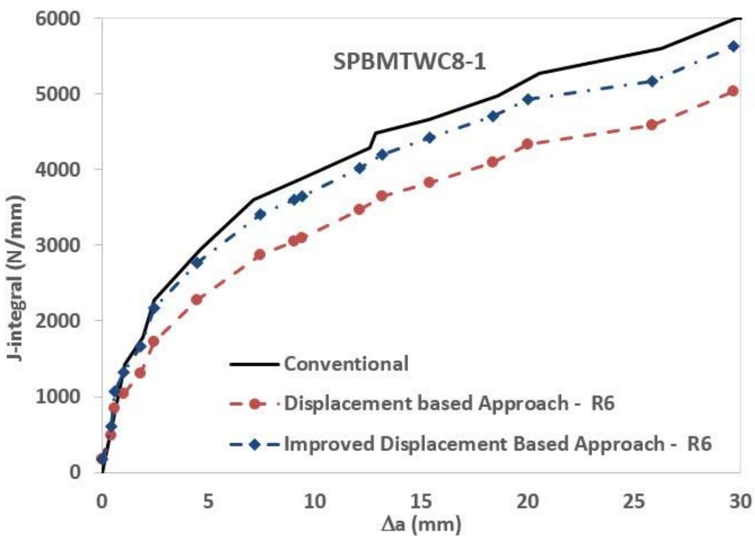

Fig. 5.13. Fracture toughness curve for pipe SPBMTWC8-1 calculated using improved displacement based approach and comparison with earlier calculated results.

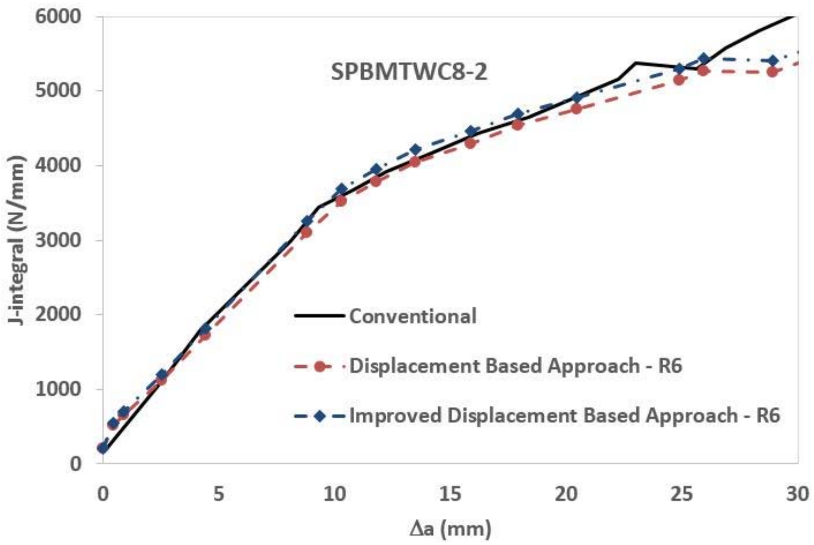

Fig. 5.14. Fracture toughness curve for pipe SPBMTWC8-2 calculated using improved displacement based approach and comparison with earlier calculated results.

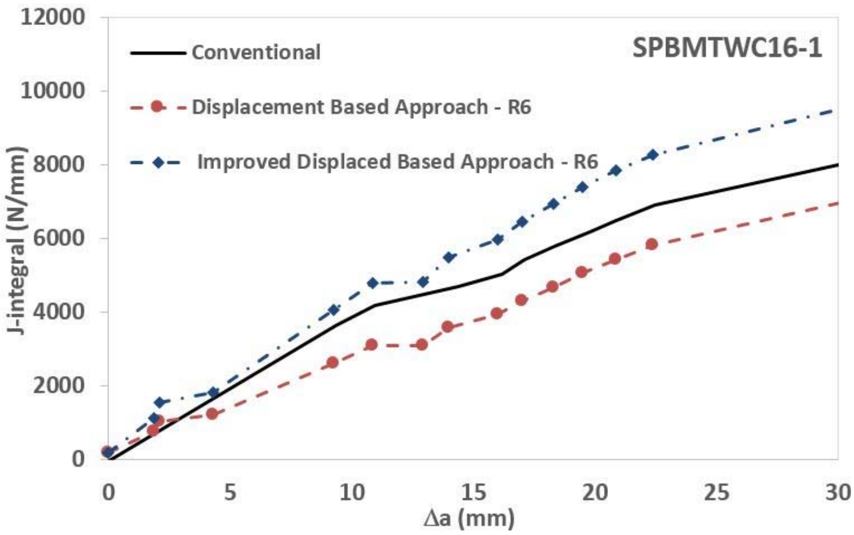

Fig. 5.15. Fracture toughness curve for pipe SPBMTWC16-1 calculated using improved displacement based approach and comparison with earlier calculated results.

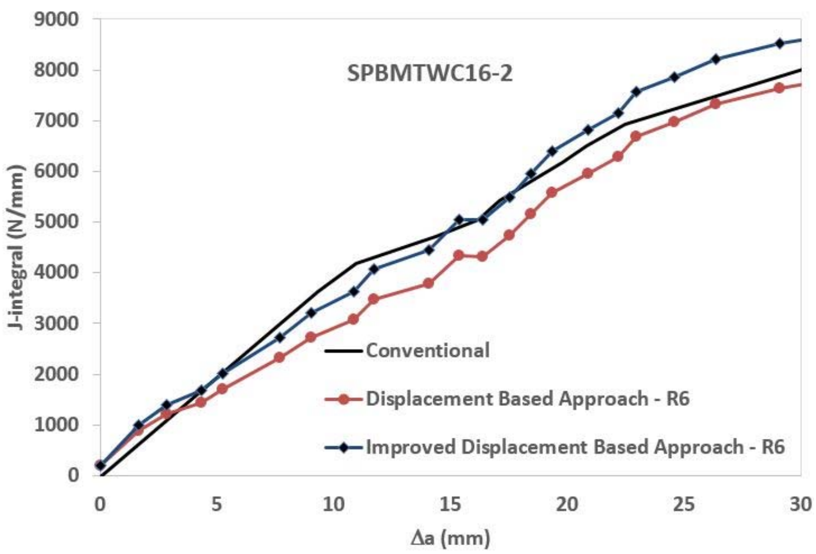

Fig. 5.16. Fracture toughness curve for pipe SPBMTWC16-2 calculated using improved displacement based approach and comparison with earlier calculated results.

Fig. 5.16 for pipes SPBMTWC16-1 and SPBMTWC16-2 and compared with those already calculated using displacement based approach. It can be observed that the recalculated results using improved approach are showing better agreement than simple displacement based R6 approach with the conventionally calculated J-R curves for all pipes of both sizes.

5.6 Discussion

The calculated fracture properties, J-R curves using displacement based R6 approach are in good agreement with conventionally calculated values. This method is more appropriate for the pipes with larger crack sizes rather than shallow/smaller crack sizes because of the assumption that deformation is concentrated on cracked section only. However, for shallow/lower cracked cases the prediction will be slightly conservative based on this assumption. Displacement based method is further improved for smaller cracked pipes by choosing the parameter, y, related to largest cracked pipe for calculation. This parameter y with LLD of any chosen lower cracked same size pipe is used for calculation of reference strain and eventually fracture property with more accuracy. For 8 inch and 16 inch pipes the available normalized deepest crack sizes, θ⁄π are 0.33 and 0.42 respectively, which are used for calculation of y. These values of y are efficiently used for recalculation of J_{mat} of same size pipes with smaller crack sizes.

5.7 Closure

The load based R6 approach to predict J-R curve is not applicable beyond limit load point. Because, depending on the type of loading i.e. load or displacement-controlled, load may not always be rising beyond limit load point but J-integral always rises with applied load/displacement. Consequently, a novel displacement-based R6 approach is proposed in this work to predict the pipe J-R curve from experimental data of load, load-line-displacement and crack growth. One parameter 'y' in the derivation of displacement-based R6 approach is used to calculate the reference strain. This was evaluated individually for each pipe with varying crack sizes. The predicted J-R curves based on this approach improved with respect to load-based R6 approach and compared better with conventionally obtained J-R curves by 'η' factor approach. One of the major advantages of this displacement based approach is that unlike conventional η-factor approach, this approach can be utilized to obtain pipe J-R curve even when experimental load data is not available due to any reason.

The methodology of this approach uses applied displacement instead of experimental load for calculation of stress intensity factor K_I. In this methodology, the assumption is that the cracked section remains circular even during significant plastic deformation. This assumption is broadly valid for cracked pipes under bending moment. However, for elbows the cracked cross section significantly ovalizes during plastic deformation under bending moment and inherent assumption is violated. Hence, in the cases of significant geometric softening/hardening, this methodology should be tested. In the next chapter, these load based and displacement based approaches will be attempted for cracked elbows for calculation of J-R curves.

Chapter 6

Hybrid Approach for Calculation of J-R Curve

6.1 Introduction

Based on limited literatures available [103, 105], it is established that for fracture assessment of any cracked component under large plastic deformation, the applied displacement is better parameter instead of applied load. Thus, a displacement based R6 approach for calculation of J-R curve is proposed in the previous chapter instead of conventional load based approach. In displacement based R6 approach, the reference stress σ_{ref} and stress intensity factor K_I both parameters are evaluated using the applied displacement. This procedure have been applied for calculation of J-R curves for total six pipes of two sizes 8 inch and 16 inch nominal diameters with different crack sizes. For these pipes, using fracture test data of load, Load Line Displacement (LLD) and relevant crack growth, J-R curves are already calculated and reported using conventional load-LLD integration approach using η and γ functions by Chattopadhyay et. al. [19].In this research work, using load based and displacement based R6 approach, J-R curves have been predicted using experimental LLD and load data respectively. Displacement based R6 predictions are found to be in better agreement with conventionally calculated J-R curves than the predictions of load based R6 approach.

For more validation of this displacement based approach, this method should be tested with other geometries and/or loading configurations. Under plan projects in Bhabha Atomic

Research Centre (BARC), total five numbers of 8 inch and 16 inch elbows with different sizes of throughwall cracks were tested by Chattopadhyay et.al. [51]. For adoption of R6 approach for prediction of J-R curve, required experimental fracture test results are available related to these cracked elbows tested under bending moment. Fracture test results like load, LLD, etc., with relevant crack extension data are available for further analyses. Using these experimental data, J-R curves evaluated using conventional approach of load vs. displacement integration using η and γ factors were calculated by Chattopadhyay et.al. [51]. Considering the availability of sufficient data of the elbows, the displacement based R6 calculation methodology is extended for elbows. The evaluated J-R curves are found to be significantly deviated from those conventionally calculated values especially for elbows tested under closing mode of bending. This displacement based method is further modified to displacement –load (hybrid) based R6 method. In this proposed method, normalized loading L_r is calculated using the applied LLD using curved beam theory. First, LLD is used to calculate the reference strain ε_{ref}. Further, using this ε_{ref}, reference stress σ_{ref} is estimated from material tensile properties. Finally, this reference stress is used for calculation of normalised loading L_r as $L_r = \sigma_{ref}/\sigma_y$. Thus, L_r is calculated using the displacement based approach as explained in detail in chapter 5. However, stress intensity factor K_I is calculated using the experimental load data like it is done in load based R6 approach as explained in chapter 4. Hence, this method is named as 'displacement-load' or 'hybrid' R6 approach. The estimated J-R curves using displacement–load based R6 approach are compared with those values already reported for elbows which were calculated using conventional approach. The results are found to be in good agreement with conventionally calculated J-R curves for elbows. This hybrid approach is further extended to the pipes investigated in the previous chapters and the estimated J-R curves are also found to be in very good agreement with conventional J-R curves for all the pipes. Thus, proposed method is found to be more appropriate and a simpler method for calculation of J-R curve using

R6 failure assessment diagram.

6.2 Experimental Data of Elbows

The elbows to be investigated here are already explained in details in Chapter 2. The geometries and loading configurations are depicted in Fig. 2.3. The elbows with extrados crack and intrados crack were loaded in closing and opening mode respectively as shown in the figure to ensure the crack initiation and growth. The relevant dimensions of the elbows are shown in Table 2.3 and Table 2.4 for elbows loaded under closing and opening mode respectively. The relevant dimensions, Outer diameter, D_0, bend radius, R_b, thickness, t, circumferential crack size, 2θ and moment arm length L are shown in the Fig. 2.3. These parameters including ratio R_m/t and crack initiation loads $P_{0.2}$ are tabulated in Table 2.3 and Table 2.4. These data were already utilized in Chapter 3 for predicting the crack initiation loads using R6 approach which are found be reasonably good agreement with experimental crack initiation loads for all the elbows. In this method, crack initiation load are predicted using the TPB specimen crack initiation toughness J_i^{TPB} based on assumption that crack initiation fracture toughness will be same for specimen and elbows. This R6 based methodology will be applied beyond crack initiation point in reverse way to calculate J_{mat} using the experimental load and/or LLD for any arbitrary loading point with relevant crack extension value.

6.3 Closed Form Expressions

The mathematical expressions of stress intensity factor, K_I and limit load P_L are given as following:

6.3.1 Stress Intensity Factor for Elbows

For elbows with throughwall crack under bending moment the stress intensity factor is calculated identically as shown for pipes given by Eqns. (3.1) and (3.2). However, the geometry factor, F_b is given by Chattopadhyay [96] as:

$$F_b = (-3.4628 + 4.446\lambda^{0.1366}) + (-52.429 + 52.445\lambda^{-0.1848})\left(\frac{\theta}{\pi}\right)^{2.6137} + \left[(-2.2524 + 1.1102\lambda^{0.1267}) + (0.8634 + 1.7283\lambda^{0.0695})\left(\frac{\theta}{\pi}\right)^{0.4587}\right](t/R_m)^{-0.5119} \tag{6.1}$$

where $\lambda = tR_b/R_m^2$ with t, R_b and R_m are thickness, bend radius and mean radius of the elbow respectively. Other parameter θ/π is normalized crack size with 2θ being the angular size of the through wall crack. These expressions are applied for calculation of K_I for all the elbows tested under both opening and closing mode of loadings.

It should be noted that Eqn. (6.1) have been developed for closing mode of moment. Because of non-availability of any mathematical expression of K_I for elbows under opening mode of moment that time, Eqn.(6.1) is used by Chattopadhyay et.al. [51] for determination of linear stress intensity factor K_I and finally for calculation of J-R curves for all elbows tested under opening and closing mode of loadings. Hence, this same expression of K_I is used in this investigation for determination of J-R curves for all elbows in all the proposed R6 approaches.

6.3.2 Limit Load for Elbows

The limit load expressions for circumferentially cracked elbows under in-plane bending moment are proposed by Chattopadhyay et. al. [32] for both opening and closing mode of loadings. The basic form of limit moment equations for both mode of loadings are represented by following expression:

$$M_L = M_0 X \tag{6.2}$$

where M_0 is the limit moment for defect free elbow and X is the weakening factor due to existing flaw, which will obviously follow the condition of $X \leq 1$.

6.3.2.1 Opening Mode

The limit moment for defect-free elbows, M_0, for opening mode of moment is proposed as

$$M_0 = 4{R_m}^2 t\sigma_y\left(1.048\lambda^{1/3} - 0.0617\right) \quad (6.3)$$

The weakening factor X due to existing crack is given as:

$$\mathrm{X} = 1.127 - 1.8108\left(\frac{\theta}{\pi}\right) \quad (6.4)$$

6.3.2.2 Closing Mode

The limit moment for defect free elbow under closing mode is proposed as:

$$M_0 = 4{R_m}^2 t\sigma_y.\,1.075\lambda^{2/3} \quad (6.5)$$

For our all elbow cases, the ratio, $R_m/t \approx 5$. Thus calculations of J-R curves using conventional approach are calculated by Chattopadhyay et.al. [51] with this assumption.

Weakening factor, X for $R_m/t = 5$ is proposed as:

$$\mathrm{X} = 1.1194 - 0.7236\left(\frac{\theta}{\pi}\right) - 2.0806\left(\frac{\theta}{\pi}\right)^2 \quad (6.6)$$

for $45^o \leq 2\theta \leq 150^o$.

It can be observed that for all elbow cases investigated, the existing crack sizes are within the validity limit.

It should be noted that many researchers have proposed different closed form expressions of limit load P_L with slight variations. However, the explained expressions of P_L in Eqns (6.2) to (6.6) have been used for getting η and γ functions which were used for prediction of conventional J-R curves for the elbows. Hence, this set of closed form expressions of limit load have been chosen for calculation of J-R curves.

6.4 Tensile Properties in terms of α and n

Tensile stress-strain data obtained for the piping material carbon steel SA333Gr6 is already reported in section literature review 2.2.1. For displacement based R6 approach, tensile stress –strain data is fitted in average way to remove the Luder regime as shown in Fig. 5.3. This Ramberg-Osgood fitted curve is quantified by two parameters α and strain hardening exponent n as shown in Table 5.1. These parameters will be used for estimation of reference stress σ_{ref} from reference strain ε_{ref} with Ramberg-Osgood equation as shown in Eqn. (5.5). This approach removes the Luder regime from stress strain data and ensures the smooth increase of reference stress σ_{ref} and material fracture toughness J_{mat} with applied reference strain ε_{ref}.

6.5 Pipes under Bending Moment

Relevant geometries and loading configurations are already discussed in subsection 2.2.2 for cracked pipes tested under four point bending moment.

Closed form expression of stress intensity factor, K_I and limit load P_L is also discussed in previous subsections 3.2.1 and 3.2.2 respectively for the pipes, which are reused here for calculation of material fracture parameters, J-R curves.

6.6 Application of R6 for Prediction of J-R Curves for Elbows

Load based and displacement based approaches are used for prediction of J-R curves for cracked pipes in chapter 4 and chapter 5 respectively. The results are found to be in good agreement with conventionally calculated J-R curves especially for displacement based approach. This approach is further adopted for an elbow ELTWEX16-4 which is fabricated

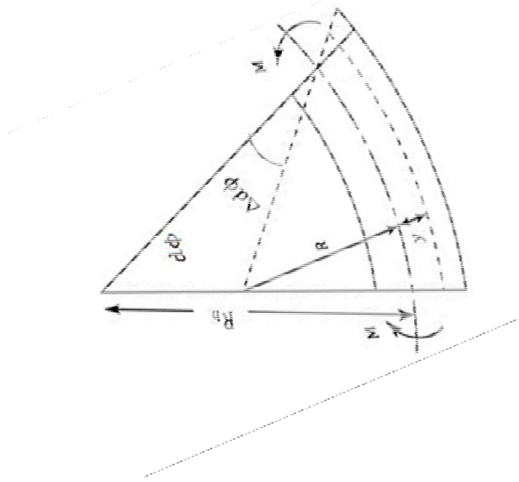

(a)

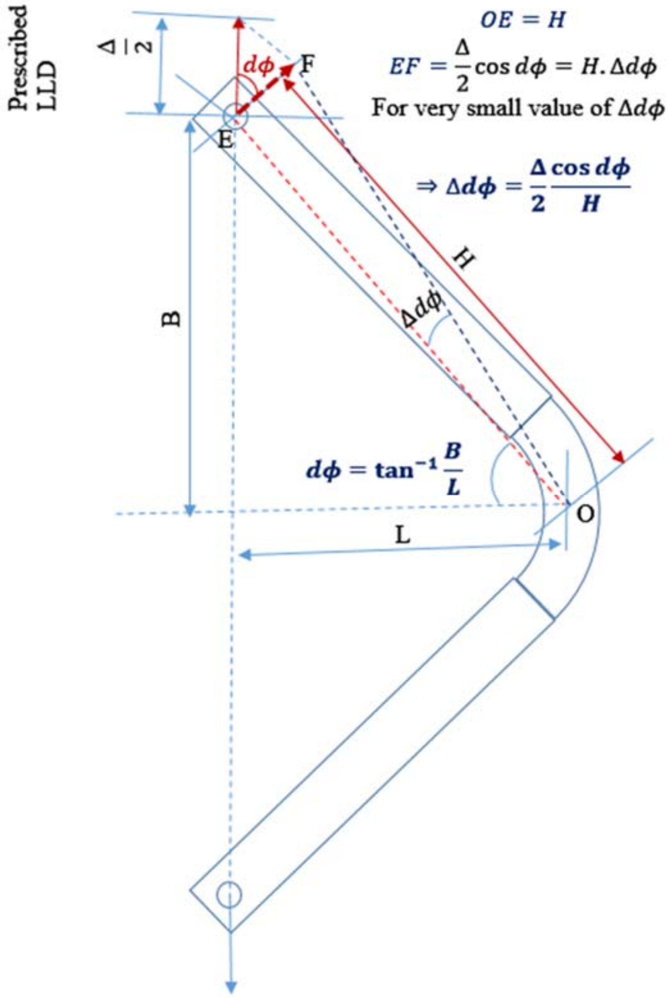

(b)

Fig. 6.1.(a) Curved beam theory. (b) Schematic representation of deformed elbow

with extrados throughwall crack and tested under closing mode of loading .The details are already given in Table 2.3 and loading configuration is schematically shown in Fig. 2.3.

6.6.1 Displacement Based Approach

For application of displacement based approach, nominal loading L_r is calculated using applied LLD instead of experimental load which is the established methodology in the R6 approach in failure assessment also. For using LLD, elastic beam theory is applied in Chapter 5 and a mathematical relation between reference strain ε_{ref} and LLD was proposed for a cracked pipe. Similarly, for elbows, curved bar theory is going to be used for getting the similar mathematical relation to calculate reference strain using LLD.

6.6.1.1 Curved Bar Theory for Elbow for Displacement Based R6 Approach

Using the angular rotation $\Delta d\phi$, curved bar theory is applied as shown in Fig. 6.1(a), for the deformed curved beam and elastic strain ε_e at distance y from neutral axis is calculated as,

$$\varepsilon_e = \frac{\Delta d\phi}{d\phi} k \tag{6.7}$$

Where $d\phi$ is the total angle created by the curved beam at centre as shown in the Fig. 6.1(a). Parameter k is a non-dimensional parameter of y and eccentricity e as explained by Timoshenko [125]. It should be noted that for an elbow centroid and neutral axis are not same unlike a pipe. Hence, for an elbow an additional parameter e other than y, is needed for getting strain distribution on cross section. This parameter e is the distance between centroid and neutral axis which is a non-dimensional function of bend radius, R_b, mean radius R_m and thickness t for an elbow.

For application of this theory, it is assumed that all the deformation/rotation in elbow due to LLD is concentrated at cracked section only. This assumption is quite reasonable because all the elbows under investigation, are cracked throughwall. Hence, all the deformation is mainly concentrated at cracked section and, deformations in other parts may be neglected for practical purpose.

The deformed elbow at cracked section is shown schematically in Fig. 6.1(b). The angular rotation $\Delta d\phi$ is shown as,

$$\Delta d\phi = \frac{\Delta}{2} \frac{\cos d\phi}{H} \tag{6.8}$$

where Δ is applied LLD, $H = \sqrt{L^2 + B^2}$ and $d\phi = \tan^{-1}(B/L)$ as shown in Fig. 6.1(b). Here

L and B are moment arm length and vertical distance between cracked section and loading point as shown in the figure.

Putting value of $\Delta d\phi$ from Eqn. (6.8) in Eqn. (6.7) and renaming elastic strain ε_e to reference strain ε_{ref} because this strain will represent the material stress strain data for converting to reference stress σ_{ref}.

Thus ε_{ref} in terms of applied LLD, Δ

$$\varepsilon_{ref} = \frac{\Delta}{2}\left(\frac{\cos d\phi}{d\phi H}\right)k \tag{6.9}$$

where k is now the function of crack size 2θ of the elbow also including other parameters. The parameter k is still not known. For determination of k, ε_{ref} is calculated by using load and displacement data corresponding to crack initiation point.

Reference strain at crack initiation $\varepsilon_{ref(i)}$ in terms of crack initiation load using Eqn. (5.6).

$$\varepsilon_{ref(i)} = (1+\alpha)\frac{\sigma_{ref(i)}}{\sigma_y}\varepsilon_y = (1+\alpha)\frac{P_i}{P_L(\sigma_y)}\varepsilon_y \tag{6.10}$$

Now, $\varepsilon_{ref(i)}$ can also written as

$$\varepsilon_{ref(i)} = \frac{\Delta_i}{2}\left(\frac{\cos d\phi}{Hd\phi}\right)k \tag{6.11}$$

Now using Eqns. (6.10) and (6.11), k can be written in terms of crack initiation parameters,

$$k = \varepsilon_y(1+\alpha)\frac{P_i}{P_L(\sigma_y)}\frac{2}{\Delta_i}\left(\frac{Hd\phi}{\cos d\phi}\right) \tag{6.12}$$

Using Eqn. (6.12) with $d\phi = \pi/4$, parameter can be calculated for crack initiation point with parameters P_i and Δ_i.

Once, k is known for an elbow, it is assumed constant for an elbow and it is used with further loading points LLD= Δ for determination of reference strain using Eqn. (6.11). Rest of the methodology is similar as explained for pipes for determination of reference stress, σ_{ref} and bending stress, σ_b which are used for calculation of nominal loading, L_r and stress intensity factor, K_I. Finally J_{mat} is calculated using Eqn. (4.1).

6.7 Calculation for Elbow ELTWEX16-4

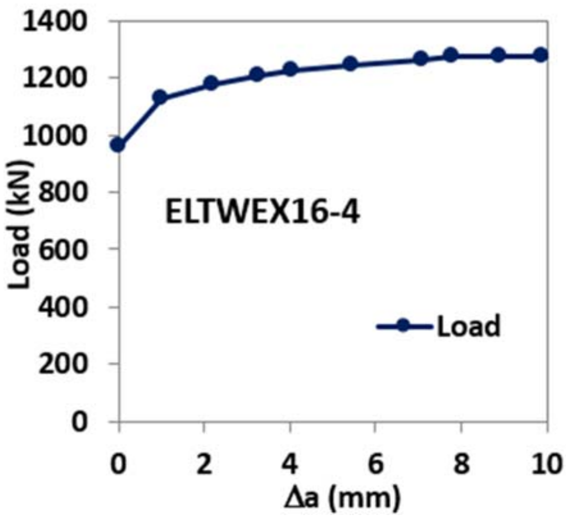

Fig. 6.2. Experimental load vs. crack growth data for elbow ELTWEX16-4

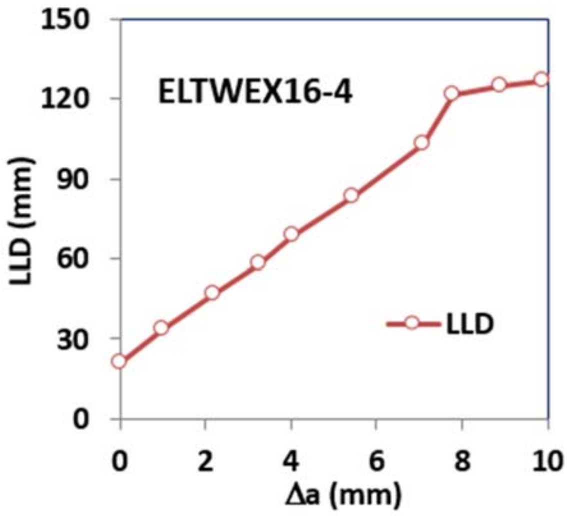

Fig. 6.3. Experimental load line displacement (LLD) vs. crack growth data for elbow ELTWEX16-4

First, R6 based approaches are employed here for the elbow ELTWEX16-4. Fracture test data load vs. crack growth and LLD vs. crack growth are shown in Fig. 6.2 and Fig. 6.3 respectively for this elbow.

6.7.1 Load Based Calculation

Load based R6 approach where reference stress σ_{ref} and stress intensity factor, K_I both the parameters are directly calculated using the applied load as explained in detail in Chapter 4. For employing the load based approach, experimental load vs. crack extension data is required. In this approach, each point of this experimental data of Fig. 6.2 can be converted to a point in the fracture property J-R curve. Reference stress is calculated using the experimental load P using the established load approach i.e. $L_r = \sigma_{ref}/\sigma_y = P/P_L(a, \sigma_y)$. Similarly, the bending

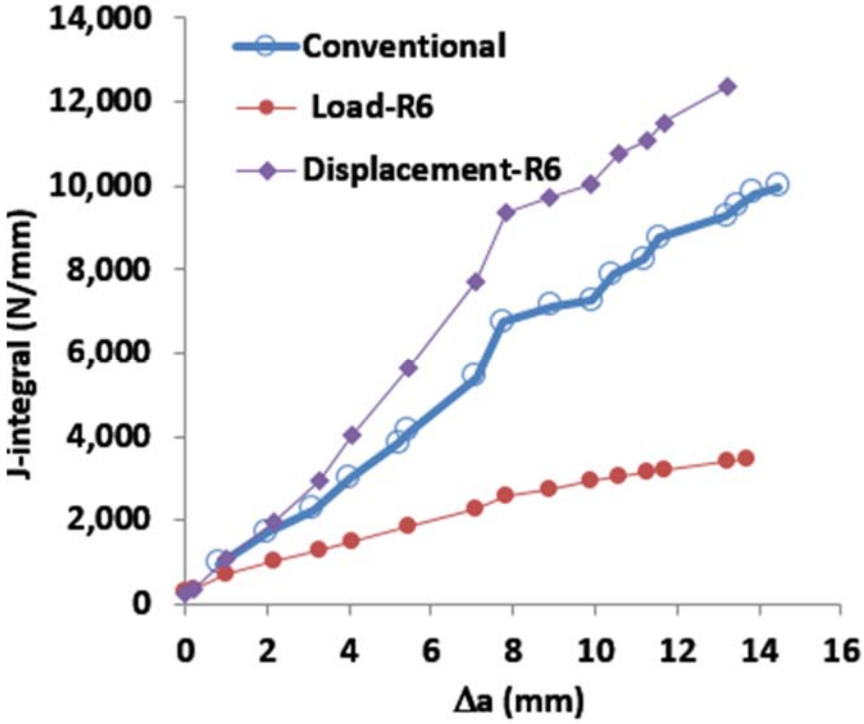

Fig. 6.4. J-R curves calculated by different methods for elbow ELTWEX16-4

stress σ_b is also calculated by converting experimental load to corresponding bending moment as shown in Eqn. (3.2). Finally using this bending stress σ_b, stress intensity factor K_I is evaluated using the Eqn. (3.1). The calculated J-R curve using this fracture data is shown in Fig. 6.4. It should be noted that the load based calculation is quite lower than the conventional J-R curve. The reason of this deviation is that the load is not an appropriate parameter for this case to quantify the instantaneous plastic deformation level and consequent reference stress σ_{ref} and reference strain ε_{ref} near crack tip. Reference stress σ_{ref} is a parameter which is an important factor to evaluate the J_{mat} in forms of $f\left(L_r = \sigma_{ref}/\sigma_y\right)$ as shown in Eqn. (4.1).

6.7.2 Displacement Based Calculation

For using displacement based approach, the input is experimental LLD vs. crack extension data which is shown for elbow ELTWEX16-4 in Fig. 6.3. In this approach, each point of this experimental curve is converted to the corresponding point of fracture property J-R curve as explained in displacement based approach in Chapter 5. First, using the curved beam theory, LLD is converted to reference strain ε_{ref} and then corresponding reference stress σ_{ref} is obtained from the fitted material stress –strain data. This σ_{ref} will now represent the fracture property J-R curve which is always rising with more and more loading. If this parameter σ_{ref} would have been predicted by load as in case of load approach, it may not have represented properly the energy absorbed during more and more applied LLD which is quantified as J_{mat}. Another parameter which is very important for determination of J_{mat} is elastic J-integral, J_e, which is determined from σ_{ref}. This approach is already adopted for a cracked pipe and shown in Eqns. (5.8) and (5.9) in chapter 5.

It should be noted that employed mathematical expression of elastic SIF K_I for an elbow have been proposed for uncracked bending stress σ_b. Here, this bending stress is related to global bending moment M as $M = \pi R_m^2 t \sigma_b$ which is corresponding to similar pipe section. Hence, this reference stress σ_{ref} is calculated by balancing the moment for uncracked section of a pipe in terms of bending stress σ_b and for cracked section of an elbow in terms of σ_{ref}. For a closing moment case of an cracked elbow, using Eqns. (6.2), (6.5) and (6.6), the moment in terms of reference stress σ_{ref} can be written as shown in Eqn. (6.13).

$$M = 4{R_m}^2 t \sigma_{ref} 1.075\lambda^{2/3}\left[1.1194 - 0.7236\left(\frac{\theta}{\pi}\right) - 2.0806\left(\frac{\theta}{\pi}\right)^2\right] \tag{6.13}$$

This is equalized with bending moment of similar pipe section as explained earlier. The bending stress σ_b can be written in terms of the reference stress σ_{ref} as shown in Eqn. (6.14).

$$\sigma_b = \left(\frac{4}{\pi}\right) 1.075\lambda^{2/3}\left[1.1194 - 0.7236\left(\frac{\theta}{\pi}\right) - 2.0806\left(\frac{\theta}{\pi}\right)^2\right]\sigma_{ref} \tag{6.14}$$

It should be noted that the mathematical expression of limit moment M_L is different for opening moment than closing moment. Hence, using relevant Eqns. (6.2), (6.3) and (6.4) the mathematical expression can be easily derived for calculating bending stress σ_b from reference stress σ_{ref} for opening mode as shown in Eqn. (6.15).

$$\sigma_b = \left(\frac{4}{\pi}\right)\left(1.048\lambda^{1/3} - 0.0617\right)\left[1.127 - 1.8108\left(\frac{\theta}{\pi}\right)\right]\sigma_{ref} \tag{6.15}$$

For calculation of bending stress σ_b from reference stress σ_{ref}, Eqn. (6.14) and (6.15) are used for cracked elbows tested under closing mode and opening mode, respectively.

Thus, bending stress σ_b is evaluated from applied LLD which finally is used for calculation of J_e. Thus, in this approach only displacement vs. crack extension data is required for prediction of fracture property J-R curve and experimental load data is not required. For elbow ELTWEX16-4, the experimental LLD vs. crack extension data as shown in Fig. 6.3, is converted to fracture property i.e. J_{mat} vs. Δa plot as shown in Fig. 6.4.

These predicted J-R curves using load based and displacement based R6 approaches are compared with conventional J-R curve as shown in Fig. 6.4. It can be observed that predicted J-R curves by load based approach is under predicting the fracture property J-R curve while displacement based approach is over predicting. The reason of deviation of load based approach is that load is not an appropriate parameter in plastically deformed regime to represent the crack driving force J as explained in detail in Chapter 5. However, the deviation of displacement based R6 approach from conventional value suggests a probable modification in this proposed displacement based approach.

6.7.3 Reason of Deviation of Displacement Based R6 Approach

In the previous chapter it was observed that predictions of J-R curves by displacement based R6 approach are in very good agreement with conventional values for all the pipes. However, here the predictions by this R6 approach for the elbow ELTEEX16-4 is showing significant deviation from conventional J-R curve. Thus, an attempt is made to investigate the possible reason of not working of the displacement based approach for the elbow.

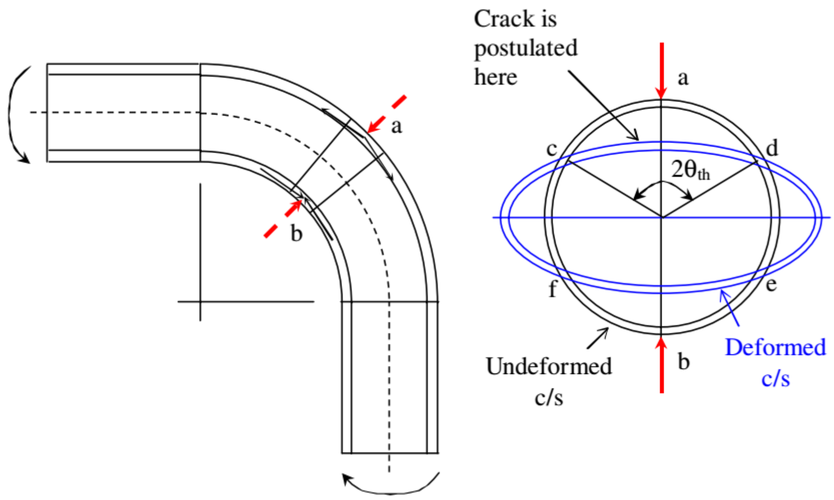

Fig. 6.5. Schematic representation of weakening of an elbow under closing mode of moment [121]

It should be noted that the uncracked bending stress σ_b is calculated using the Eqn. (6.14), which is based on the assumption that the cracked cross section will remain circular during loading. Though, it is observed by Chattopadhyay et. al. [121] that if elbow is subjected to closing mode of moment with some threshold crack size $2\theta_{th}$ then its load carrying capacity is weakened significantly due to ovalization of cross section as shown schematically in Fig. 6.5. Thus, the inherent assumption of circular cross section is not valid for elbows. Applied LLD is used for calculation of reference strain ε_{ref} and further this ε_{ref} is used for estimation of reference stress σ_{ref}, which is finally used for calculation of bending stress σ_b. Hence, the calculation is based on the assumption that the crack section at crack is circular while it has actually turned to oval shape because of loading configuration and significant plastic deformation. In reality, this shape change has caused significant reduction in the load carrying capacity of the cross section. Thus the prediction of the load from LLD based on circular cross section is an erroneous approach. This approach will give significant over prediction of the bending stress/load because of the present ovalization in closing mode of the loading. This over

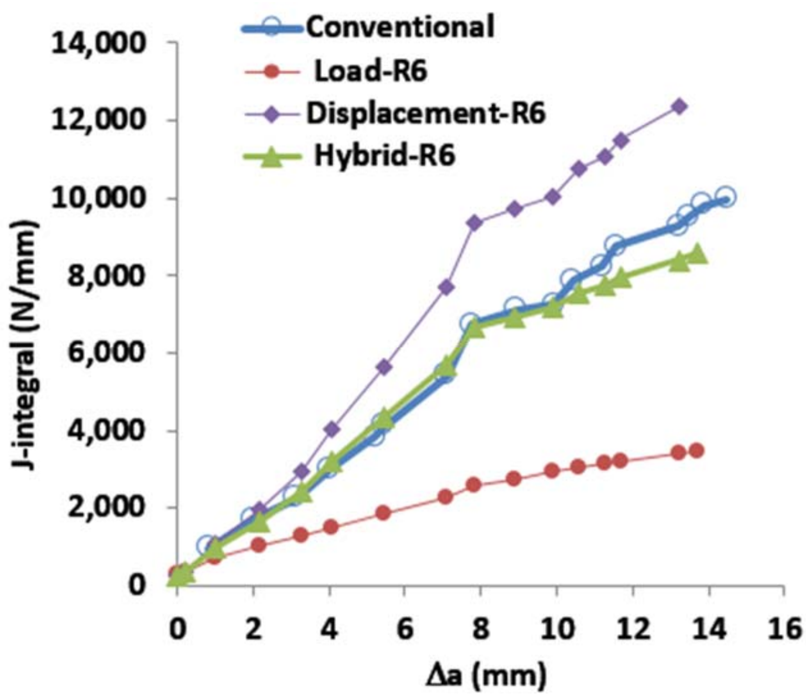

Fig. 6.6. J-R curve by hybrid approach is in agreement with conventional one for elbow ELTWEX16-4

prediction of σ_b will lead to higher estimate of K_I or J_e, which will eventually lead to significant over prediction of material fracture toughness J_{mat} based on relation, $J_{mat}(\Delta a) = J_e[f(L_r)]^{-2}$ as shown in Fig. 6.4.

6.7.4 Displacement-Load (Hybrid) Based Approach

It is observed that using the LLD for calculation of σ_b and further K_I is not an appropriate approach in case of an elbow.

a) Load based approach for J-elastic

Instead of LLD, directly experimental measured load P should be used for more accurate prediction of bending stress σ_b and consequent K_I using Eqns. (3.1) and (3.2) respectively. Thus, load based approach is adopted for calculation of stress intensity factor K_I and consequent J-elastic, $J_e = K_I^2/E'$.

b) **Displacement based approach for normalized loading 'L_r'**

It should be noted that displacement is used for calculation of reference strain and reference stress and finally for calculating the L_r. So L_r and $f_1(L_r)$ is predicted by displacement based approach. The Eqn. (4.1), $J_{mat}(\Delta a) = J_e[f(L_r)]^{-2}$ is used for calculation of fracture property J_{mat}.

First term J_e is calculated by using experimental load P, while second term $f(L_r)$ is evaluated by displacement based approach using experimental LLD. Thus, this methodology is termed as, "hybrid approach" because it is using both the experimental results load and displacement with relevant crack extension data. Comparison of hybrid based calculation with other approaches are shown in Fig. 6.6. It can be observed that prediction by hybrid approach is in better agreement with conventional J-R curve than load based and displacement based approaches for the elbow ELTWEX16-4.

6.8 Results

6.8.1 Different Parameters in the Steps of J_{mat} - Estimation

Relevant experimental parameters crack initiation load P_i and corresponding LLD Δ_i are given in Table 6.1 for all the elbows. Different important parameters e.g. non-dimensional parameter 'k', normalized reference strain $\varepsilon_{ref(i)}/\varepsilon_y$, normalized reference stress, $L_{r(i)}$ and J-elastic $J_{e(i)}$ evaluated in the steps of determination of J-R curve are also shown in the table. It should be noted that the parameters like normalized reference stress $L_{r(i)}$ and J-elastic $J_{e(i)}$ are

Table 6.1. Different parameters at crack initiation point during J-R curve calculation for the elbows

Elbow Designation	P_i (KN)	Δ_i (mm)	'k'	$\varepsilon_{ref(i)}/\varepsilon_y$	$L_{r(i)} = \sigma_{ref(i)}/\sigma_y$	$J_{e(i)}$ (N/mm)
ELTWEX16-4	1004.16	22.81	1.05	6.43	0.88	173.58
ELTWEX16-5	741.1	21.0	0.98	5.52	0.76	249.58
ELTWIN16-1	639.48	19.26	0.77	4.62	0.64	75.44
ELTWIN16-2	607.43	24.8	0.71	5.47	0.75	165.81
ELTWIN8-1	114.26	27.81	0.88	6.66	0.94	28.69

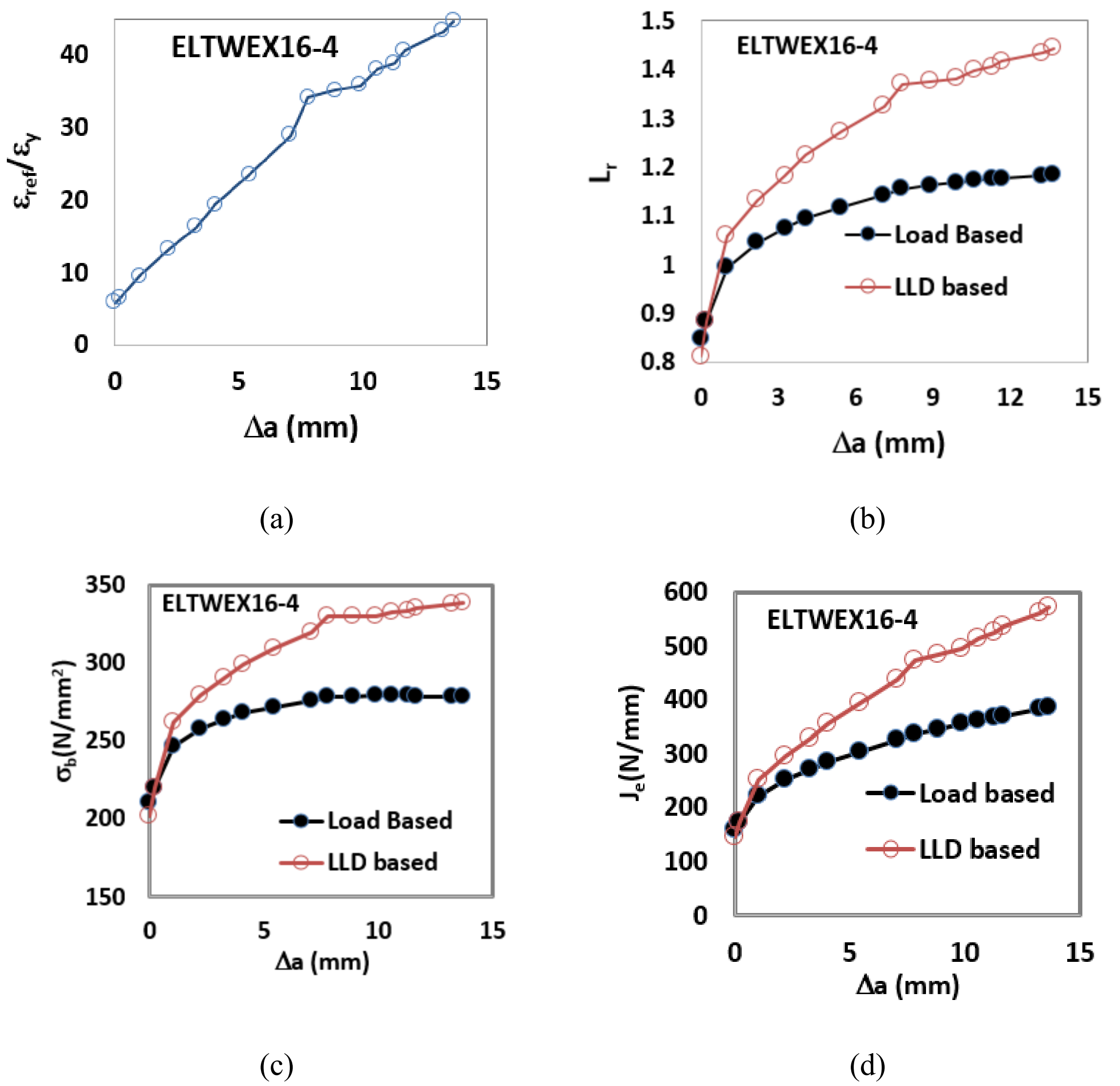

Fig. 6.7. Variation of different parameters with crack extension Δa for elbow ELTWEX16-4. (a) Normalized reference strain, $\varepsilon_{ref}/\varepsilon_y$. (b) Normalized reference stress, $L_r = \sigma_{ref}/\sigma_y$. (c) Bending stress, σ_b for uncracked section. (d) J-elastic, J_e calculated by different methods.

identical for load based and displacement based approaches because the loading level is within elastic regime. In the elastic regime, reference stress is in elastic limit i.e. $P \leq P_L$ or $\sigma_{ref} \leq \sigma_y$. Hence, reference stress σ_{ref} is linear to reference strain ε_{ref} as explained schematically in Fig. 5.4.

Variation of different important parameters namely normalized reference strain $\varepsilon_{ref(i)}/\varepsilon_y$, normalized reference stress, $L_{r(i)}$, bending stress σ_b, and J-elastic $J_{e(i)}$with crack extension are shown in Fig. 6.7 for elbow ELTWEX16-4. The parameters are initially in agreement near crack initiation point because of elastic loading regime where load based and displacement based approaches yield identical results. However, on higher crack growth range, the significant differences in the parametric values are quite evident because of large scale plastic deformation.

6.8.2 J-R Curves for Remaining Elbows

Hybrid approach is also employed for calculation of J-R curves for remaining four elbows. Experimental fracture data of load and LLD curves with relevant crack extension is shown in Fig. 6.8 for the elbow ELTWEX16-5. The calculated J-R curves using this fracture data by different approaches are shown in Fig. 6.9. Similarly, for remaining 16 inch elbows with intrados cracks, these curves are shown in Fig. 6.10 and Fig. 6.11 for elbow ELTWIN16-1, and, in Fig. 6.12 and Fig. 6.13 for elbow ELTWIN16-2. For an 8 inch elbow ELTWIN8-2 investigated, the experimental load and LLD vs. crack extension data are plotted in Fig. 6.14 and calculated J-R curves using this experimental data by the different proposed approaches are shown in Fig. 6.15.

It can be observed that the predictions of J-R curves using hybrid approach are in better agreement with conventional values compare to both load based and displacement based R6.

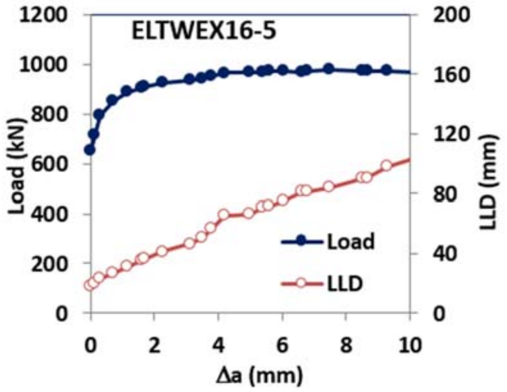

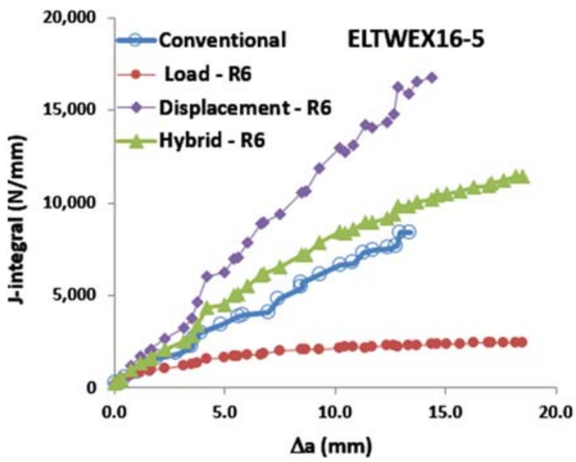

Fig. 6.8. Experimental load and LLD curves with corresponding crack growth for elbow ELTWEX16-5

Fig. 6.9. J-R curves calculated by different methods for elbow ELTWEX16-5

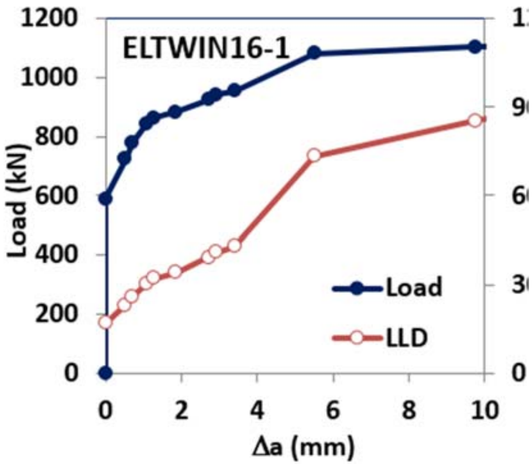

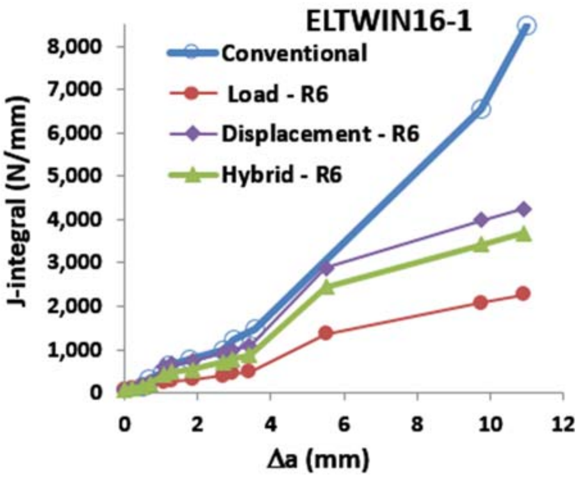

Fig. 6.10. Experimental load and LLD curves with corresponding crack growth for elbow ELTWIN16-1

Fig. 6.11. J-R curves calculated by different methods for elbow ELTWIN16-1

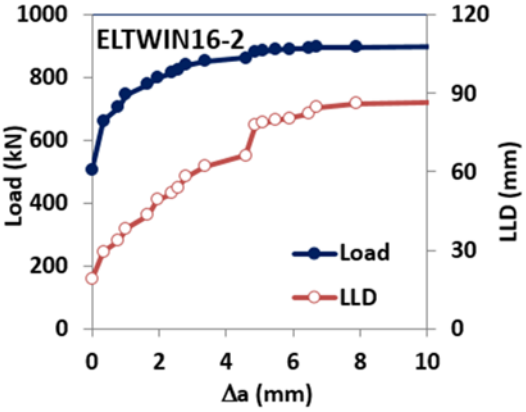

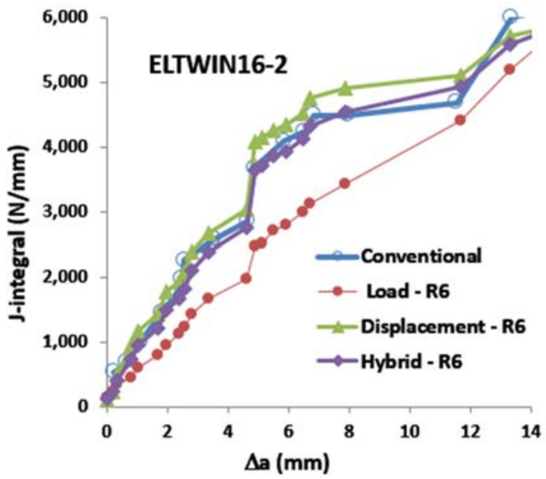

Fig. 6.12. Experimental load and LLD curves with corresponding crack growth for elbow ELTWIN16-2.

Fig. 6.13. J-R curves calculated by different methods for elbow ELTWIN16-2.

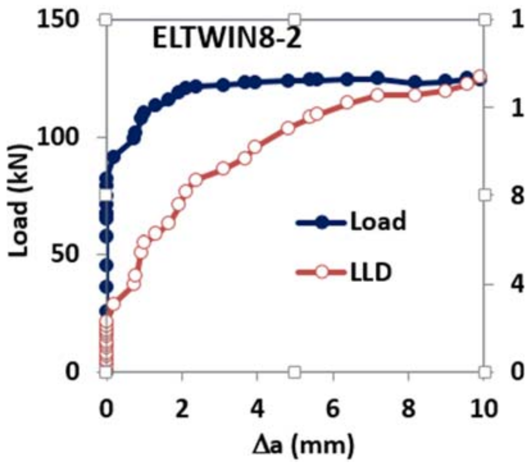

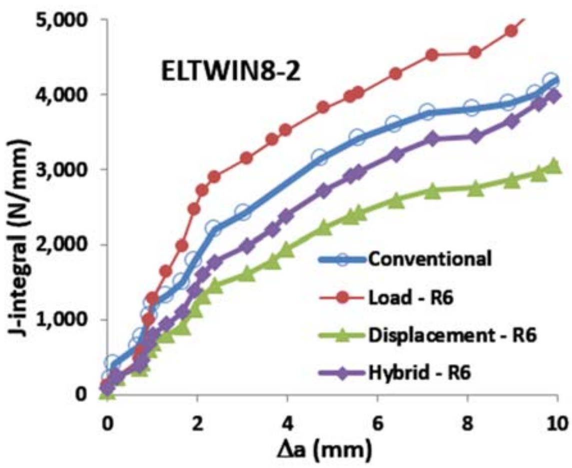

Fig. 6.14 Experimental load and LLD curves with corresponding crack growth for elbow ELTWIN8-2.

Fig. 6.15. J-R curves calculated by different methods for elbow ELTWIN8-2.

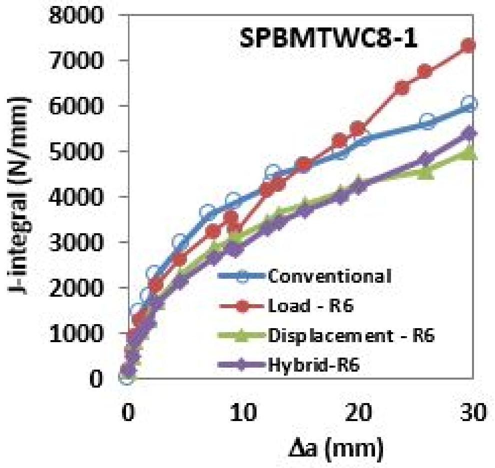

(a)

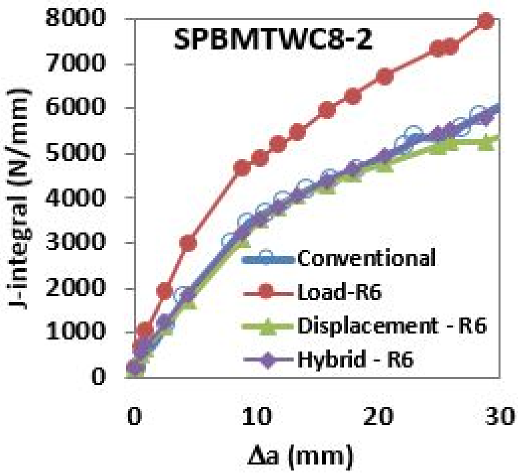

(b)

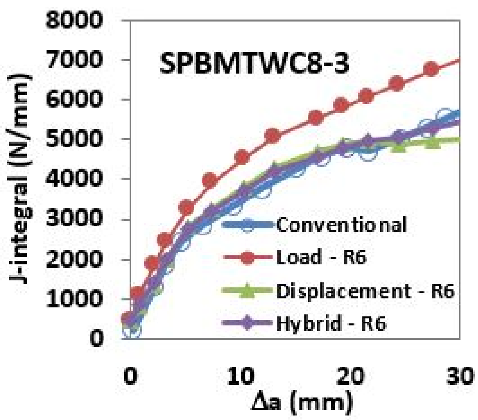

(c)

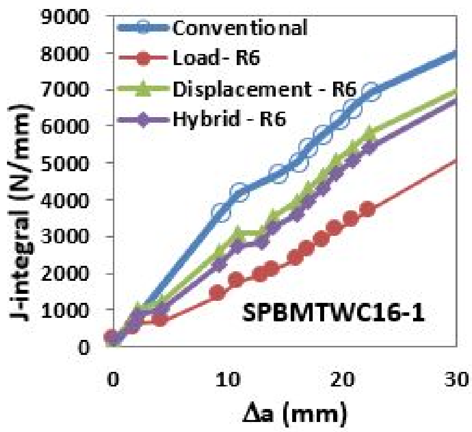

(d)

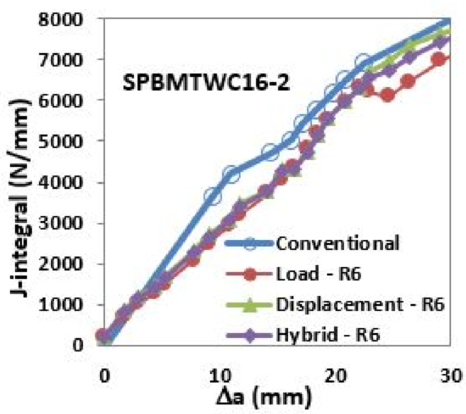

(e)

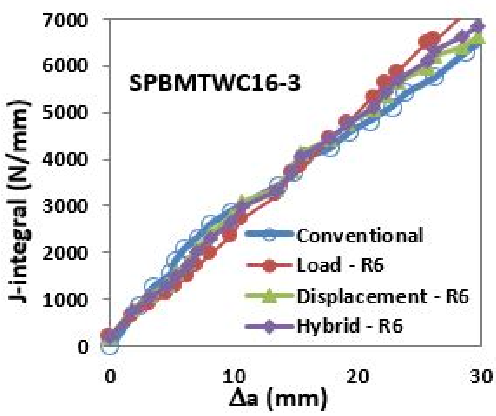

(f)

Fig. 6.16. Comparative plot of J-R curves calculated by hybrid- R6 approach for pipes. Figures (a), (b), (c), (d), (e) and (f) respectively for pipes SPBMTWC8-1, SPBMTWC8-2, SPBMTWC8-3, SPBMTWC16-1, SPBMTWC16-2 and SPBMTWC16-3.

6.8.3 J-R Curves for Pipes by Hybrid Approach

It is already observed in previous chapter that the predictions by displacement cased approach are in good agreement with conventional values for all six pipes. However, for elbows instead of displacement based approach, prediction by hybrid approach is in good agreement with conventional values. Thus, this hybrid approach is extended to the pipes for prediction of J-R curves. These J-R curves are compared with J-R curves predicted by other approaches and shown in Fig. 6.16 for all pipes. It can be observed that predictions by hybrid approach are in very good agreement with conventional J-R curves approaches for all the pipes also.

6.9 Comparison of Different Approaches for Calculation of J-R curve

In conventional approach of calculation of J-R curve from experimental fracture test data, load and load line displacement (LLD) with related crack extension are required. Load and LLD curve is integrated using relevant η and γ functions. The values of these functions depend on the instantaneous geometry, so it has to be updated for changed crack size due to crack growth. Hence, this approach requires both experimental load and LLD data as shown in part A of Fig. 6.17, with related crack extension. This is fundamentally appropriate approach because it is based on the energy consumed by the cracked component during the crack extension.

In the usual R6 approach, for assessment of failure, the normalized parameters, like crack driving force, $K_r = K_e/K_{mat}$ and remote loading, $L_r = P/P_L$ are evaluated by the applied load only. As shown in Eqn.(4.1) $J_{mat}(\Delta a) = J_e[f(L_r)]^{-2}$, material fracture toughness, J_{mat} is multiplication of two variables J elastic, J_e and functional value of L_r, $[f(L_r)]^{-2}$. Thus, the value of fracture toughness J_{mat} at this crack extension point Δa is dependent on these two parameters. In established R6 methodology, both these parameters are evaluated by using the instantaneous value of experimental load P with crack extension Δa as shown in part B of Fig. 6.17. Thus, this approach is termed as load based R6 approach.

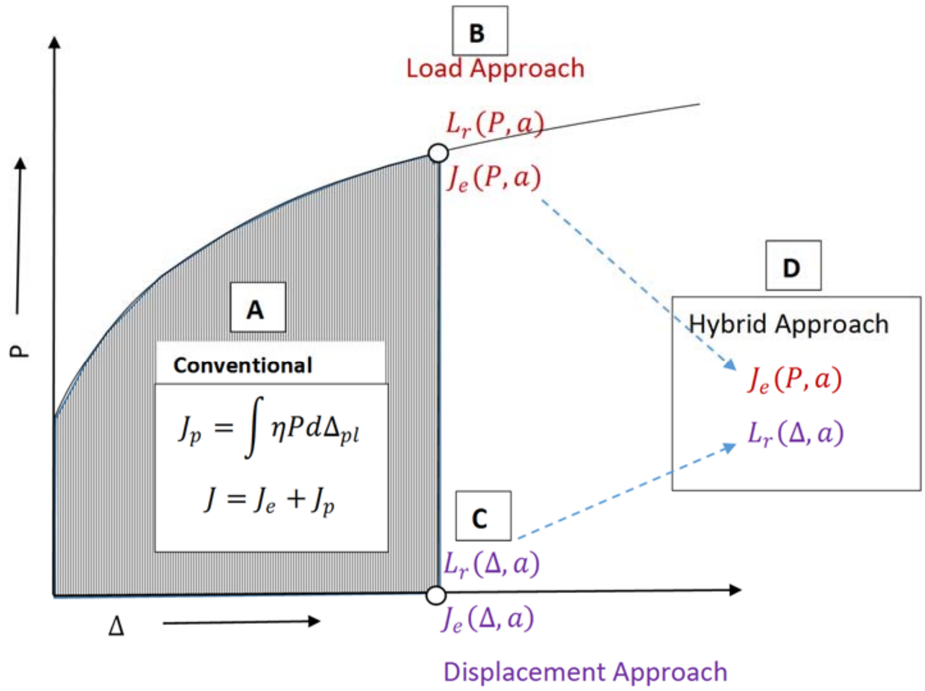

Fig. 6.17. Conventional and different R6 –approaches for calculation of J-R curve using experimental load and displacement data

In displacement based approach, both these parameters J_e and L_r are evaluated by the instantaneous experimental LLD value Δ at this crack extension value Δa as shown in part C of Fig. 6.17. The extent of plastic deformation is better quantified by the applied displacement unlike by the applied load in load based approach. Hence, this approach is appropriate in prediction of material fracture toughness in the regime of significant plastic deformation near crack tip. However, the limitation of this approach is that in this approach bending stress σ_b is also calculated by applied displacement. In case of significant plastic deformation and/or geometric hardening or softening, this approach is not able to correctly predict bending stress σ_b.On using this parameter to calculate J_e, it results in to erroneous prediction of fracture toughness J_{mat}.

This limitation of displacement based approach is corrected by calculating the J elastic (J_e) by using the experimental load P like load based approach. Therefore, to have the best predictions, displacement based approach is used for calculating the normalized loading L_r, and load based approach is adopted for calculating J_e as shown in part D of Fig. 6.17. Thus, this approach is termed as hybrid approach, which significantly improves the prediction of J-R curve.

6.10 Closure

Predictions of J-R curves based on displacement based R6 approach were found to be in very good agreement with conventional values for all the pipes in Chapter 5. This approach as well as load based approach are extended to cracked elbows for which all necessary experimental data like load, LLD and crack growth were already available. The predictions of J-R curves by displacement based and load based R6 approaches are found to be showing significant deviation from conventionally calculated values.

The inability of displacement based approach for estimation of fracture property lead to the hybrid approach when displacement and load both are required for calculation. This inability is attributed to ovalization of the cross section of elbow. Experimental load, P is used for determination of stress intensity factor, K_I and consequently J_e. However for determination of reference stress, σ_{ref}, applied LLD is used like displacement based approach. The calculated J-R curves using hybrid approach, are found to be in very good agreement with conventional values for all pipes and elbows. Thus, hybrid R6 approach is proposed as the most appropriate methodology for estimation of fracture property J-R curve using R6 method.

Chapter 7

Discussions and Conclusions

7.1 Discussions

For obtaining the material fracture property J-R curve for a ductile material, a fracture test is conducted and test data like load, Load Line Displacement (LLD), crack growth, etc., are obtained. These test data are post processed using conventional approach of integration of load vs. LLD curve using geometry functions η and γ. The issue with this methodology is that η and γ functions are available for very limited geometries with specific loading configurations. Determination of fracture property is not possible for any arbitrary geometries without having these functions for these cases. Thus, an extensive literature survey is conducted for seeking an alternative approach to bypass the need of these functions for post processing the fracture test data.

In this thesis, an alternative and simpler approach to post process the fracture test data is proposed and validated. The proposed methodology is based on the R6 failure assessment diagram (FAD). Usually, R6 FAD is used for prediction of failure in terms of ductile initiation in elastic plastic fracture regime. The failure assessment line $f(L_r)$ is normalised form of J-integral in terms of applied loading P. On increasing the load P, J-integral increases and failure point is achieved when applied J-integral becomes equal to fracture initiation toughness J_{ic}. The loading point corresponding to this failure point is crack initiation point for that cracked geometry and gives crack initiation load. Usage of this methodology is reversed for achieving the main objective of the present investigation. Fracture test data is providing the crack initiation load. Using this crack initiation load P_i, ductile initiation toughness J_{ic} is obtained. Finally this methodology is adopted for all loading points and experimental load vs. crack extension curve is converted to fracture property J-R curve i.e. J_{mat} vs. Δa curve. The final proposed methodology is achieved by step wise investigation using different fracture test data. First investigation is attempted using conventional approach of R6 using experimental load with relevant crack growth data. Later LLD, and finally both of load and LLD are utilized for calculation of fracture property. This investigation is clearly divided in four parts as shown in Fig. 7.1 and explained in following points:

1. Efficacy of the R6 failure assessment diagram is assessed for the piping material SA333Gr6 in determination of crack initiation load in elastic plastic fracture regime. (Chapter 3.)
2. In this part, an innovative approach for calculating the J-R curve using R6 failure assessment diagram is proposed. Using this methodology, entire load vs. crack extension curve is converted to fracture property J_{mat} vs. crack extension curve for total six cracked pipes. (Chapter 4.)
3. Based on extensive literature survey, it is established that for highly plastically deformed cases the applied strain/displacement is a better parameter to quantify the fracture response instead of conventionally used load parameter. Hence, displacement based R6 approach is proposed in this investigation for determination of fracture property J-R curve for cracked pipes using LLD vs. crack growth data. (Chapter 5.)
4. Based on adoption of these R6 based methods for determination of fracture property for elbows, it is found that displacement based approaches has limitations for elbows. Hence a 'hybrid' approach is proposed where load is used for determination of crack driving force characterized by stress intensity factor K_I, whereas displacement is used for calculating loading parameter 'L_r'. (Chapter 6.)

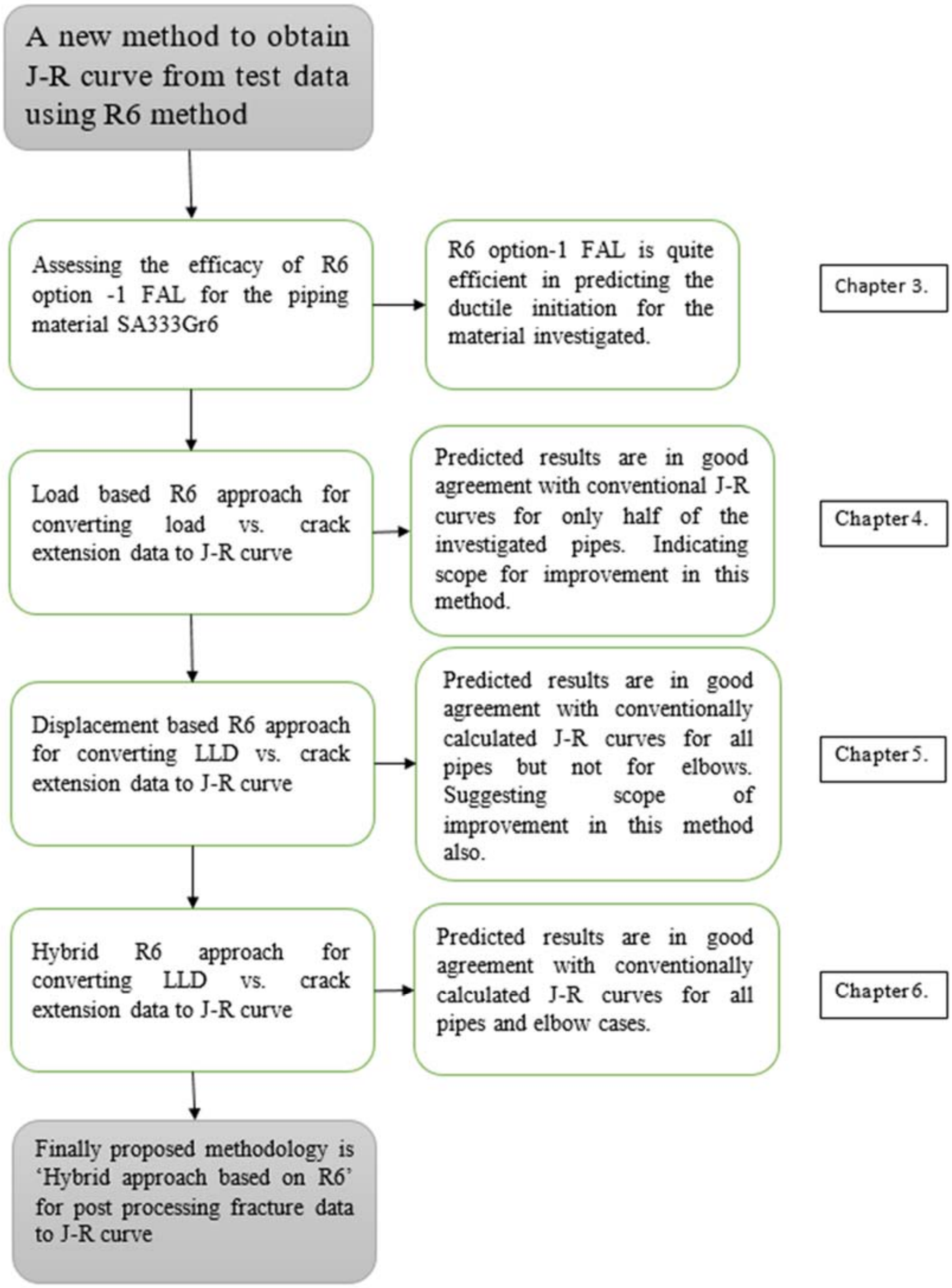

Fig. 7.1. Hierarchy of the evolvement of the hybrid approach based on R6 FAD

In all the proposed R6 based approaches, the closed form expressions of linear stress intensity factor (SIF), K_I and limit load ,P_L, are required. Hence, on using these R6 based approaches, the closed form expressions of limit load P_L are required which are available for wider range of geometries and loading configurations than η and γ functions. It should also be noted that that η and γ functions are obtained generally by using first and second order derivatives of limit load expressions [12], which may exaggerate the approximation error associated with the limit load expressions. Hence, using the proposed approaches with directly limit load P_L, are better than conventional approach to avoid those possible errors related with limit load based η and γ functions.

7.2 Conclusions

The conclusion for each chapter is already explained at the last section of every chapter. However, most salient points observed in the course of this investigation are outlined below.

1. R6 failure assessment diagram option-1 curve is found to be efficient in predicting the crack initiation load which are in good agreement with corresponding experimental values. This observation shows that R6 is quite efficient in predicting the ductile initiation point in elastic-plastic fracture regime for the investigated piping material SA333Gr6.
2. The load based predictions are found to be, in very good agreement with conventionally calculated J-R curves already reported in the literature for three out of the total six investigated pipes. The significant deviation of remaining three cases shows that there is a scope of improvement in the proposed methodology.
3. The predicted J-R curves using displacement based R6 approach are found to be in very good agreement for all six investigated pipes with conventionally calculated J-R curves.

4. For getting material fracture property J-R curve using displacement based approach, only LLD vs. crack growth data is needed as input fracture test data. Experimental load data is not required for this R6 approach unlike conventional η-factor approach.
5. On adaptation of displacement based R6 approach for the elbows, it is observed that the predicted J-R curves are not in good agreement with conventional values for elbows especially under closing moment loading. On further investigation, the reason of the deviation is found to be the severe ovalization of elbow at cracked cross section. Because of this ovalization, the prediction of J −elastic (J_e) from LLD tends to be erroneous, which results in the wrong prediction of J-R curve. Hence, a 'hybrid approach' is proposed where parameter L_r is predicted using the applied LLD while another parameter J-elastic (J_e) is calculated using experimental load P.
6. The predicted J-R curves using hybrid R6 approach, are found to be in very good agreement with conventionally calculated J-R curves for all the pipes and elbows. Hence, hybrid approach is recommended as a final methodology for prediction of J-R curves from fracture test data using R6 method.

7.3 Contributions

1. An innovative methodology based on R6, is proposed to calculate the fracture property J-R curve using fracture test data without the need of η and γ functions unlike conventional approach.
2. An innovative approach is developed and utilized to calculate the reference stress and reference strain for the deeply cracked cases using simple beam theories.
3. The utility of R6 is extended from just failure assessment to calculation of fracture toughness J_{mat}.

7.4 Recommendations for Future Works

A complete methodology is proposed and validated for post processing the fracture test data to material fracture property J-R curve for cracked pipes and elbows under bending moment. These cases were chosen for investigation because of the available fracture test data and corresponding conventionally calculated J-R curves using those test data. However, following complementary studies will corroborate and extend the utility of this proposed approach.

1. The proposed methods may be employed for the prediction of η factor in a simpler way than conventional approach. First, the crack driving force J for the loading P, may be predicted by the R6 method. By using the load vs. LLD curve and predicted J, η factor can be calculated in a simpler way. In this procedure, the effect of crack extension in terms of γ factor on J, has to be neglected.
2. In this work, elastic beam theory approach is utilized for proposing methodology to calculate references strain ε_{ref} and J_{mat} using experimental LLD in this work. It is recommended to validate this methodology by extensive finite element analyses. This work will substantiate the proposed methodology.
3. This investigation is performed for piping material SA333Gr6, which is the material of investigated pipes and elbows. For this purpose, smooth hardening fit is done in this work for material tensile true stress strain data of piping material SA333Gr6 from yield point (including Luder regime) to ultimate true stress point. This methodology may be attempted for other materials.
4. In recent investigations, a relationship between ε_{ref} and crack driving force J-integral is derived for very shallow cracked cases using extensive finite element analyses and, strain based R6 failure assessment diagram is proposed. That approach is not applicable for deeply cracked cases because of the assumptions involved. The

proposed approach of this thesis may be utilized to calculate a reference strain based R6 failure assessment diagram for deeply cracked cases.

5. Under this investigation, deeply cracked pipes and elbows were analyzed for determination of reference strain ε_{ref} from applied LLD. The proposed methodology requires the assumption that all the deformation is concentrated at the cracked section only. This assumption is valid for larger crack sizes but not for shallower cracks. Some recent investigations have proposed similar methodology for the very shallow cracks where the reference strain ε_{ref} is assumed to be same as strain at remote uncracked section significantly away from the crack. For mid-sized crack both of these assumptions will be violated partially. Hence, the investigation of mid-sized cracked cases may be attempted, which may involve some modification in the proposed methodology.
6. All the investigated pipes and elbows were tested purely/predominantly under bending moment. This methodology may be attempted for other loading modes like tension, combinations of loading and bending, etc. The efficacy of the proposed methodology may also be tested with fracture test data of standard fracture specimens, miniature specimens, etc., for getting material fracture property J-R curve.

References

[1] G. R. Irwin, “Anaysis of stresses and strains near the end of a crack traversing a plate,” *Journal of Applied Mechanics,* vol. 24, pp. 361-364, 1957.

[2] H. M. Westergaard, “Bearing pressures and cracks,” *Journal of Applied Mechanics,* vol. 6, pp. 49-53, 1939.

[3] J. R. Rice, “A path independent integral and the approximate analysis of strain concentraion by notches and cracks,” *Journal of Applied Mechanics,* vol. 35, pp. 379-386, 1968.

[4] J. W. Hutchinson, “Singular behaviour at the end of a tensile crack tip in a hardening material,” *Journal of the Mechanics and Physics of Solids,* vol. 16, pp. 13-31, 1968.

[5] B. F. Beaudoin, D. F. Quinones and T. C. Hardin, “Leak-before-break application in US light water reactor balance-of-plant piping,” *International Journal of Pressure Vessesls and Piping,* vol. 43, pp. 67-83, 1990.

[6] B. L. Kee and J. S. Nathwani, “Leak-before-break approach for large diameter heat transport piping,” Darlington NGS A, 1985.

[7] N. P. O'Dowd and C. F. Shih, “Family of crack tip fields characterized by a triaxiality parameter - I: structure of fields.,” *Journal of Mechanics and Physics of Solids,* vol. 39, pp. 898-1015, 1991.

[8] J. A. Joyce and R. E. Link, “Application of two parameter elastic-plastic fracture mechanics to analysis of structures,” *Engineering Fracture Mechanics,* vol. 57, no. 4, pp. 431-446, 1997.

[9] “ASTM E1820-99a: Annual book ASTM standards,” in *Standard test method for*

measurement of fracture toughness., vol. vol. 03.01, 1999.

[10] H. A. Ernst, P. C. Paris and J. D. Landes, "Estimations of J-integral and tearing modulus T from a single specimen test record," in *Fracture Mechanics: Thirteenth Conference, ASTM STP 743*, Philadelphia: American Society for Testing and Materials, 1981.

[11] J. Chattopadhyay, B. K. Dutta and H. S. Kushwaha, "Derivation of gamma parameter from limit load expressions of cracked component to evaluate J-R curve," *International Journal of Pressure Vessels and Piping,* vol. 78, pp. 401-427, 2001.

[12] J. Chattopadhyay, B. K. Dutta and H. S. Kushwaha, "New eta and gamma functions to evaluate J-R curve from cracked pipes and elbows. Part I: theoretical derivations.," *Engineering Fracture Mechanics,* vol. 71, pp. 2635-2660, 2004.

[13] V. Tvergaard and A. Needleman, "Analysis of the cup- cone fracture in a round tensile bar," *Acta. Metall.,* vol. 32, pp. 157-169, 1984.

[14] B. K. Dutta, S. Guin, M. K. Sahu and M. K. Samal, "A phenomenological form of the q2 parameter in the Gurson model," *International Journal of Pressure Vessels and Piping,* vol. 85, no. 4, pp. 199-210, 2008.

[15] R6, "Assessment of the integrity of structures containing defects, Revision 4, including subsequent updates," Gloucester, UK, 2013.

[16] A. R. Dowling and A. C. Townley, "The effects of defects on structural failure: a two-criterion approach.," *International Journal of Pressure Vessels and Piping,* vol. 3, pp. 77-107, 1975.

[17] R. P. Harrison, K. Loosemore and I. Milne, "Assessment of the Integrity of Structures Containing Defects," CEGB Report R/H/R6-Rev.1, London, 1977.

[18] R. A. Ainsworth, "The Assessment of defects in dtructures of strain hardeing material," *Engineering Fracture Mechanics,* vol. 19, no. 4, pp. 633-642, 1984.

[19] J. Chattopadhyay, B. K. Dutta and H. S. Kushwaha, “Experimental and Analytical Study of Three Point Bend Specimens and Throughwall Cicumferentially Cracked Straight Pipes,” *International Journal of Pressure Vessels and Pipings,* vol. 77, pp. 455-471, 2000.

[20] J. Chattopadhyay, T. Pavan Kumar, B. K. Dutta and H. S. Kushwaha, “Fracture Experiments on Throughwall Cracked Elbows under In-plane Bending Moment: Test Results and Theoretical/Numerical Analyses,” *Engineering Fracture Mechanics,* vol. 72, pp. 1461-1497, 2005.

[21] T. L. Anderson, Fracture Mechanics: Fundamentals and Applications, 3rd Ed. ed., New York: CRC Press, 2005.

[22] P. J. Budden, “Validation of the new R6 strain-based failure assessment diagram approach using finite element data,” British Energy, Gloucester, 2009.

[23] P. J. Budden and R. A. Ainsworth, “The shape of strain based failure assessment diagram,” *International Journal of Pressure Vessels and Piping,* vol. 89, pp. 59-66, 2012.

[24] P. K. Singh, J. Chattopadhyay, H. S. Kushwaha, S. Tarafder and V. R. Ranganath, “Tensile and fracture properties evaluation of PHT system piping material of PHWR,” *Internaitonal Journal of Pressure Vessels and Piping,* vol. 75, pp. 271-280, 1998.

[25] “ASTM E8-91: Annual book of ASTM standards,” in *Test methods for tension testing of metallic materials, vol. 03.01*, 1991.

[26] S. Tarafder, S. Shivaprasad , M. Tarafder, P. Prasad, V. R. Raghunath and D. Swapan, “Specimen size and constraint effect on J-R curves of SA333Gr-6 Steel,” Jamshedpur, India, 2000.

[27] J. Chattopadhyay, H. S. Kushwaha and E. Roos, “Some recent developments on

integrity assessment of pipes and elbows. Part II: Experimental investigations," *International Journal of Solids and Structures,* vol. 43, pp. 2932-2958, 2006.

[28] J. Chattopadhyay, "Improved J and COD estimation by GE/EPRI method in elastic to fully plastic transition zone.," *Engineering Fracture Mechanics,* vol. 73, pp. 1959-1979, 2006.

[29] J. Chattopadhyay, A. K. S. Tomar, B. K. Dutta and H. S. Kushwaha, "Elastic-plastic J and COD estimation schemes for throughwall circumferentially cracked elbow under in-plane closing moment," *Engineering Fracture Mechanics,* vol. 72, pp. 2186-2217, 2005.

[30] T. V. Pavankumar, M. K. Samal, J. Chattopadhyay, B. K. Dutta, H. S. Kushwaha, E. Roos and M. Seidenfuss, "Transferability of fracture parameters from specimens to component level," *International Journal of Pressure Vessels and Piping,* vol. 82, pp. 386-399, 2005.

[31] T. V. Pavankumar, J. Chattopadhyay, B. K. Dutta and H. S. Kushwaha, "Transferability of specimen J-R curve to straight pipes with throughwall circumferential flaws.," *International Journal of Pressure Vessels and Piping,* vol. 79, pp. 127-134, 2002.

[32] J. Chattopadhyay, A. K. S. Tomar, B. K. Dutta and H. S. Kushwaha, "Closed form collapse moment equation of throughwall circumferentially cracked elbows subjected to in-plane bending moment," *ASME Journal of Pressure Vessel Technology,* vol. 126, pp. 307-317, 2004.

[33] A. Gurson, "Continuum theory of ductile rupture by void nucleation and gorwth: Part-I-Yield criteria and flow rules for porous ductile media," vol. 105, pp. 2-15, 1977.

[34] I. N. Sneddon, "The distribution of stress in the neighbourhood of a crack in an elastic solid," *Proceedings, Royal Society of London,* Vols. A-187, pp. 229-260, 1946.

[35] M. L. Williams, “On the stress distribution at the base of a stationary crack,” *Journal of Applied Mechanics,* vol. 24, pp. 109-114, 1957.

[36] J. R. Rice and G. F. Rosengren, “Plane strain deformation near a crack tip in a power law hardeing material,” *Journal of the Mechanics and Physics of Solids,* vol. 16, pp. 1-12, 1968.

[37] J. W. Hutchinson, “Fundamentals of the phenomenological theory of nonlinear fracture mechanics,” *Journal of Applied Mechanics,* vol. 79, pp. 1042-1051, 1983.

[38] X. K. Zhu and S. K. Jang, “J-R curve corrected by load-independent constraint parameter in ductile crack growth,” *Engineering Fracture Mechanics,* vol. 68, pp. 285-301, 2001.

[39] C. Betegen and J. W. Hancock, “Two parameters of characteristics of elastic-plastic crack-tip field,” *Journal of Applied Mechanics,* vol. 58, pp. 104-110, 1991.

[40] N. P. O'Dowd and C. F. Shih, “Family of crack tip fields characterized by a triaxiality parameter - II: structure of fields.,” *Journal of Mechanics and Physics of Solids,* vol. 40, pp. 939-963, 1992.

[41] H. Clausmeyer, K. Kussmaul and E. Roos, “Influence of stress state on the failure behaviour of cracked components made of steel,” *ASME Applied Mechanics Reviews,* vol. 44, no. 2, pp. 77-92, 1991.

[42] W. Brocks and W. Schmitt, “Quantitative assessment of the role of crack tip constraint on ductile tearing,” in *American Society of Testing and Materials*, Philadelphia, 1993.

[43] Y. J. Chao and W. Ji, “Cleavage fracture quantified by J and A2, constraint effects in fracture theory and applications,” in *American Society for Testing and Materials*, Philadelphia, PA, 1995.

[44] N. O. Larrosa and R. A. Ainsworth, “A transferability approach for reducing excessive

conservatism in fracture assessments," *Engineering Fracture Mechanics,* vol. 174, pp. 54-63, 2017.

[45] J. Yang, "Matching of crack-tip constraint between standard and non-standard specimen," *Advances in Mechanical Engineering,* vol. 10, pp. 1-8, 2018.

[46] J. R. Rice, P. C. Paris and J. G. Merkle, "Some further results of J-integral analysis and estimates, in: Progress in Flaw Growth and Fracture Toughness Testing," in *ASTM STP 536, American Society for Testing and Materials*, Philadelphia, 1973.

[47] H. A. Ernst, P. C. Paris, M. Rossow and J. W. Hutchinson, "Analysis of load diplacement relation to determine J-R curve and tearing instabilities material properties, in:," in *Fracture Mechanics, ASTM STP, American Society for Testing and Materials*, Philadelphia, 1979.

[48] J. W. Hutchinson and P. C. Paris, "Stability analysis of J-controlled crack growth.," *In: Elastic–Plastic Fracture, ASTM STP 668.,* pp. 37-64, 1979.

[49] M. D. Rajab and A. Zahoor, "Fracture analysis of pipes containing full circumferential internal part-through flaw," *International Journal of Pressure Vessels and Piping,* vol. 41, pp. 11-23, 1990.

[50] J. Chattopadhyay, B. K. Dutta and H. S. Kushwaha, "New eta and gamma functions to evaluate J-R curve from from cracked pipes and elbows, Part II:experimental and numerical validation," *Engineering Fracture Mechanics,* vol. 71, pp. 2661-2675, 2004.

[51] J. Chattopadhyay, T. V. Pavankumar, B. K. Dutta and H. S. Kushwaha, "J-R curves from through-wall cracked elbow subjected to in-plane bending moment.," *Jounal of Pressure Vessel Technology, Transactions of ASME,* vol. 125, pp. 36-45, 2003.

[52] S. Webster and A. Bannister, "Stuructural integrity procedure for Europe - of the SINTAP programme overview," *Engineering Fracture Mechanics,* vol. 67, pp. 481-

554, 2000.

[53] BSi, “Guidance on Methods for Assessing the Accessibility of Flaws in Mettalic Structures,” London, 2000.

[54] P. Anderson, M. Bergman, B. Brickstad, L. Dahlberg, F. Nilsson and I. Sattari-Far, “A Procedure for Safery Assessment of Components with Cracks - Handbook,” Stockholm, 1996.

[55] H. Kobayashi, S. Sakai, M. Asano, K. Miyazaki, T. Nagasaki and Y. Takahashi, “Developement of a flaw evalation handbook of the high pressure institute of Japan,” *International Journal of Pressure Vessels and Piping,* vol. 77, pp. 929-936, 2000.

[56] H. Kobayashi and K. Kashima, “Overview of JSME flaw evaluation code for nuclear power plants,” *International Journal of Pressure Vessesls and Piping,* vol. 77, pp. 937-944, 2000.

[57] P. N. Li, Y. Lei, Q. P. Zhang and X. R. Li, “A Chinese structural integrity assessment procedure for pressure vessels containing defects,” *International Journal of Pressure Vessels and Piping,* vol. 77, pp. 945-952, 2000.

[58] T. L. Anderson and D. A. Osage, “API 579: a comprehensive fitness-for-service guide,” *International Journal of Pressure Vessesls and Piping,* vol. 77, pp. 953-963, 2000.

[59] “RSE-M Code. In-service inspection rules for the mechanical components of PWR nuclear islands. Appendix 5.4-analytical methods for calculating stress ingrity factors and J-inegral,” Paris, 2010.

[60] B. A. Bilby, A. H. Cotrell and K. H. Swinden, “The spred of plastic yield from a notch,” *Proceedings of the Royal Society London A,* vol. 444, pp. 461-482, 1963.

[61] P. T. Heald, G. M. Spink and P. J. Worthington, “Post yield fracture mechanics,” *Material Science and Engineering,* vol. 10, pp. 129-138, 1972.

[62] R. P. Harrison, K. Loosemore and I. Milne, “Assessment of the integrity of the structures containing defects. CEGB Report R-H-R6,” UK: Central Electricity Generation Board, 1976.

[63] R. P. Harrison, K. Loosemore and I. Milne, “Assessment of the Integrity of Structures Containing Defects,” Central Electricity Generating Board report, London, 1980.

[64] R. P. Harrison, K. Loosemoore, I. MIlne and A. R. Dowling, “Assessment of the Integrity of Stuctures Containing Defects,” CEGB Report R/H/R6-Rev.2, London, 1980.

[65] C. E. Turner, “A J-based design curve,” in *In Advances in Elastic - Plastic Fracture Mechanics*, Larson, Ed., 1980.

[66] N. L. Goldman and J. W. Hutchinson , “Fully Plastic Crack Problems: The Centre Cracked Strip Under Plain Strain,” *International Journal Solids Structures,* vol. 11, pp. 577-591, 1975.

[67] I. Milne, “Failure Assessment Diagrams and J Estimates: A Comparision for Ferritic and Austenitic Steels,” *CEGB report RD/L/2208N81,* 1982.

[68] C. F. Shih, “J-integral estimates for strain hardeing materials in antiplane shear using fully plastic solutions,” in *Mechanics of crack growth, ASTM STP 590*, 1976.

[69] N. L. Goldman and J. W. Hutchinson, “Fully plastic crack problems: The centre cracked strip under plane strain,” Cambridge Mass., February, 1974.

[70] J. C. Amazigo, “Fully plastic crack in an infinite body under antiplane shear,” Cambridge, Mass., December, 1973.

[71] C. F. Shih and J. W. Hutchinson, “Fully Plastic Solutions and Large Scale Yielding Estimates for Plane Stress Crack Problems,” *Journal of Engineering Materials and Technology,* vol. 98, pp. 289-295, 1976.

[72] J. M. Bloom and S. N. Malik, “"Procedure for the Assessment of the Integrity of Nuclear Pressure Vessels and Piping Containing Defects,",” Palo Alto, 1982.

[73] J. M. Bloom, “A procedure for the assessment of the structural integrity of nuclear pressure vessels,” *ASME Journal Presssure Vessel Technology,* vol. 105, pp. 28-34, 1983.

[74] J. M. Bloom, “Validation of a deformation plasticity failure assessment diagram approach to flaw evaluation. In: ‘‘Elastic–Plastic Fracture: Second Symposium, Volume-II-Fracture Resistance Curves and Engineering Applications, ASTM 803,’’,” in *American Society for Testing and Materials*, Philadelphia, PA, 1983.

[75] V. Kumar, M. D. German and C. F. Shih, “An Engineering Approach for Elastic–Plastic Fracture Analysis,” Palo Alto, 1981.

[76] I. Milne, “Failure analysis in the presence of ductile crack growth,” *Material Science Engineering,* vol. 39, pp. 65-79, 1979.

[77] R. K. Penny and D. L. Marriott, Design for Creep, New York: McGraw-Hill, 1971.

[78] A. G. Miller and R. A. Ainsworth, “Consistency of numerical results for power-law hardeing materials and the accuracy of the reference stress approximation of J,” *Engineering Fracture Mechanics,* vol. 32, pp. 233-247, 1989.

[79] I. Milne, R. A. Ainsworth, A. R. Dowling and A. T. Stewart, “Background to and validation of CEGB report R/H/R6—Revision 3,” *International Journal of Pressure Vessels and Piping,* vol. 32, pp. 105-196, 1988.

[80] I. Milne, R. A. Ainsworth, A. R. Dowling and A. T. Stewart, “Assessment of the integrity of structures containing defects,” *International Journal of Pressure Vessels and Piping,* vol. 32, pp. 3-104, 1988.

[81] U. Zerbst, R. A. Ainsworth and K. H. Schwalbe, “Basic principles of analytical flaw

assessment methods.," *International Journal of Pressure Vessels and Pipings.,* vol. 77, pp. 855-867, 2000.

[82] N. Nourpanah and F. Taheri, "Developement of reference strain approach for assessment of fracture response of reeled pipelines.," *Engineering Fracture Mechanics,* vol. 77, pp. 2337-2353, 2010.

[83] R. A. Ainsworth, F. Gutierrez-Solana and J. Ruiz Ocejo, "Analysis levels within the SINTAP defect assessment procedures," *Engineering Fracture Mechanics,* vol. 67, pp. 515-527, 2000.

[84] R. A. Ainsworth, "7.03- Failure Assessment Diagram Methods,," in *Comprehensive Structural Integrity*, 2003, pp. 89-132.

[85] British Energy, "Assessment of the Integrity of Structures Containing Defects," Gloucester, 2001.

[86] J.-H. An, S.-P. Hong, Y.-J. Kim and P.-J. Budden, "Elastic stresses for 90 degree elbows under in-plane bending," *International Journal of Mechanical Sciences,* vol. 53, pp. 762-776, 2011.

[87] T. C. Micheal, A. R. Verappan and S. Shanmugam, "Effect of ovality and variable wall thickness on collapse loads in pipe bends subjected to in-plane bending closing moment," *Engineering Fracture Mechanics,* vol. 79, pp. 138-148, 2012.

[88] A. Buckshumian, A. R. Verappan and S. Shanmugam, "Plastic collapse loads in shape-imperfect pipe bends under in-plane opening bending moment," *International Journal of Pressure Vessels and Piping,* Vols. 111-112, pp. 21-62, 2013.

[89] S. Zhang, X. Wang, B. Song and D. Zhao, "Limit analysis based on GM criterion for defect-free pipe elbow under internal pressure," *International Journal of Mechanical Sciences,* vol. 78, pp. 91-96, 2014.

[90] J.-J. Han, K.-H. Lee, N.-H. Kim, Y.-J. Kim, D. W. Jerng and P. J. Budden, “Comparison of existing plastic collapse load solutions with experimental data for 90o elbows,” *International Journal of Pressure Vessels and Piping,* vol. 89, pp. 19-27, 2012.

[91] Y.-J. Kim, Y.-I. Kim and T.-K. Song, “Finite element plastic loads for circumferential cracked pipe bends under in-plane bending,” *Engineering Fracture Mechanics,* vol. 74, pp. 643-668, 2007.

[92] Y. Lei, Y. Li and Z. Gao, “Global limit load solutions for thick-walled cylinders with circumferential cracks under combined internal pressure, axial force and bending moment, Part I: Theoretical solutions,” *International Journal of Pressure Vessels and Piping,* Vols. 114-115, pp. 23-40, 2014.

[93] Y. Lei, “Review of Limit Load Solutions for Defective Pipe Bends, Report E/REP/BBGB/0060/GEN/09 Revision 000,” EDF Energy Nuclear Generation, , Gloucester, UK, 2011.

[94] J.-H. An, Y.-J. Kim and P. Budden, “Elastic stress intensity factors and crack opening displacements for circumferential through-walled cracked elbows,” *Engineering Fracture Mechanics,* vol. 77, pp. 2821-2839, 2010.

[95] A. Zahoor, “Closed form expressions for fracture mechanics analysis of cracked pipes,” *ASME, Journal of Pressure Vessel and Technology,* vol. 107, pp. 203-205, 1985.

[96] J. Chattopadhyay, B. K. Dutta, H. S. Kushwaha, S. C. Mahajan and A. Kakodkar, “A database to evaluate stress intensity factors of elbows with throughwall flaws under combined internal pressure and bending moment,” *International Journal of Pressure Vessels and Pipings* , vol. 60, pp. 71-83, 1994.

[97] BS7019, “Guide for assessing the significance of flaws in metallic structures,” British Standards, London, 2005.

[98] American Petroleum Institute, “Fitness-for-Service,” 2007.

[99] H. A. Bratfos, “Use of strain-based ECA for the assessment of flaws in pipeline girth welds subjected to plastic deformations linepipes in hostile environments,” in *Proceedings of International conference on application and evaluation of high grade*, Yokohoma, Japan, 7-8 November, 2002.

[100] K.-H. Schwalbe, “The crack tip opening displacement and J integral under strain control and fully plastic conditions estimated by the engineering treatment model for plane stress tension,” in *ASTM STP, 1207*, Philadelphia, 1994.

[101] Y.-Y. Wang, D. Rudland, R. Denys and D. Horseley, “A preliminary strain-based design criterion for pipeline girth welds,” in *Proceedings of the IPC'02, 4th international pipeline conference, Calgary, September 29–October 3, 2002*, Newyork: ASME;2002, 2002.

[102] D. Linkens, C. L. Formby and R. A. Ainsworth, “A strain-based approach to fracture assessment—example applications,” in *Proceedings of fifth International Conference on engineering structural integrity assessment, EMAS*, Cambridge, 2000.

[103] K. R. Jayadevan, E. Ostby and C. Thaulow, “Fracture response of pipelines subjected to large plastic deformation under tension.,” *Internal Journal of Pressure Vessels and Pipings,* vol. 81, no. 9, pp. 771-83, 2004.

[104] E. Otsby, K. R. Jayadevan and C. Thaulow, “Fracture response of pipelines subjected to large plastic deformation under bending.,” *International Journal of Pressure Vessels and Pipings,* vol. 82, pp. 201-215, 2005.

[105] E. Otsby and A. O. Hellesvik, “Large-Scale Experimental Investigation of the Effect of Biaxial Loading on the Deformation Capacity of Pipes with Defects,” *International Journal of Pressure Vessels and Piping,* vol. 85, no. 11, pp. 814-824, 2008.

[106] L. F. S. Parise, C. Ruggieri and N. P. O'Dowd, “Fully-Plastic Strain Based J-estimation scheme for circumferential surface cracks in pipes subjected to reeling,” *ASME Journal of Pressure Vessel Technology,* vol. 137, pp. 041204-04 -- 041204-8, August 2015.

[107] T. Tkaczyk, N. P. O'Dowd and K. Nikbin, “Fracture assessment procedures for steel pipelines using a modified reference stress solution,” *Journal of Pressure Vessel Technology,* vol. 131, pp. 1243-1257, 2009.

[108] Y. J. Kim and P. J. Budden, “Reference stress approximations for J and COD of circumferential through-wall cracked pipes,” *International Journal of Fracture,* vol. 116, pp. 195-218, 2002.

[109] W. E. Kastner, E. Rohrich, W. Schmitt and R. Steinbuch, “Critical crack sizes in ductile piping,” *International Journal of Pressure Vessels and Piping,* vol. 9, pp. 197-219, 1981.

[110] D. J. Smith, A. J. Fookes, M. Lamb and D. W. Dean, “Development of a strain-based FAD for prediction of creep cracking in welds,” in *In: Proceedings of the international conference on integrity of high temperature welds*, Nottingham, 1998.

[111] A. J. Fookes and D. J. Smith, “Using a strain based failure assessment diagram for creep-brittle materials,” *International Journal of Pressure Vessels and Piping,* vol. 78, pp. 951-961, 2001.

[112] R. A. Ainsworth, “Methods for treating displacement-controlled loading using the R6 defect assessment procedure,” Berkeley Technology Centre, Berkeley, 1993.

[113] Y. Lei, “J-integral and limit load analysis of semi-elliptical surface cracks in plates under tension,” *International Journal of Pressure Vessels and Piping,* vol. 81, pp. 21-30, 2004.

[114] Y. Lei, “J-integral and limit load analysis of semi-elliptical surface cracks in plates

under bending," *International Journal of Pressure Vessels and Piping,* vol. 81, pp. 31-41, 2004.

[115] Y. Lei, "J-integral and limit load analysis of semi-elliptical surface cracks in plates under combined tension and bending," *International Journal of Pressure Vessels and Piping,* vol. 81, pp. 43-56, 2004.

[116] Y. Lei, "A comparison of 3-D finite element and simplified estimates of J under thermal and mechanical loads," in *ASME 2002 Pressure Vessels and Piping Conference*, Vancouver, BC, Canada, 2002.

[117] P. J. Budden and M. C. Smith, "Numerical validation of a strain-based failure assessment diagram approach to fracture," in *In: Proc ASME PVP2009,PVP2009-77377*, Prague, July 26-30, 2009.

[118] P. J. Budden, "Fracture assessment diagram methods for strain based fracture," *Engineering Fracture Mechanics,* vol. 73, pp. 537-552, 2006.

[119] W. Xu and W. He, "Strain-based engineering critical assessment of pipeline girth welds," Cambridge:TWI; 2007, 2007.

[120] R. A. Ainsworth, P. J. Budden, C.-Y. Oh and Y.-J. Kim, "The treatment of secondary strains within a strain-based failure assessment diagram," *International Journal of Pressure Vessels and Piping,* vol. 104, pp. 14-20, 2013.

[121] J. Chattopadhyay and A. K. S. Tomar, "New plastic collapse moment equations of defect-free and throughwall circumferentially cracked elbows subjected to internal pressure and in-plane bending moment," *Engineering Fracture Mechanics,* vol. 73, pp. 829-854, 2006.

[122] M. R. Jones and J. M. Eshelby, "Limit load solutions for circumferentially cracked cylinders under internal pressure and combined tension and bending," Nuclear Electric

Report, TD/SID/REP/0032, 1990.

[123] M. K. Sahu, J. Chattopadhyay and B. K. Dutta, “Fracture studies of straight pipes subjected to internal pressure and bending moment,” *International Journal of Pressure Vessels and Pipings,* vol. 134, pp. 56-71, 2015.

[124] M. K. Sahu, J. Chattopadhyay and B. K. Dutta, “Application of R6 Failure Assessment Method to obtain fracture toughness,” *Theoretical and Applied Fracture Mechanics,* vol. 81, pp. 67-75, 2015.

[125] S. Timoshenko, Strength of Materials, New Delhi: CBS Publishers, 1986.